A signal-processing-based approach for damage detection of steel structures

by

Amin Moghadam

B.S., University of Qom, 2012
M.S., Sharif University of Technology, 2014

A THESIS

submitted in partial fulfillment of the requirements for the degree

MASTER OF SCIENCE

Department of Civil Engineering
College of Engineering

KANSAS STATE UNIVERSITY
Manhattan, Kansas

2019

Approved by:

Major Professor
Professor Hani Melhem

Copyright

Abstract

This study reports the results of an analytical, experimental and a numerical study (proof of concept study) on a proposed method for extracting the pseudo-free-vibration response of a structure using ambient vibration, usually of a random nature, as a source of excitation to detect any change in the dynamic properties of a structure that may be caused by damage. The structural response contains not only a random component but also a component reflecting the dynamic properties of the structure, comparable to the free vibration for a given initial condition. Structural response to the arbitrary excitation is recorded by one or several accelerometers with a desired data-collection frequency and resolution. The free-vibration response of the structure is then extracted from this data by removing the random component of the response by the method proposed in this study. The features of the free-vibration response of the structure extracted by a suitable method, namely Fast Fourier Transform (FFT) in this study, can be used for change detection. Possible change of the pattern of these features is dominantly linked to the change in dynamic properties of the system, caused by possible damage.

To show the applicability of the concept, besides an analytical verification using Newmark's linear acceleration method, two steel portal frames with different flexural stiffness were made in the steel workshop of the structural laboratory for an experimental study. These structures were also numerically modeled using a finite element software. A wireless accelerometer with a sampling frequency rate of 2046 Hz was affixed on the top of the physical structure, at the same location where the acceleration was recorded for the corresponding numerical model. The physical structure was excited manually by an arbitrary hit and the response of the structure to this excitation, in terms of the acceleration on the top of the structure, was recorded. The pseudo-free-vibration response was extracted and transferred into frequency domain

using FFT. The frequency with the largest magnitude which is the fundamental frequency of the structure was traced. This was repeated for several independent excitations and the fundamental frequencies were observed to be the same, showing that the process can correctly identify the natural frequencies of the structure. Similarly, the numerical model was excited and for several base excitation cases, the fundamental frequencies were found to be the same. Considering the acceptable accuracy of the results from the two numerical models in simulating the response of their corresponding physical models, additional numerical models were analyzed to show the consistency and applicability of the proposed method for a range of flexural stiffness and damping ratio. The results confirm that the proposed method can precisely extract the pseudo-free-vibration response of the structures and detect the structural frequencies regardless of the excitation. The fundamental frequency is tied to the stiffness and a larger stiffness leads to a higher frequency, as expected, regardless of the simulated ambient excitation.

Table of Contents

List of Figures vii
Acknowledgements xvi
Dedication xvii
Chapter 1 - Introduction 1
1.1 Introduction 1
1.2 Objectives 3
Chapter 2 - Literature Review 5
2.1 Direct Use of Modal Parameters 5
2.1.1 Change in the Natural Frequencies 5
2.1.2 Identification Based on the Frequency Contours Methods 8
2.1.3 Change in Damping 9
2.1.4 Mode Shapes and Changes in Node Positions 10
2.1.5 MAC and Other Related Assurance Criteria 12
2.1.6 Mode Shapes Curvature 13
2.1.7 Modal Strain Energy 15
2.1.8 Changes in Dynamic Flexibility 15
2.1.9 Sensitivity-Based Approach 17
2.1.10 Changes in Antiresonances 17
2.2. Changes in Frequency Response Function 19
2.2.1 Extension of the MAC Criteria for the Frequency Response Function 20
2.3. Coupling Responses Measurements 21
2.3.1 Applications for Damage Detection in Practical Cases 21
Chapter 3 - The Proposed Approach and Procedure 24
3.1 The Proposed Approach to Extract the Pseudo-Free-Vibration Response 24
3.2 The Procedure for Damage Detection 26
Chapter 4 - Geometry, Material, and Modeling 28
4.1 Analytical Model 28
4.2 Numerical Models 29
4.3 Experimental Models 30

4.4 Modeling 32
4.4.1 ABAQUS Software 32
4.4.2 MATLAB Software 39
Chapter 5 - Results 40
5.1 Analytical Study 40
5.2 Numerical Study 43
5.3 A proposed procedure to determine the exact values of u_0 and Δt_1 47
5.4 Evaluation of the effects of damping ratio on the results 50
5.5 Experimental Study 54
5.6 Thirty different numerical models 58
Chapter 6 - Conclusion and Future Study 60
6.1 Conclusions 60
6.1 Future Study 61
References 64
Appendix A - Pseudo-Free-Vibration and FFT Diagrams for Changing Δt_1 while u_0 is constant 72
Appendix B - Pseudo-free-vibration and FFT Diagrams for changing u_0 while Δt_1 is constant ... 98
Appendix C - MATLAB Codes 117

List of Figures

Figure 1.1 Structural Health Monitoring and damage detection categories 2
Figure 3.1 A sampled acceleration-time response 24
Figure 3.2 The extracted part shown in Figure 3.1 25
Figure 3.3 All steps required to pass for damage detection 27
Figure 4.1 The considered single degree of freedom system (m=44.36 kg, c=0, k=1751.27 N/m) 28
Figure 4.2 Geometrical characteristics of structure one 29
Figure 4.3 Geometrical characteristics of structure two 30
Figure 4.4 The experimental structures one and two and the accelerometer 31
Figure 4.5 The instances characteristics 33
Figure 4.6 Defining of the modulus of elasticity and the Poisson's ratio of steel 33
Figure 4.7 Defining of steel density 34
Figure 4.8 Defining of the section characteristics 34
Figure 4.9 The independent instances 35
Figure 4.10 Using linear perturbation, modal dynamics analysis to obtain the ambient response of the structure 35
Figure 4.11 The fixed supports of the structures 36
Figure 4.12 The elements properties 37
Figure 4.13 Views of the numerical model of structure one (Side view) 37
Figure 4.14 Views of the numerical model of structure one (Isometric view) 38
Figure 4.15 An example of the actual random excitations used 38
Figure 4.16 Job analysis in ABAQUS 39
Figure 5.1 Comparing the free-vibration responses of the single degree of freedom system using two different methods namely Newmark's linear acceleration method and exact free-vibration 41
Figure 5.2 Comparing the pseudo-free-vibration responses of the single degree of freedom system with the exact free-vibration response 42
Figure 5.3 The natural frequency of the single degree of freedom system extracted using the 8-step MATLAB code 43

Figure 5.4 Signal processing results of structure one subjected to dynamic load one (pseudo-free-vibration response diagram) 45
Figure 5.5 Signal processing results of structure one subjected to dynamic load one (FFT diagram) 45
Figure 5.6 Signal processing results of structure two subjected to dynamic load one (pseudo-free-vibration response diagram) 46
Figure 5.7 Signal processing results of structure two subjected to dynamic load one (FFT diagram) 46
Figure 5.8 Comparison of the fundamental frequency of the numerical results of structures one and two subjected to dynamic loads one, two and three 47
Figure 5.9 Fundamental frequencies of structure one when Δt_1 is varying while u_0 is constant .. 48
Figure 5.10 Fundamental frequencies of structure one when u_0 is varying while Δt_1 is constant 49
Figure 5.11 Pseudo-free-vibration response diagram of structure one subjected to dynamic load one (damping ratio=0%) 51
Figure 5.12 FFT diagram of structure one subjected to dynamic load one (damping ratio=0%). 51
Figure 5.13 Pseudo-free-vibration response diagram of structure one subjected to dynamic load one (damping ratio=4%) 52
Figure 5.14 FFT diagram of structure one subjected to dynamic load one (damping ratio=4%). 52
Figure 5.15 Pseudo-free-vibration response diagram of structure one subjected to dynamic load one (damping ratio=7%) 53
Figure 5.16 FFT diagram of structure one subjected to dynamic load one (damping ratio=7%). 53
Figure 5.17 The fundamental frequency of structure one subjected to dynamic load one for different damping ratios varying from 0 to 7 percent 54
Figure 5.18 Signal processing results of experimental model one subjected to dynamic load one (pseudo-free-vibration response diagram) 55
Figure 5.19 Signal processing results of experimental model one subjected to dynamic load one (FFT diagram) 55
Figure 5.20 Signal processing results of experimental model two subjected to dynamic load one (pseudo-free-vibration response diagram) 56
Figure 5.21 Signal processing results of experimental model two subjected to dynamic load one (FFT diagram) 56

Figure 5.22 Comparing of the fundamental frequencies of the experimental and numerical results of structures one and two subjected to dynamic loads one, two and three (structure one)... 57
Figure 5.23 Comparing of the fundamental frequencies of the experimental and numerical results of structures one and two subjected to dynamic loads one, two and three (structure two)... 57
Figure 5.24 The fundamental frequency of the signal processing results of different models with different column heights under dynamic load one (For example, C250 refers to a structure for which all geometrical characteristics are the same as Figures 4.2 and 4.3 except that the column height is 250 mm) 59
Figure 5.25 The fundamental frequency of the signal processing results of different models with different column heights under dynamic load two (For example, C250 refers to a structure for which all geometrical characteristics are the same as Figures 4.2 and 4.3 except that the column height is 250 mm..... 59
Figure A.1 Signal processing results of structure one subjected to dynamic load one (pseudo-free-vibration response diagram-Δt_1= 3.5%, u_0= 0.1D_{max})72
Figure A.2 Signal processing results of structure one subjected to dynamic load one (FFT diagram- Δt_1= 3.5%, u_0= 0.1D_{max}) 72
Figure A.3 Signal processing results of structure one subjected to dynamic load one (pseudo-free-vibration response diagram- Δt_1= 3.4%, u_0= 0.1D_{max}) 73
Figure A.4 Signal processing results of structure one subjected to dynamic load one (FFT diagram- Δt_1= 3.4%, u_0= 0.1D_{max}) 73
Figure A.5 Signal processing results of structure one subjected to dynamic load one (pseudo-free-vibration response diagram- Δt_1= 3.3%, u_0= 0.1D_{max}) 74
Figure A.6 Signal processing results of structure one subjected to dynamic load one (FFT diagram- Δt_1= 3.3%, u_0= 0.1D_{max}) 74
Figure A.7 Signal processing results of structure one subjected to dynamic load one (pseudo-free-vibration response diagram- Δt_1= 3.2%, u_0= 0.1D_{max}) 75
Figure A.8 Signal processing results of structure one subjected to dynamic load one (FFT diagram- Δt_1= 3.2%, u_0= 0.1D_{max}) 75
Figure A.9 Signal processing results of structure one subjected to dynamic load one (pseudo-free-vibration response diagram- Δt_1= 3.1%, u_0= 0.1D_{max}) 76

Figure A.10 Signal processing results of structure one subjected to dynamic load one (FFT diagram- Δt_1= 3.1%, u_0= 0.1D_{max}) 76
Figure A.11 Signal processing results of structure one subjected to dynamic load one (pseudo-free-vibration response diagram- Δt_1= 3.0%, u_0= 0.1D_{max}) 77
Figure A.12 Signal processing results of structure one subjected to dynamic load one (FFT diagram- Δt_1= 3.0%, u_0= 0.1D_{max}) 77
Figure A.13 Signal processing results of structure one subjected to dynamic load one (pseudo-free-vibration response diagram- Δt_1= 2.9%, u_0= 0.1D_{max}) 78
Figure A.14 Signal processing results of structure one subjected to dynamic load one (FFT diagram- Δt_1= 2.9%, u_0= 0.1D_{max}) 78
Figure A.15 Signal processing results of structure one subjected to dynamic load one (pseudo-free-vibration response diagram- Δt_1= 2.5%, u_0= 0.1D_{max}) 79
Figure A.16 Signal processing results of structure one subjected to dynamic load one (FFT diagram- Δt_1= 2.5%, u_0= 0.1D_{max}) 79
Figure A.17 Signal processing results of structure one subjected to dynamic load one (pseudo-free-vibration response diagram- Δt_1= 2.4%, u_0= 0.1D_{max}) 80
Figure A.18 Signal processing results of structure one subjected to dynamic load one (FFT diagram- Δt_1= 2.4%, u_0= 0.1D_{max}) 80
Figure A.19 Signal processing results of structure one subjected to dynamic load one (pseudo-free-vibration response diagram- Δt_1= 2.3%, u_0= 0.1D_{max}) 81
Figure A.20 Signal processing results of structure one subjected to dynamic load one (FFT diagram- Δt_1= 2.3%, u_0= 0.1D_{max}) 81
Figure A.21 Signal processing results of structure one subjected to dynamic load one (pseudo-free-vibration response diagram- Δt_1= 2.2%, u_0= 0.1D_{max}) 82
Figure A.22 Signal processing results of structure one subjected to dynamic load one (FFT diagram- Δt_1= 2.2%, u_0= 0.1D_{max}) 82
Figure A.23 Signal processing results of structure one subjected to dynamic load one (pseudo-free-vibration response diagram- Δt_1= 2.0%, u_0= 0.1D_{max}) 83
Figure A.24 Signal processing results of structure one subjected to dynamic load one (FFT diagram- Δt_1= 2.0%, u_0= 0.1D_{max}) 83

Figure A.25 Signal processing results of structure one subjected to dynamic load one (pseudo-free-vibration response diagram- Δt_1= 1.4%, u_0= 0.1D_{max}) 84
Figure A.26 Signal processing results of structure one subjected to dynamic load one (FFT diagram- Δt_1= 1.4%, u_0= 0.1D_{max}) 84
Figure A.27 Signal processing results of structure one subjected to dynamic load one (pseudo-free-vibration response diagram- Δt_1= 1.3%, u_0= 0.1D_{max}) 85
Figure A.28 Signal processing results of structure one subjected to dynamic load one (FFT diagram- Δt_1= 1.3%, u_0= 0.1D_{max}) 85
Figure A.29 Signal processing results of structure one subjected to dynamic load one (pseudo-free-vibration response diagram- Δt_1= 1.2%, u_0= 0.1D_{max}) 86
Figure A.30 Signal processing results of structure one subjected to dynamic load one (FFT diagram- Δt_1= 1.2%, u_0= 0.1D_{max}) 86
Figure A.31 Signal processing results of structure one subjected to dynamic load one (pseudo-free-vibration response diagram- Δt_1= 1.1%, u_0= 0.1D_{max}) 87
Figure A.32 Signal processing results of structure one subjected to dynamic load one (FFT diagram- Δt_1= 1.1%, u_0= 0.1D_{max}) 87
Figure A.33 Signal processing results of structure one subjected to dynamic load one (pseudo-free-vibration response diagram- Δt_1= 1.0%, u_0= 0.1D_{max}) 88
Figure A.34 Signal processing results of structure one subjected to dynamic load one (FFT diagram- Δt_1= 1.0%, u_0= 0.1D_{max}) 88
Figure A.35 Signal processing results of structure one subjected to dynamic load one (pseudo-free-vibration response diagram- Δt_1= 0.9%, u_0= 0.1D_{max}) 89
Figure A.36 Signal processing results of structure one subjected to dynamic load one (FFT diagram- Δt_1= 0.9%, u_0= 0.1D_{max}) 89
Figure A.37 Signal processing results of structure one subjected to dynamic load one (pseudo-free-vibration response diagram- Δt_1= 0.8%, u_0= 0.1D_{max}) 90
Figure A.38 Signal processing results of structure one subjected to dynamic load one (FFT diagram- Δt_1= 0.8%, u_0= 0.1D_{max}) 90
Figure A.39 Signal processing results of structure one subjected to dynamic load one (pseudo-free-vibration response diagram- Δt_1= 0.7%, u_0= 0.1D_{max}) 91

Figure A.40 Signal processing results of structure one subjected to dynamic load one (FFT diagram- Δt_1= 0.7%, u_0= 0.1D_{max}) 91
Figure A.41 Signal processing results of structure one subjected to dynamic load one (pseudo-free-vibration response diagram- Δt_1= 0.6%, u_0= 0.1D_{max}) 92
Figure A.42 Signal processing results of structure one subjected to dynamic load one (FFT diagram- Δt_1= 0.6%, u_0= 0.1D_{max}) 92
Figure A.43 Signal processing results of structure one subjected to dynamic load one (pseudo-free-vibration response diagram- Δt_1= 0.5%, u_0= 0.1D_{max}) 93
Figure A.44 Signal processing results of structure one subjected to dynamic load one (FFT diagram- Δt_1= 0.5%, u_0= 0.1D_{max}) 93
Figure A.45 Signal processing results of structure one subjected to dynamic load one (pseudo-free-vibration response diagram- Δt_1= 0.4%, u_0= 0.1D_{max}) 94
Figure A.46 Signal processing results of structure one subjected to dynamic load one (FFT diagram- Δt_1= 0.4%, u_0= 0.1D_{max}) 94
Figure A.47 Signal processing results of structure one subjected to dynamic load one (pseudo-free-vibration response diagram- Δt_1= 0.3%, u_0= 0.1D_{max}) 95
Figure A.48 Signal processing results of structure one subjected to dynamic load one (FFT diagram- Δt_1= 0.3%, u_0= 0.1D_{max}) 95
Figure A.49 Signal processing results of structure one subjected to dynamic load one (pseudo-free-vibration response diagram- Δt_1= 0.2%, u_0= 0.1D_{max}) 96
Figure A.50 Signal processing results of structure one subjected to dynamic load one (FFT diagram- Δt_1= 0.2%, u_0= 0.1D_{max}) 96
Figure A.51 Signal processing results of structure one subjected to dynamic load one (pseudo-free-vibration response diagram- Δt_1= 0.1%, u_0= 0.1D_{max}) 97
Figure A.52 Signal processing results of structure one subjected to dynamic load one (FFT diagram- Δt_1= 0.1%, u_0= 0.1D_{max}) 97
Figure B.1 Signal processing results of structure one subjected to dynamic load one (pseudo-free-vibration response diagram- Δt_1= 0.5%, u_0= (1/2)*D_{max}) 98
Figure B.2 Signal processing results of structure one subjected to dynamic load one (FFT diagram- Δt_1= 0.5%, u_0= (1/2)*D_{max}) 98

Figure B.3 Signal processing results of structure one subjected to dynamic load one (pseudo-free-vibration response diagram- Δt_1= 0.5%, u_0= (1/3)*D_{max}) 99
Figure B.4 Signal processing results of structure one subjected to dynamic load one (FFT diagram- Δt_1= 0.5%, u_0= (1/3)*D_{max}) 99
Figure B.5 Signal processing results of structure one subjected to dynamic load one (pseudo-free-vibration response diagram- Δt_1= 0.5%, u_0= (1/4)*D_{max}) 100
Figure B.6 Signal processing results of structure one subjected to dynamic load one (FFT diagram- Δt_1= 0.5%, u_0= (1/4)*D_{max}) 100
Figure B.7 Signal processing results of structure one subjected to dynamic load one (pseudo-free-vibration response diagram- Δt_1= 0.5%, u_0= (1/5)*D_{max}) 101
Figure B.8 Signal processing results of structure one subjected to dynamic load one (FFT diagram- Δt_1= 0.5%, u_0= (1/5)*D_{max}) 101
Figure B.9 Signal processing results of structure one subjected to dynamic load one (pseudo-free-vibration response diagram- Δt_1= 0.5%, u_0= (1/6)*D_{max}) 102
Figure B.10 Signal processing results of structure one subjected to dynamic load one (FFT diagram- Δt_1= 0.5%, u_0= (1/6)*D_{max}) 102
Figure B.11 Signal processing results of structure one subjected to dynamic load one (pseudo-free-vibration response diagram- Δt_1= 0.5%, u_0= (1/7)*D_{max}) 103
Figure B.12 Signal processing results of structure one subjected to dynamic load one (FFT diagram- Δt_1= 0.5%, u_0= (1/7)*D_{max}) 103
Figure B.13 Signal processing results of structure one subjected to dynamic load one (pseudo-free-vibration response diagram- Δt_1= 0.5%, u_0= (1/10)*D_{max}) 104
Figure B.14 Signal processing results of structure one subjected to dynamic load one (FFT diagram- Δt_1= 0.5%, u_0= (1/10)*D_{max}) 104
Figure B.15 Signal processing results of structure one subjected to dynamic load one (pseudo-free-vibration response diagram- Δt_1= 0.5%, u_0= (1/11)*D_{max}) 105
Figure B.16 Signal processing results of structure one subjected to dynamic load one (FFT diagram- Δt_1= 0.5%, u_0= (1/11)*D_{max}) 105
Figure B.17 Signal processing results of structure one subjected to dynamic load one (pseudo-free-vibration response diagram- Δt_1= 0.5%, u_0= (1/14)*D_{max}) 106

Figure B.18 Signal processing results of structure one subjected to dynamic load one (FFT diagram- Δt_1= 0.5%, u_0= (1/14)*D_{max}) 106
Figure B.19 Signal processing results of structure one subjected to dynamic load one (pseudo-free-vibration response diagram- Δt_1= 0.5%, u_0= (1/16)*D_{max}) 107
Figure B.20 Signal processing results of structure one subjected to dynamic load one (FFT diagram- Δt_1= 0.5%, u_0= (1/16)*D_{max}) 107
Figure B.21 Signal processing results of structure one subjected to dynamic load one (pseudo-free-vibration response diagram- Δt_1= 0.5%, u_0= (1/19)*D_{max}) 108
Figure B.22 Signal processing results of structure one subjected to dynamic load one (FFT diagram- Δt_1= 0.5%, u_0= (1/19)*D_{max}) 108
Figure B.23 Signal processing results of structure one subjected to dynamic load one (pseudo-free-vibration response diagram- Δt_1= 0.5%, u_0= (1/20)*D_{max}) 109
Figure B.24 Signal processing results of structure one subjected to dynamic load one (FFT diagram- Δt_1= 0.5%, u_0= (1/20)*D_{max}) 109
Figure B.25 Signal processing results of structure one subjected to dynamic load one (pseudo-free-vibration response diagram- Δt_1= 0.5%, u_0= (1/50)*D_{max}) 110
Figure B.26 Signal processing results of structure one subjected to dynamic load one (FFT diagram- Δt_1= 0.5%, u_0= (1/50)*D_{max}) 110
Figure B.27 Signal processing results of structure one subjected to dynamic load one (pseudo-free-vibration response diagram- Δt_1= 0.5%, u_0= (1/100)*D_{max}) 111
Figure B.28 Signal processing results of structure one subjected to dynamic load one (FFT diagram- Δt_1= 0.5%, u_0= (1/100)*D_{max}) 111
Figure B.29 Signal processing results of structure one subjected to dynamic load one (pseudo-free-vibration response diagram- Δt_1= 0.5%, u_0= (1/200)*D_{max}) 112
Figure B.30 Signal processing results of structure one subjected to dynamic load one (FFT diagram- Δt_1= 0.5%, u_0= (1/200)*D_{max}) 112
Figure B.31 Signal processing results of structure one subjected to dynamic load one (pseudo-free-vibration response diagram- Δt_1= 0.5%, u_0= (1/1000)*D_{max}) 113
Figure B.32 Signal processing results of structure one subjected to dynamic load one (FFT diagram-ΔT_1= 0.5%, u_0= (1/1000)*D_{max}) 113

Figure B.33 Signal processing results of structure one subjected to dynamic load one (pseudo-free-vibration response diagram- Δt_1= 0.5%, u_0= (1/10000)*D_{max}) 114
Figure B.34 Signal processing results of structure one subjected to dynamic load one (FFT diagram- Δt_1= 0.5%, u_0= (1/10000)*D_{max}) 114
Figure B.35 Signal processing results of structure one subjected to dynamic load one (pseudo-free-vibration response diagram- Δt_1= 0.5%, u_0= (1/100000)*D_{max}) 115
Figure B.36 Signal processing results of structure one subjected to dynamic load one (FFT diagram- Δt_1= 0.5%, u_0= (1/100000)*D_{max}) 115
Figure B.37 Signal processing results of structure one subjected to dynamic load one (pseudo-free-vibration response diagram- Δt_1= 0.5%, u_0= (1/1000000)*D_{max}) 116
Figure B.38 Signal processing results of structure one subjected to dynamic load one (FFT diagram- Δt_1= 0.5%, u_0= (1/1000000)*D_{max}) 116

Acknowledgements

I would like to gratefully thank Dr. Hani G. Melhem, my advisor, for his guidance, support and help during my PhD studies at Kansas State University (KSU). Gratitude is also extended to the members of the supervisory committee: Dr. Hayder Rasheed and Dr. Dunja Peric.

I would like to express my deepest gratitude to my wife. She was always there cheering me up and stood by me through the good times and bad times, and her support, encouragement and love helped me to get to another achievement in my life.

Finally, I would like to thank my family specially my mother and father for their faith in me and allowing me to be as ambitious as I wanted.

Dedication

This work is dedicated to my wife, Mansoureh Jalali, and my parents,

Reza Moghadam and Zahra Moghadam.

Chapter 1 - Introduction

1.1 Introduction

Different structures like towers, bridges, retaining walls, wind turbines, and so forth are susceptible to damage from extreme loads such as earthquakes, wind, floods, fires, undermining from adjacent construction, landslides, and overloading with heavy contents. Moreover, these structures status can be changed by aging and environmental effects that significantly affect the performance of structures during their service life. Examples of such deterioration are corrosion, wood decay, concrete attack by adverse chemicals, fatigue, foundation settlement, slope creep, or vibrations from adjacent construction.

The state of the structure must remain in the situation determined in design. Structural Health Monitoring (SHM) aim is diagnosing of the "state" of the constituent materials, different parts, and full assembly of these parts constituting the structure as a whole to monitor the performance of structure, detect and assess any damage at the earliest stage in order to reduce the life-cycle cost of structure and improve its reliability and safety.

In structural health monitoring, both Destructive Damage Detection (DDD) and Non-destructive Damage Detection (NDD) techniques are used to evaluate the structure to detect any possible damage available in the structure. However, NDD techniques are more convenient and less costly than DDD techniques due to recent advances in electronic technologies like sensors, computers, and so forth. Meanwhile, despite of DDD techniques that find any defect in the structure by testing samples removed from the structure, NDD techniques do not damage the structure.

NDD techniques can be categorized into two clusters: local methods; and global methods. Some of highly effective methods are acoustic or ultrasonic methods, magnetic field methods,

radiograph, microwave/ground penetrating radar, fiber optics, eddy current methods and thermal field methods. These methods are visual or localized experimental methods that detect damage on or near the surface of the structure by measuring light, sound, electromagnetic field intensity, displacements, or temperature [1]. The following are some Non-destructive tests (NDTs) that are commonly used in structural engineering practice: Schmidt Hammer, also known as the rebound or impact hammer, to evaluate reinforced concrete strength [2]; Concrete ultrasonic tester to measure crack depth [3]; Ground penetrating radar for rebar detection [4]; Digital coating thickness gauge to measure painting thickness of steel members [5]; eddy current is very effective for crack detection at welded joint [6]. Figure 1.1 illustrates a general classification based on different damage detection categories, methods, and basic algorithms [7].

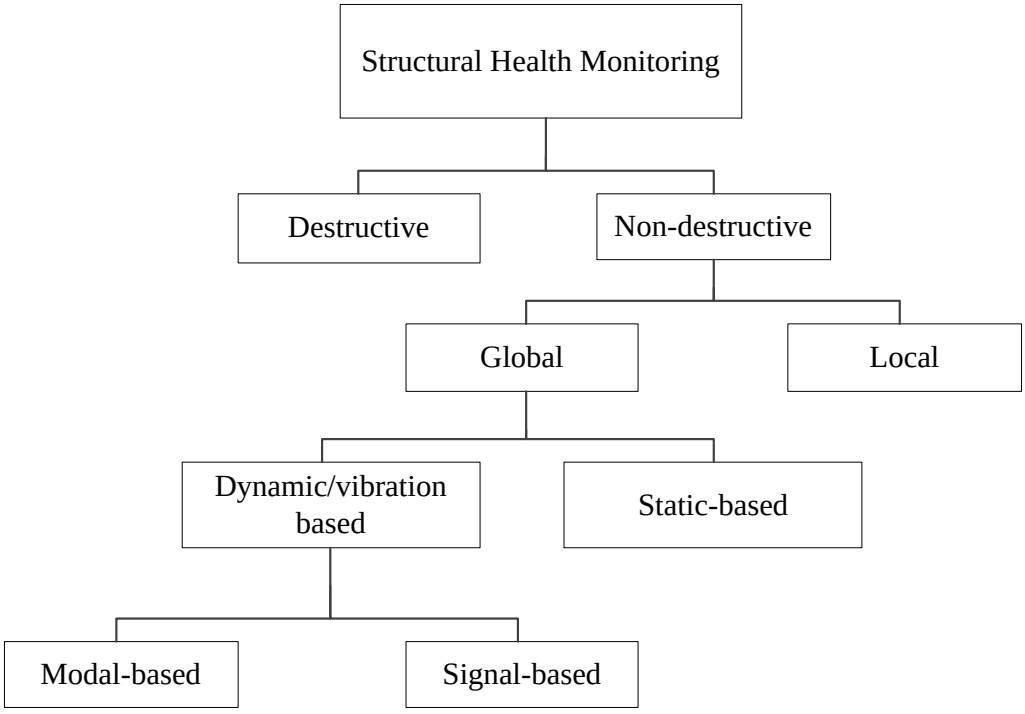

Figure 1.1 Structural Health Monitoring and damage detection categories

1.2 Objectives

There are two different forms of vibration test on civil structures, forced vibration test (FVT) and ambient vibration test (AVT) [8], [9]. In the past, rotating eccentric mass (REM) shakers have been used for forced vibration testing for buildings [10]. In rare cases, shakers driven by hydraulic or electro-dynamic actuators have been used to excite a building with a broad band signal [8], [10]. Because of the fact that machinery associated with FVT are generally logistics and large, except of a few cases, AVT is preferable. In ambient vibration tests, a set of accelerometers are needed to be set on the structure to measure the response of structures subjected to the vibrations of the wind, traffic and so forth [11]. Additionally, measured signals are possibly contaminated by noise so that information from tiny damage in structures may be covered by the random vibration and noise, and the selection and construction of the feature index of structural damage are variable [1]. Thus, in this study, the author has adopted a novel random-vibration-based approach using ambient vibration, as a source of excitation, to detect any change in the dynamic properties of a structure that may be caused by damage. Under any excitation, the response of a structure is composed of free and forced vibrations, as long as the structure remains in its linear and elastic range. So, the free vibration response of the structure can be extracted by eliminating the forced response. Filtering out the random component of the response, leads to the free vibration response of the structure. Averaging the response for each time step on a large number of data points is one of the methods to filter out the forced vibration of the response to a random excitation. In this study, the forced vibration is eliminated for a pre-determined initial acceleration, for which the free vibration is extracted. The free vibration response can then be used to detect change using various methods. Here, the free-vibration response called pseudo-free-vibration response is transferred into frequency domain using Fast Fourier Transform (FFT) and

the changes in structural frequencies are used for detection of changes in the dynamic properties of the structure. The frequency with the maximum intensity in frequency domain which is the fundamental frequency of the structure is traced in this study to detect changes in the stiffness of the structure.

Chapter 2 - Literature Review

2.1 Direct Use of Modal Parameters

2.1.1 Change in the Natural Frequencies

The change of natural frequencies is one of the common damage detection methods in structural health monitoring. When any damage occurs in a structure, the stiffness will decrease, and therefore natural frequencies of the system decreases as well. One of the greatest advantages of this method is that structural frequencies can be easily measured. Also, to determine the resonant frequencies, usually, classical vibrational measurement techniques can be used as experimental techniques that make the vibrational measurements with a great number of measurements to be cheaper compared to other methods. Another advantage is that having a great control of experimental conditions makes the frequency measurements to be with a relatively acceptable accuracy, and uncertainties in the measured frequencies will be determinable. Moreover, using analytical developments or finite element models makes obtaining the knowledge about undamaged systems very easy; thus, having the measurement points adequately chosen allows one to have a quick and efficient detection of the frequencies changes as well as the identification of the damage location.

According to Doebling et al. [12], for the first time, in 1969, Lifshitz and Rotem [13] proposed a damage detection method by using vibration measurements. This technique is a damage detection method in elastomers based upon measuring of natural frequencies by changes in dynamic moduli and damping of tensile specimens. Hearn and Testa [14] proposed a formula that approximates the i^{th} natural frequency. This formula, assuming that the damage does not change the mass matrix, provides a relationship between M (the mass matrix), Φi (the i^{th} mode shape vector), and the element deformation vector that can be computed from the mode shapes. They

also concluded that the ratio of the variations of two natural frequencies of mode *i* and *j* is dependent to the damage location, however, it does not show the damage severity. Many other researchers have attempted to detect damage in structures by using changes in natural frequencies. Salawu proposed an intensive review in [6]. Some other researchers used natural frequencies changes for damage detection by comparing the natural frequencies of the undamaged and damaged structures [15]–[25]. In some of these studies, the ratio of the natural frequencies of damaged structure to the natural frequencies of the damaged structure will be used for damage detection [16]. The mentioned study [16] used the linear fracture mechanics theory to determine the crack location and depth of a cantilever beam. Also, to obtain the natural frequencies and mode shapes, the finite element model of the cracked beam was constructed. From the theoretical analysis and experimental measurements, it is found that the crack location and crack size noticeably affect the first and second natural frequencies of the cantilever beam. This study provides a useful tool for detection of medium size cracks in a beam that also has reliable and accurate results for crack depth, besides an acceptable error for the crack location. On the other hand, some other studies use the percentage change of the natural frequencies [26]–[29]. The percentage change of the natural frequencies can be very small (for instance 1% for small cracks or specific locations of the crack); so, the natural frequencies of the intact structure should be accurately measured in order to be able to determine if the obtained frequencies are smaller than expected. So, inaccurate measures of the natural frequencies may cause one to miss the small amount of damage that may be caused by small amount of frequency changes. Results show that a crack located near a node of the mode vibration has little effect on. For those places that are near the largest bending moment of i^{th} mode, the crack will change the natural frequencies more noticeably.

An approach similar to the methods explained above estimates the crack gravity and location (by only obtaining the frequencies of the damaged structures) without any need to compare the frequencies of undamaged frequencies with damaged frequencies. In this case, the crack detection requires the knowledge of the material properties (Young's modulus *E* and the density for example), that are estimated by using the uncracked natural frequencies. Although this method may be introduced as a different method that does not require the natural frequencies of the undamaged structures, the undamaged frequencies are used, and the material properties are implicitly considered. So, this last approach can be equivalent to the procedures previously explained. Sinou proposed another indicator based on the changes of the frequencies [30] shown in Equation 2.1. This indicator shows the effect of the damage on two different modes (*i* and *j*); if the value of the indicator is larger than 0, it can be concluded that the mode of i^{th} pulsation is more affected by the crack than another pulsation.

$$\text{indicator} = \left(\frac{\text{undamaged frequency of mode i}}{\text{undamaged frequency of mode j)}} - \frac{\text{damaged frequency of mode i}}{\text{damaged frequency of mode j}}\right) \tag{2.1}$$

Messina et al. also defined an indicator for Damage Location Assurance Criterion (DLAC) based on the changes in natural frequencies [31]. The values of the Damage Location Assurance Criterion (DLAC) vary between zero and unity. Values of zero and unity indicate no correlation and exact match, respectively, and consequently when the indicator value for *i* is one, the location of the damages has been found. Messina et al. extended the Damage Location Assurance Criterion (DLAC) for multiple damage cases as well [32]. The Multiple Damage Location Assurance Criterion (MDLAC) contains sensitivity matrix that contains the first order derivatives of *n* natural frequencies with respect to *m* damage variables *x*. The objective of MDLAC method is to find a

variable vector included in the formula of MDLAC that makes the MDLAC equal to one. MDLAC, was then extended for long-span civil engineering structures by Koh and Dyke [33].

2.1.2 Identification Based on the Frequency Contours Methods

The identification of the crack parameters can be done by using the different factors and the combined effects of the crack in changes of frequencies of the damage structure.

Nikolakopoulos and Papadopoulos using eigenfrequency measurements, evaluated the crack depth and position identification in frame structures and the general idea is to present in contour graph from the dependency of the first two structural eigenfrequencies on crack depth and location [34]. For that, determining the intersecting point of the superposed contours that correspond to the measured eigenfrequency variations caused by the crack presence is needed. They verified the proposed methodology using a number of structure examples included in the paper.

Using the frequency contours method and the intersection of contours from different modes Yang et al. [35] identified the cracks in a simply supported beam. They showed that the intersecting point of three contours corresponding to the measured frequency indicates a crack depth. They also showed that this method can determine the probable location of two cracks because of the structural symmetry in the simply supported beam.

To avoid the non-uniqueness of the damage detection, Dong et al. provided an approach to use the evolution of mode shape [36]. Swamidas et al. claimed that adding an off-center mass to the original structure helps to remove symmetrical solutions [37]. Sinou showed that the preceding method is not a suitable method to eliminate symmetrical solution for all cases, and in some cases will be pretty hard to use [30]. In some experimental cases, because of uncertainties, three contour lines do not have only one intersection for each case, and the centroid of the three pairs of

intersections have been considered as the crack location and size [38], [39]. Therefore, Sinou extended the methodology of mass adding using two different methods [30]. The first method was adding a mass at one of the ends of the symmetrical structure, and the second was testing at the other end. However, the results of the tests on experimental cases show that the methodology works for general structures because of uncertainties. Another method was removing the non-uniqueness of the damage location by the appropriate use of resonances and antiresonances [40], [41]. The advantage of this method is that, with a relevant accuracy, the crack location and size will be obtained without any need to additional tests. Sinou also proposed an extension of the frequencies contour line method by considering the orientation of the front crack besides the crack size and location.

2.1.3 Change in Damping

It is reasonable to expect that a great indicator for damage detection can be damping changes because it is expected that the friction between crack surfaces can increase the damping ratio. Modena et al. [42] claimed that uncertainties or small changes of natural frequencies might make some cracks impossible to detect. However, cracks cause important changes in the damping factor that makes crack identification more probable. It is obvious that increasing the crack severity increases the damping factor.

Bovsunovsky using experimental results with an edge fatigue crack of mode *i* at bending vibrations, showed that the energy dissipation in a non-propagating crack is not caused by the friction between crack surfaces [43]. However, he claimed that energy dissipation change can be used for damage detection based on change prediction of the damping factor.

Kyriazoglou et al. proposed an indicator, specific damping capacity (SDC), for damage detection in composite laminates which is the ratio of the energy dissipated in one cycle to the total

energy stored in that cycle [44]. They illustrated that the changes of SDC strongly correspond to damping properties such that initial damage in composites will be determined before the occurrence of further damage. They also claimed and showed that the SDC is very sensitive to small changes in the crack depth. Interestingly, although large changes were observed in SDC for carbon fiber-reinforced laminates, no detectable changes in the resonant frequencies was found.

Panteliou et al. showed that the larger the crack depth, the larger damping factor is [45]. They also mentioned that the crack identification using damping factor change is relatively insensitive to boundaries conditions compared to the change in natural frequencies.

Leonard et al. illustrated that vibration amplitudes affects the modal damping value of a damaged structure [46]. For example, working on a cantilever beam, they showed that when the amplitudes are too small such that they are not able to generate an open crack, the modal damping decreases. When the opening and closing cracks provides contact effects, the modal damping will be really important. They also concluded that using modal damping to detect damage is difficult because of the evolution dependence of modal damping to the vibration amplitude. Also, uncertainties and modal damping shifts may be observed when the temperature increases.

2.1.4 Mode Shapes and Changes in Node Positions

Mode shapes approach has also received considerable attention in conjunction with changes in natural frequencies due to the fact that a mode shape is a unique characteristic and spatial description of the amplitude of a mechanical structure for each resonant frequency [47]; Therefore, a local damage changes the mode shapes. and the evolution of the spatial description of the amplitude of each resonance can be a damage indicator [47]. Moreover, change of mode shapes depends on both the severity and the location of the damage and the spatial description of

magnitude change with respect to each mode may vary from one to another due to the crack location [47].

Gladwell and Morassi [48] investigated the effect of damage on the nodes in an axially vibrating thin rod. It was illustrated that nodes of the mode shapes move toward the damage. If the node is located to the right of the damage, it moves to the left, and if the node is located to the left, it moves to the right. So, from the movement of the nodes, one can realize the location of the damage.

Then, Dilena and Morassi [49] introduced the positive nodal displacement domain (PNDD) and negative nodal displacement domain (NNDD) that define the direction by which nodal points move. So, when there is any bending vibration, these domains allow to detect the damage. The advantage of using this method is that node positions are easier to measure than mode shapes because they only need the modal component signs not the amplitudes measurement. They also showed the capability of the method by conducting some experimental studies on cracked steel beams.

Study of modal parameters for damage detection such as natural frequencies change and mode shapes change was conducted by Adams et al. [50], Cawley and Adams [51], and Yuen [52] for the vibration of bridges using only the few lower modes.

Natke and Cempel [53] used eigenfrequencies change and mode shapes change for damage detection in a cable-stayed steel bridge. Kullaa [54] demonstrated that the method used by Natke and Campel is reliable for damage detection on the bridge Z24 in Switzerland [55].

Law and Zhu [56] used the mode shapes deflection as an indicator of damage in bridge structures. They showed that the deflection will increase once any damage occurs in the structure. However, they also noticed that the deflection of the damaged structure is sometimes larger than

the deflection measured for the weight of light vehicle. They explained that a moving load such as a vehicle affects the damage opening consequently inducing evolutions of the natural frequencies and mode shapes. So, the crack behavior of the structure subjected to a moving load and the associated non-linear analysis are pretty important to be taken into consideration.

2.1.5 MAC and Other Related Assurance Criteria

Based on the study conducted by Doebling et al. [57], [58], West [59], without having a prior FE model, presented the first systematic use of mode shape information damage localization of the structures. The Modal Assurance Criterion (MAC) is used to determine the level of correlation between modes from the test of an undamaged Space Shuttle Orbiter body flap and the modes from the test of the flap after it has been exposed to acoustic loading.

The MAC value will be always between 0 and 1. MAC uses of the orthogonality properties of the mode shapes to compare two modes. A value of one means that the mode shapes of the two sets of data are identical otherwise a value of zero is calculated. So, a low MAC value can be indicator for a damage. Srinivasan and Kot [60] showed that change in MAC values for damage detection of a cylindrical shell is a more sensitive indicator than changes in resonant frequencies. MAC criteria are a reliable indication of the disparity between two sets of data that can be used for detection of damage. However, it does not show explicitly where the source of the damage in the structure lies.

Palacz and Krawczuk [61] showed that when more than two mode shapes are used, damage localization will be more accurate. On the other hand, a small number of measurements may cause worse damage detection by using the MAC criteria. Other related assurance criteria can be proposed: the frequency response assurance criterion (FRAC), coordinate orthogonality check (CORTHOG), frequency scaled modal assurance criterion (FMAC), partial modal assurance

criterion (PMAC), Modal assurance criterion square Root (MACSR), scaled modal assurance criterion (SMAC), and modal assurance criterion using reciprocal modal vectors (MACRV). A review of the significant of each criterion may be found in [62].

One of the main disadvantage of using MAC criterion or the other assurance criteria as damage indicators is that measurements at a lot of points are required and the duration of measurements should be increased if the mode shapes change is used as an indicator.

Parloo et al. [63] used the modes shapes and the modal assurance criterion (MAC) and co-ordinate modal assurance criterion (COMAC) for damage detection on I-40 highway bridge in New Mexico. However, they showed that only the most severe damage of the bridge was identified, and that the environmental noise significantly affects the damage detection method such that when using this method some of the damages were missed.

2.1.6 Mode Shapes Curvature

As an alternative to mode-shape, curvature is widely used for damage detection from mode shape changes to obtain information about vibration changes. For example, the absolute change in mode shape curvature is an efficient indicator of damage used by Pandey et al. [64]. In this method, as result of a local reduction in stiffness once damage occurs, a local increase happens in the curvature.

Ho and Ewins [65] proposed other criteria based on the mode shapes curvatures as damage indicators including Mode Shape Amplitude Comparison (MSAC), Flexibility Index (FI), Mode Shape Slope (MSS), and Mode Shape Curvature Square (MSCS). Ho and Ewins also indicated that the previous indicators and absolute changes in mode shape curvature are relatively reliable for damage detection but uncertainties at the boundaries conditions and the measurement quality are two of disadvantages of this method.

Maeck and De Roeck [55] used the mode shape curvatures in a direct stiffness calculation technique for the prestressed concrete bridge Z24 in Switzerland, and tested the framework of the Brite Euram project SIMCES. Then, a damage detection indicator (CDF) was introduced using the changes of the dynamic stiffness given by changes in the modal bending moment over the modal curvature. Moreover, they showed that modal curvatures are very sensitive to damage in the bridge.

AbdelWahab and De Roeck [66] proposed Curvature Damage Factor using the application of modal curvatures change for damage detection concrete bridge Z24. They showed that unlike the classical mode shape curvature that is pretty hard for detection of multi damages from the results of only one mode, Curvature Damage Factor will provide a reliable indentation for the damage location. They also mentioned that irregularities in the measured mode shapes or uncertainties need to be carefully examined in order to avoid worse diagnostic.

The mode shape curvatures were applied by Parloo et al. [63] for different damages on I-40 highway bridge in New Mexico. However, they concluded that the mode shape curvature is not a suitable method for actual structures in practical cases for the detection of small damages or in early state, and that this method can only be effective for the most severe damage.

Dutta and Talukdar [67] used Curvature Damage Factor for damage detection of continuous bridges containing damaged parts at different locations. They evaluated changes in natural frequencies, modes shapes and curvature mode shapes. The results illustrated that considering curvature of the mode shapes will provide a stronger method for damage location compared to the mode shapes. They also showed that besides the choice of the modes as a very important fact, adequate numbers of modes are needed for multiple damage locations.

2.1.7 Modal Strain Energy

A damage detection technique based on modal strain energy between two structural degrees of freedom was proposed by Stubbs et al. [68], [69]. They also presented a formula based on fractional strain energies for the i^{th} mode of the undamaged and damaged structures for a Bernoulli-Euler beam.

Alvandi and Cremona [70] also used the strain energy method for damage detection on different civil engineering structures with experimental data. They showed that the strain energy method is more efficient than changes in flexibility, change in mode shape curvature, and change in flexibility curvature that will be discussed later. However, the modes strain energy was also performed by Parloo et al. [63] for the identification of various damages on the I-40 highway bridge in New Mexico, and the results showed that the method does not provide a robust detection of small damage due to noise in the environment.

2.1.8 Changes in Dynamic Flexibility

The dynamic flexibility matrix can be used as a damage detection method in the static behavior of the structure [73]. The dynamic flexibility matrix G is defined as the inverse of the static stiffness matrix. By only keeping the first few modes of the structure, the expression of the flexibility matrix can be approximated by equation 2.2.

$$G=\sum_{i=1}^{n} \frac{1}{\omega_i^2} \phi_i \phi_i^T \quad (2.2)$$

where ω_i is the i^{th} resonant frequency of the structure, ϕ is the mode shape matrix, and ϕ_i defines the i^{th} mode shape. Each column of the flexibility matrix represents the displacement pattern of the structure associated with a unit force applied at the associated degree of freedom. Any small changes in the lower order modes will cause a highly evolutions of the dynamic flexibility matrix due to the inverse relation to the square of the resonant frequencies ω_i [71]. The variation matrix

is defined as changes in the flexibility matrices of undamaged and damaged structures ($\Delta G = G_{damaged} - G_{undamaged}$) such that the maximum variation corresponds to the damage location [71].

Unity check method was proposed by Lin [72] for damage location in structures. This method was presented earlier by Lin [73] for location of modeling errors using modal test data. The error matrix can be defined as equation 2.3.

$$E=GK_{undamaged}-I \quad (2.3)$$

where G is the dynamic flexibility matrix of the damaged structure, $K_{undamaged}$ is the structural stiffness matrix of the undamaged structure, and I is an identity matrix which is a square matrix in which all the elements of the principal diagonal are ones and all other elements are zeros. The error matrix is going to be zero when no damage occurred in the structure. The highest peak of the plots of the stiffness error matrix E shows the damage location. According to Gysin [74], the number of modes used to derive the stiffness error matrix will significantly affect the accuracy of the flexibility matrix method.

Park et al. [75], extending the error stiffness matrix, developed a method using weighted error matrix that magnifies the value of the stiffness error at the location of the damage in the structure. They also showed that weighted error matrix will provide a more powerful method for damage location identification.

Aktan et al. [76] concluded that dynamic flexibility change can be a suitable indicator for damage detection of bridges. Mayes [77] also used the dynamic flexibility for damage detection of I-40 bridge over Rio Grande. Park et al. [78] showed that damage can be correctly located and detected using the flexibility matrix in ten-story building, a bridge and an engine structure. Topole [81] evaluated sensitivity of dynamic flexibility matrix by performing various damage scenarios

such as multiple damages at joints. He showed that this technique works well for damage locating and of a simple damage but not for multiples damages.

2.1.9 Sensitivity-Based Approach

The sensibility-based approach is a method for damage detection that involves the mode shapes of the damaged and undamaged structures as well as the natural frequencies of the undamaged modes. This technique determines the damage location using mode shape sensitivities to changes in stiffness or/and changes in mass in structural degree of freedom and the equation is provided in reference [79].

Considering a limited number of modes to compute the sensitivity factors will provide a good approximation compared to when all modes are taken into consideration. Also, because of noise measurement, using mass sensitivities will be more stable than calculating stiffness sensitivities.

The mode shape sensitivities was compared with various damage indicators such as the modal flexibility change method, the mode shape curvature changes and the strain energy method by Parloo et al. [63]. The investigations were conducted using experimental data on a clamped board and the I-40 highway bridge in New Mexico. The results showed that the sensitivity-based approach is the most efficient damage assessment technique, and even when damage is very small, this technique detects the damage precisely, however, presence of noise in real situation will cause the method to be less efficient.

2.1.10 Changes in Antiresonances

The resonance frequencies of the system at the excitation points in the excitation directions are called antiresonance frequencies [80]. Physical interpretation of the phenomenon of antiresonances can be performed for damage detection and localization in complex structures

because damage significantly affects this phenomenon. It should be noted that the resonances and antiresonances will repeatedly change the Frequency Response Function of the point where the response co-ordinate and the excitation co-ordinate are identical [71]. Meanwhile, according to Wahl et al. [81], when the distance between the excitation coordinate and the response coordinate increases, the number of antiresonance ranges decreases.

Bamnios et al. [86] through analytically and experimentally studies, investigated the effect of damage on the mechanical impedance of different Plexiglas beams with different boundary conditions damaged in several locations and with different severity. They demonstrated that the driving-point impedance changes due to the damage in case of flexural vibrations. They also showed that the slope of the curve of the changes increases considerably in the first antiresonances near the damage. When damage severity increases, the jump will be increased as well which helps determine the damage location.

Douka et al. [82] evaluated changes in antiresonances in double-cracked beams, and as expected based on previous studies discussed above, they indicated that depending upon the damage severity and location, a jump occurs in the antiresonances of the damaged structure. However, because there were two cracks, there were also two jumps in the slope of the curve of the changes in the first resonances. Also, each slope was computed near each damage. However, they indicated that small changes in the slope of the antiresonance curve is hard to be estimated that makes the proposed method based on changes in antiresonances inefficient for small damage. Conducting experiments on a free-free beam with open cracks, Dharmaraju and Sinha [83] confirmed the previous claims that the crack location identification using the change in antiresonance is not efficient.

2.2. Changes in Frequency Response Function

Another methodology for damage detection is using Frequency Response Function (FRF). The theoretical description of FRF can be explained as follows [71]:

The equation of motion for any structure can be presented by equation 2.4:

$$M\ddot{x}+C\dot{x}+Kx=f(t) \quad (2.4)$$

where M, K and C are the mass, stiffness and damping matrices. f(t) is the vector applied to the structure, and dot is the derivative with respect to the time. x is the vector of nodal degrees of freedom of the structure. t defines the time instant.

For harmonic excitation, the force vector can be defined as equation 2.5:

$$F(t)= Fe^{i\omega t} \quad (2.5)$$

where ω is the frequency of the force, and F defines the force amplitude vector. Therefore, the response vector can be written as equation 2.6:

$$x(t)= Xe^{i\omega t} \quad (2.6)$$

So, the equation of motion can be written as equation 2.7:

$$(-\omega^2M+ i\omega C +K)\, X = F \quad (2.7)$$

Consequently, the relation between the response X(ω) and the excitation F(ω) at each frequency ω is given by equation 2.8:

$$X(\omega) = H(\omega)F(\omega) \quad (2.8)$$

where H(ω) defines the receptance matrix of the system or the Frequency Response Function matrix that is given by equation 2.9:

$$(-\omega^2M+ i\omega C +K)^{-1} = H(\omega) \quad (2.9)$$

The relation between the response at the i^{th} co-ordinate with a single excitation applied at the j^{th} coordinate defines the individual Frequency Response Function H_{ij} (ω) that is

given by equation 2.10:

$$H_{ij}(\omega) = X_i / F_j \quad (2.10)$$

with $F_n = 0$ for n = 1, . . ., m and $n \neq j$ (m is the total number of degree-of-freedom). It may be noted that Operational Deflection Shape (ODS) that describes the normalized structure shape at each frequency ω is given by the column vector of matrix $H_j(\omega)$.

2.2.1 Extension of the MAC Criteria for the Frequency Response Function

When any damage occurs in the structure, the stiffness and the damping of the structure will change so, the receptance matrix of the damaged structure $H^{damaged}_{ij}(\omega)$ that is function of stiffness and damping will also change. In the following, some of the studies that propose different indicators that are a function of the receptance matrix of the damaged and undamaged structures are provided. As an extension of the MAC criteria in the frequency domain, Heylen and Lammens [84] proposed an indicator named Frequency Response Assurance Criterion (FRAC). According to this method, the values of FRAC varies between zero to unity. The FRAC value of unity means no damage is found. The more damage in the structure, the smaller value of FRAC.

Zang et al. [85], [86] proposed the first Global Shape Correlation function (GSC) to detect damage in structure. The GCS (ω) gives a real value between zero to unity such that when the value GCS (ω) is not equal to one, damage is detected. Then Zang et al. [85], [86] proposed the second Global Amplitude Correlation function (GAC) based on response amplitudes. The GAC indicator is provided in these references [85], [86]. They also proposed the averaged integration of first Global Shape Correlation function (AIGSC) and the second Global Amplitude Correlation function (AIGAC). The AIGSC and AIGAC indicators are also real constants between zero to unity to determine if the structure is damaged or undamaged. The authors investigated these various indicators to a bookshelf structure with various case of damage, including location and

level for single or multiple presence of damage. They concluded that all the correlation criteria are able to detect the damaged structures [71].

2.3. Coupling Responses Measurements

Knowing that damage decreases the stiffness of structure at the location of the damage, the equation of motion can be written as equation 2.11:

$$M\ddot{x}+C\dot{x}+\tilde{K}x=f(t) \tag{2.11}$$

where $\tilde{K}$ is the global stiffness matrix of the structure containing the stiffness reduction of the crack at the location of the damage. So, for a harmonic force f(t), equation 2.7 can be written as equation 2.12:

$$(-\omega^2M+ i\omega C +\tilde{K})\ X = F \tag{2.12}$$

Knowing that the damage creates a stiffness matrix K_{crack} at the damage location, the equation of motion can be defined as equation 2.13:

$$(-\omega^2M+ i\omega C +K)\begin{bmatrix} X^c \\ X^{uc} \end{bmatrix}=F-F_c=\begin{bmatrix} F^c \\ F^{uc} \end{bmatrix}-\begin{bmatrix} F_c^c \\ 0 \end{bmatrix} \tag{2.13}$$

where K defines the stiffness matrix of the undamaged structure. The subscripts *c* and *uc* represent the cracked and uncracked elements, respectively. F contains the external force vector, and F_c represents the force vector only due to the contribution of the crack.

This concept has been used by many researchers.

2.3.1 Applications for Damage Detection in Practical Cases

Gounaris et al. [87] used coupled response measurements method for damage identification of structures. To identify the severity and the location of a transverse crack, one needs to dynamically excite the beam and to measure the response of the structure in two directions at a point on the beam. According to the authors of this paper [87], displacement measurement in one

direction while the beam is excited in another direction helps to detect the damage. The authors believe that the main advantage of this method is its efficiency even for small cracks.

Liu et al. [88], through analytical and experimental studies, evaluated a hollow section structure in free-free boundary conditions using coupled response measurements (lateral and axial responses). In the uncracked beam, lateral or axial force only excite the corresponding bending or axial modes. However, in the damaged structure, there is an extra peak in the bending direction near the undamaged axial natural frequency. They finally concluded that this method is a very good indicator for damage detection.

Chasalevris and Papadopoulos [89] used the coupled bending vibrations to identify two cracks of a stationary shaft. They considered the case of bending vibrations caused by a vertical excitation. They showed that the relative angular position of the cracks as well as their severity will affect this method's efficiency.

Lee et al. [90] used the coupling measurements in Frequency Response Function for damage detection. The structures used were a cantilever beam and a simply-supported beam.

The previous criteria and methodologies that are based on linear measurements can be used for damage detection of rotary machinery. But, these methods should be used during static condition of rotor that makes the process time-consuming in practical engineering. However, the application of coupling measurements for identification of open cracks has been already extended by some researchers. As far as damage detection of rotating shafts is not what civil engineers are usually concern about, some limited examples are provided in the following.

Papadopoulos and Dimaragonas [91] investigated the coupling of longitudinal and bending vibrations of a rotating shaft with a transverse crack. They also evaluated the effects of the bending vibration on the torsional vibration spectrum [92]. They finally concluded that coupling between

bending and torsion, bending and tension, and the general vibration coupling can be very efficient for rotor crack detection [93]. There are some other researches in this regard, and readers can find them in these references [94], [95].

Chapter 3 - The Proposed Approach and Procedure

In this chapter, the proposed novel random-vibration-based approach using ambient vibration for damage identification of the structures is explained in detail [96], [97]. This chapter is divided into two main sections: obtaining the free-vibration response called pseudo-free-vibration that is explained in section 3.1, and the procedure for damage detection explained in section 3.2. According to this procedure, the pseudo-free-vibration response should be transferred into frequency domain using FFT and the changes in structural frequencies should be used for detection of changes in the dynamic properties of the structure. The frequency with the maximum intensity in frequency domain of the structure (fundamental frequency) should be followed to detect changes in the stiffness of the structure.

3.1 The Proposed Approach to Extract the Pseudo-Free-Vibration Response

This section describes the proposed approach to extract the pseudo-free-vibration response of the structure implemented in a MATLAB software. Figure 3.1 depicts an example of the response of the structure physical model subjected to an ambient vibration as recorded during an experiment, with the very initial part of that signal amplified as shown in Figure 3.2.

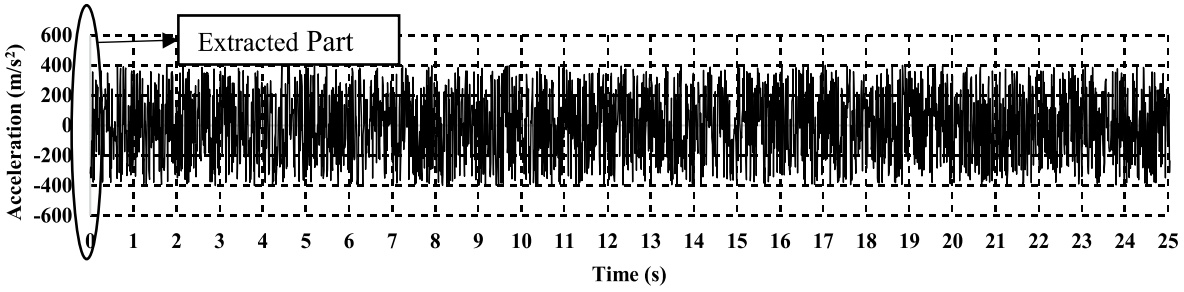

Figure 3.1 A sampled acceleration-time response

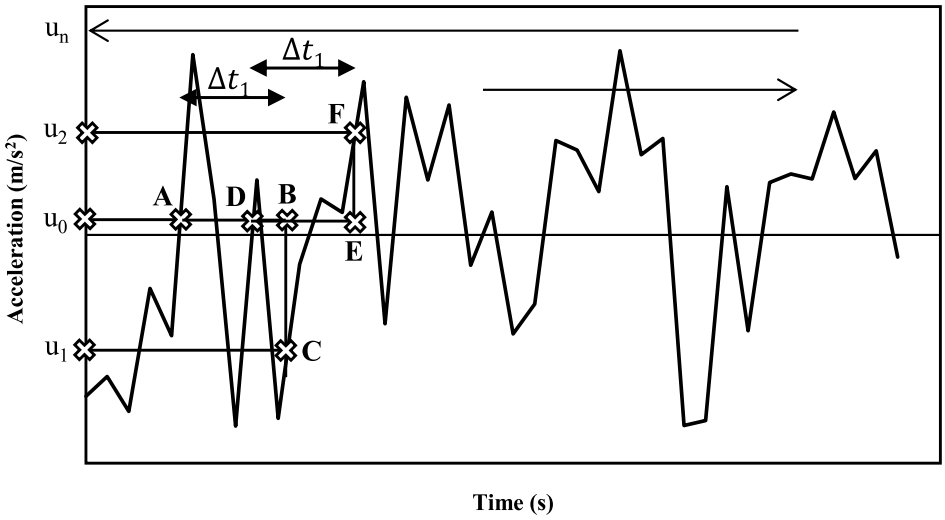

Figure 3.2 The extracted part shown in Figure 3.1

According to the proposed approach, the following steps should be used to extract the pseudo-free-vibration response:

1. An initial value of the acceleration (u_0) should be carefully chosen so that the horizontal line intersects as many points as possible on the signal curve. The author recommends a value of 1/10 of the maximum acceleration in the acceleration-time response.
2. When the horizontal line intersects the signal curve for the first time (point A in Figure 3.2), the horizontal line should be extended as much as Δt_1 to reach point B shown in the figure. Note that Δt_1 should be carefully selected. The author recommends a small value for Δt_1 (in this study, Δt_1=0.5% of the total duration of the acceleration signal) because according to the following steps, such a time step provides enough points for obtaining the pseudo-free-vibration response of the structure. Typically, one would start with a small value and then increase it to larger values later. These values, especially the largest, and the rate of increase should be carefully selected, since they would affect the large and/or small periods extracted.

3. Then, wherever the length of Δt_1 ends, a vertical line should be extended up or down till it intersects the curve at point C shown in Figure 3.2. The value of this point on the acceleration axis will be the second acceleration value (u_1).
4. In the next step, from point A, the horizontal line needs to be extended till intersects the curve (point D in Figure 3.2). If point A is on an ascending line, the extended line should intersect the curve in an ascending line otherwise it should intersect the curve in a descending line.
5. Then, from point D, the horizontal line should be extended as much as Δt_1 till it gets point E, and another acceleration value (u_2) can be obtained using the procedure explained in Step 4.
6. The procedure in Steps 4 and 5 should be repeated till the end of the curve such that the final acceleration value will be (u_n).
7. Steps 2 to 6 should be repeated with different values of (Δt). These values will be denoted as Δt_2, Δt_3…, Δt_m, where $\Delta t_2 = 2 \times \Delta t_1$, $\Delta t_3 = 3 \times \Delta t_1$…, $\Delta t_m = m \times \Delta t_1$, with Δt_m being the value of Δt in the last iteration.
8. As the final step, required points for drawing the pseudo-free-vibration response diagram are created such that (X_m, Y_m) = Δt_m, Um=$\frac{u_1+u_2+u_3+\cdots+u_n}{n}$) where n is the number of extracted acceleration values and m is the number of points in the resulting pseudo-free-vibration response diagram. The MATLAB code used for extracting pseudo-free-vibration response is provided in Appendix C.

3.2 The Procedure for Damage Detection

The approach described in the preceding section is used to generate the pseudo-free-vibration response of the system with time on the x-axis and acceleration on the y-axis. After extracting the

pseudo-free-vibration response (in the time domain) from the response of structure to random excitation for each system configuration, a Fast Fourier Transform (FFT) is applied to transform it to the frequency domain. The frequency with the largest intensity which is the fundamental frequency of the structure is traced to be used for damage detection. The following flowchart, Figure 3.3, shows all steps required to pass from extracting the acceleration versus time response to damage detection.

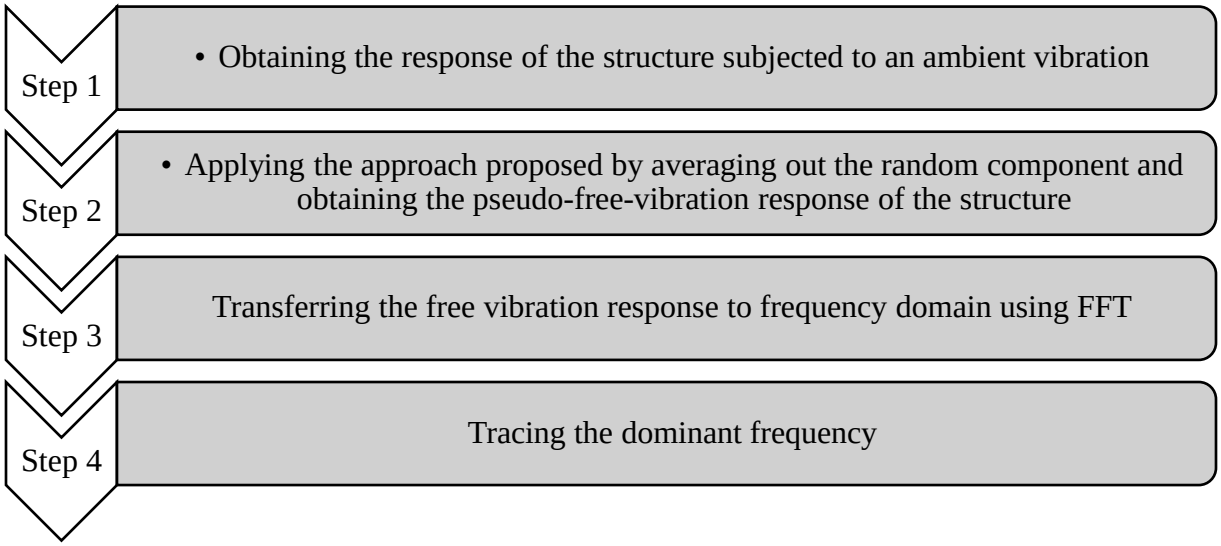

Figure 3.3 All steps required to pass for damage detection

Chapter 4 - Geometry, Material, and Modeling

In this study, besides an analytical verification using Newmark's linear acceleration method for the approach explained in chapter 3, two steel portal frames with different flexural stiffness were made in the steel workshop of the structural laboratory for an experimental study. These structures were also numerically modeled using ABAQUS. In this section, the geometry, material for all three studies including analytical, numerical, and experimental are explained in detail.

4.1 Analytical Model

This study, using a simple analytical example, verifies the capability of the proposed novel approach for extracting of the pseudo-free-vibration response of the structures explained in chapter 3. To prove that, a single degree of freedom system (m = 44.36 kg, c = 0, k = 1751.27 N/m), shown in Figure 4.1, was considered. Using Newmark's linear acceleration method introduced as the most precise analytical method of linear response of single degree of freedom systems [98], the free-vibration response of the system was obtained. To extract the free-vibration response using Newmark's linear acceleration method, time steps, p(t), initial displacement and initial velocity are taken as 0.1 sec, 0, 0, and -0.0012 m/sec respectively. To generate ambient vibration, rand function is Excel is used that generates numbers between 0 and 1. The results of the analytical study are presented in chapter 5.

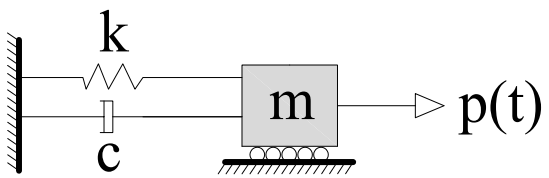

Figure 4.1 The considered single degree of freedom system (m=44.36 kg, c=0, k=1751.27 N/m)

4.2 Numerical Models

Two one-story steel portal frames were numerically simulated using ABAQUS software [99] to evaluate the capability of the approach proposed in chapter 3. In these structures, all beam-to-column connections are assumed to be fixed using thick angles; thus, there are three degrees of freedom for each structure. Steel material (ST37) is assumed to be elastic-perfectly plastic with yield strength and ultimate strain of F_y=240 MPa and ε_u=0.35, respectively [100]. The modulus of elasticity and the Poisson's ratio of steel used are *E*=200 GPa and υ=0.3, respectively. The geometrical characteristics of the structures are presented in Figure 4.2 and 4.3, and as it can be clearly observed, the only difference between these two structures is their column heights.

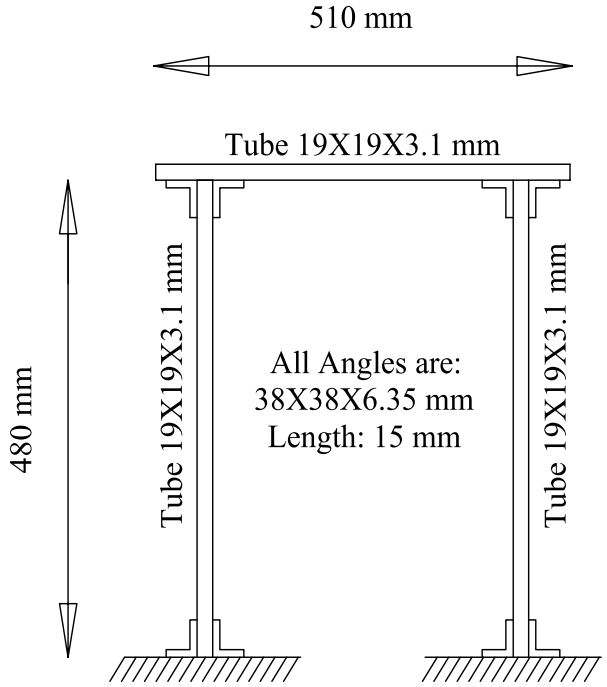

Figure 4.2 Geometrical characteristics of structure one

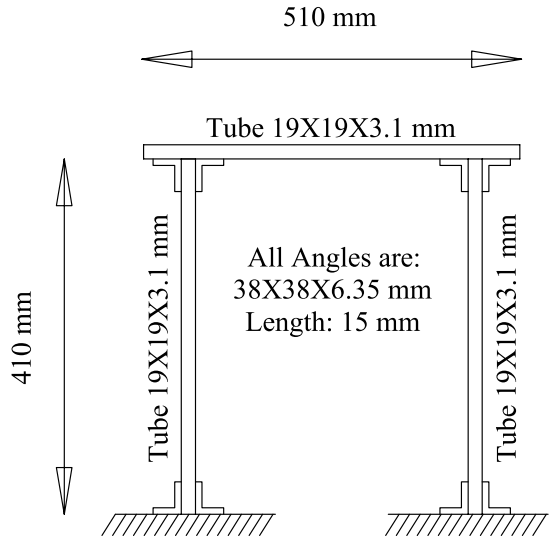

Figure 4.3 Geometrical characteristics of structure two

It should be noted that each structure has been analyzed under three different dynamic loads (denoted dynamic load one, two, and three). These dynamic loads were applied to a random point on one of the columns, and the responses of the structures were extracted from a point at the top right of the structures. Meanwhile, the dynamic loads were generated using "rand" function in Excel software which can produce random numbers between zero and one, and the maximum magnitude of each dynamic load is set to be 0.1 Newton. Each of these dynamic loads has a one-second time period with a time step equal to 0.001 second.

4.3 Experimental Models

To verify the results extracted from the numerical study, physical models for structures one and two were constructed in the laboratory of civil engineering department at Kansas State University such that all geometrical characteristics were exactly the same as what had been considered for the numerical models shown in Figure 4.2 and 4.3. As seen in Figure 4.4, the beams were connected to the columns with thick angles, and all connections were bolted except the supports which were welded. Also, the structures were tightened to the ground using clamps, so

they could not move while they are under the load. Also, to ensure that the connections are fixed, two completely tightened bolts were used in each leg of the thick angles.

The structures were analyzed under three three-second-long dynamic loads. To achieve the random vibrations, for each single dynamic load, different tools like a hammer, a piece of wood, and a metal object were used to hit, and the number of hits and the hits locations and the hits powers were not the same so that the dynamic loads may be considered causing random vibration. Furthermore, to obtain acceleration-time records corresponding to those from the numerical models in ABAQUS, the accelerometer was installed at the top right of the structures. The accelerometer used was a wire-less G-link that sends the signals to a base station as shown in Figure 4.4b which is then connected to a computer that records the response of the structure a with a sampling rate of 2048 times per second.

a) Experimental structures one and two

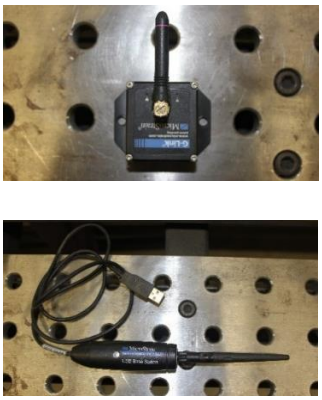

b) The accelerometer used and base station

Figure 4.4 The experimental structures one and two and the accelerometer

4.4 Modeling

In order to realize structural damage detection using signal-based pattern recognition, it is necessary to obtain in advance the vibration response of structure with different damage scenarios. Because it is nearly impossible to let a practical structure experience all kinds of damage, using numerical simulation is always a strong tool to evaluate the structure in different conditions. In this study, ABAQUS was used to simulate the physical model with different boundary condition configurations to obtain the ambient vibration response for each case. There is no doubt that using other types of finite element software should give the same results.

MATLAB software was also used to numerically implement the computational procedure presented in Chapter 3. Two computer codes were developed: The first is to extract the free vibration signal from the ambient vibration signal, and the second is to transform the signal from the time domain to the frequency domain. Both codes are combined and presented in Appendix C.

4.4.1 ABAQUS Software

In this section, the authors are going to explain all the key steps of simulating the structures in ABAQUS software. The structure shown in Figure 4.2 and 4.3 consists of eleven parts including two columns, one beam, and eight angles, and they are created as a 3D, deformable, and solid instance as shown in Figure 4.5.

As shown in Figures 4.6 and 4.7, the modulus of elasticity, the Poisson's ratio of steel, and density used are E=200 GPa, υ=0.3, and 7850 kg/m^3, respectively. Also, all the sections are defined as a solid, homogeneous sections shown in Figure 4.8.

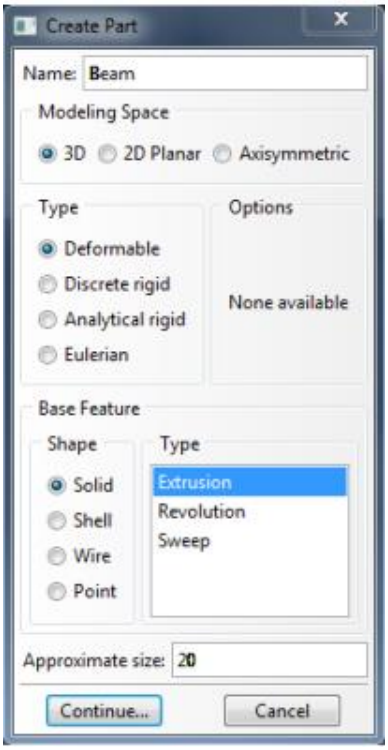

Figure 4.5 The instances characteristics

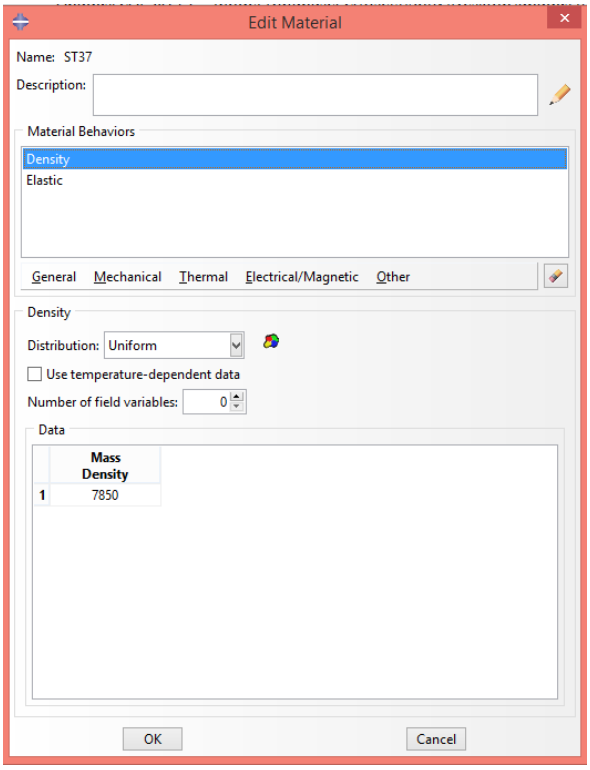

Figure 4.6 Defining of the modulus of elasticity and the Poisson's ratio of steel

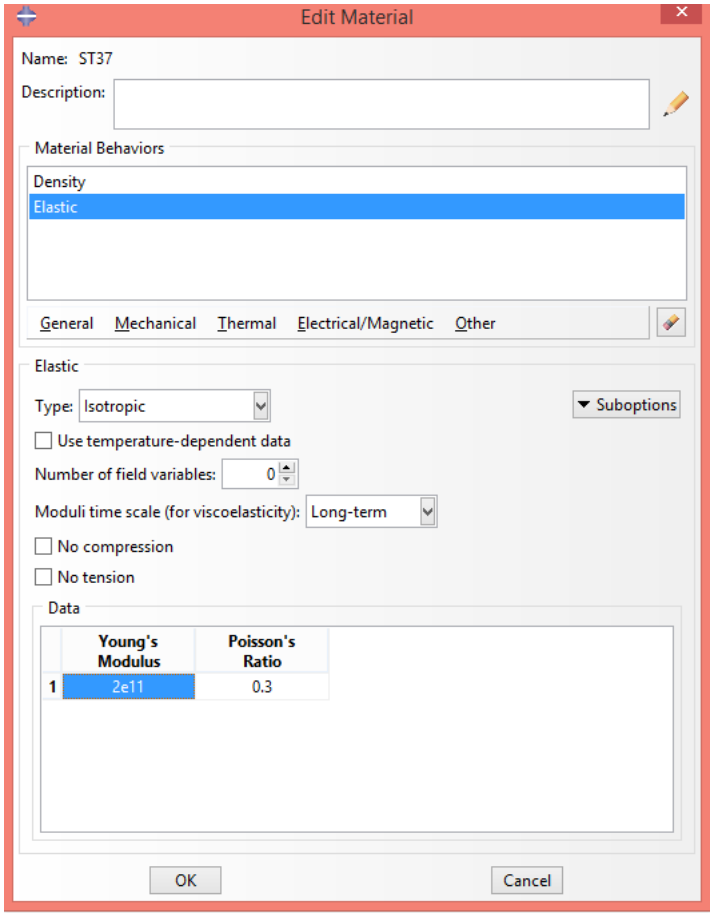

Figure 4.7 Defining of steel density

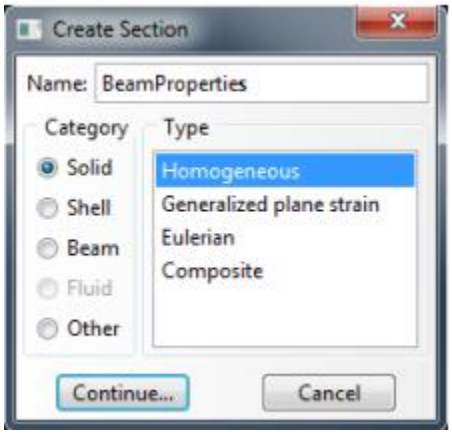

Figure 4.8 Defining of the section characteristics

As shown in Figure 4.9, all instances are independent, which helps to mesh each instance separately with different mesh sizes. To obtain the ambient response of the structure subjected to an ambient vibration, linear perturbation, modal dynamics is used, shown in Figure 4.10.

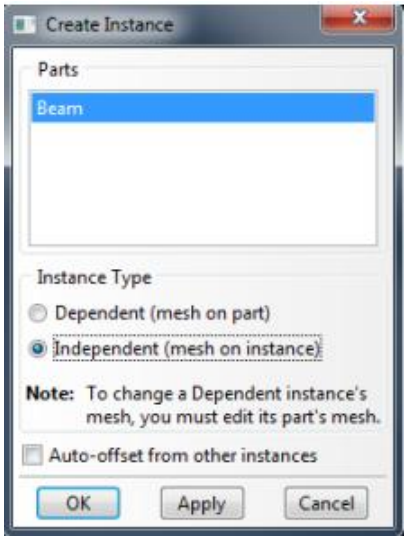

Figure 4.9 The independent instances

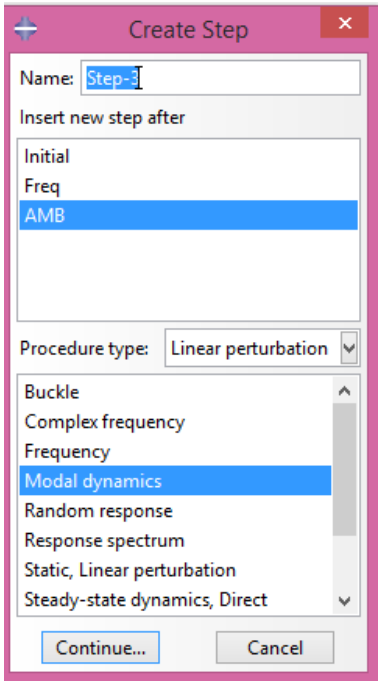

Figure 4.10 Using linear perturbation, modal dynamics analysis to obtain the ambient response of the structure

As shown in Figure 4.11, the supports are fixed. As far as the load direction applied to the structure is not in U2 direction, the structure will not move in U2 direction as well; thus, the supports are just fixed in U1 and U3, and UR3 directions.

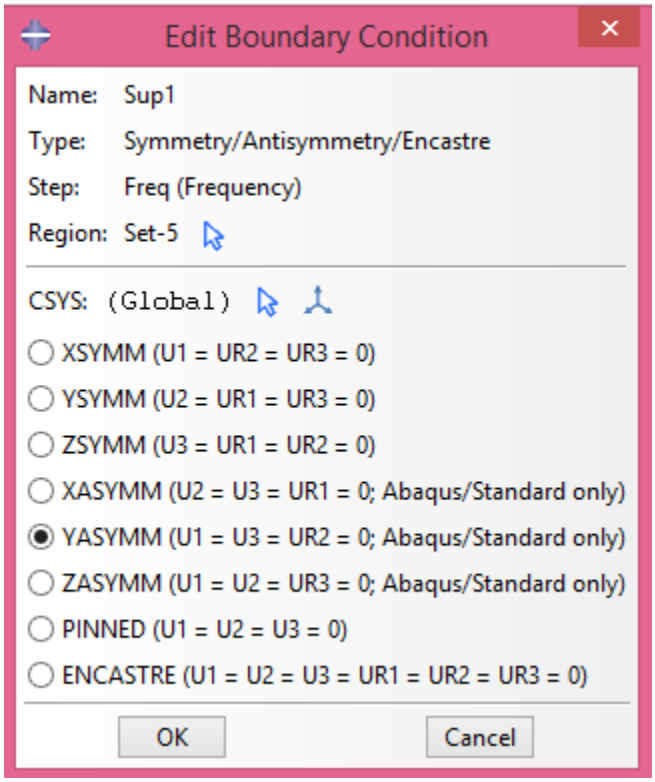

Figure 4.11 The fixed supports of the structures

According to Figure 4.12, the elements are 8-node linear brick, reduced integration, hour glass. The mesh sizes of the beams, columns, and angles of the numerical models are 1 cm, 1 cm, and 1 mm, respectively. The numerical model is presented in Figure 4.13 and 4.14.

As noted earlier, each structure has been analyzed under three different dynamic loads (denoted dynamic load one, two, and three). These dynamic loads were applied to a random point on one of the columns, and the responses of the structures were extracted from a point at the top right of the structures. Figure 4.15 shows an example of the actual random excitations applied to the structure.

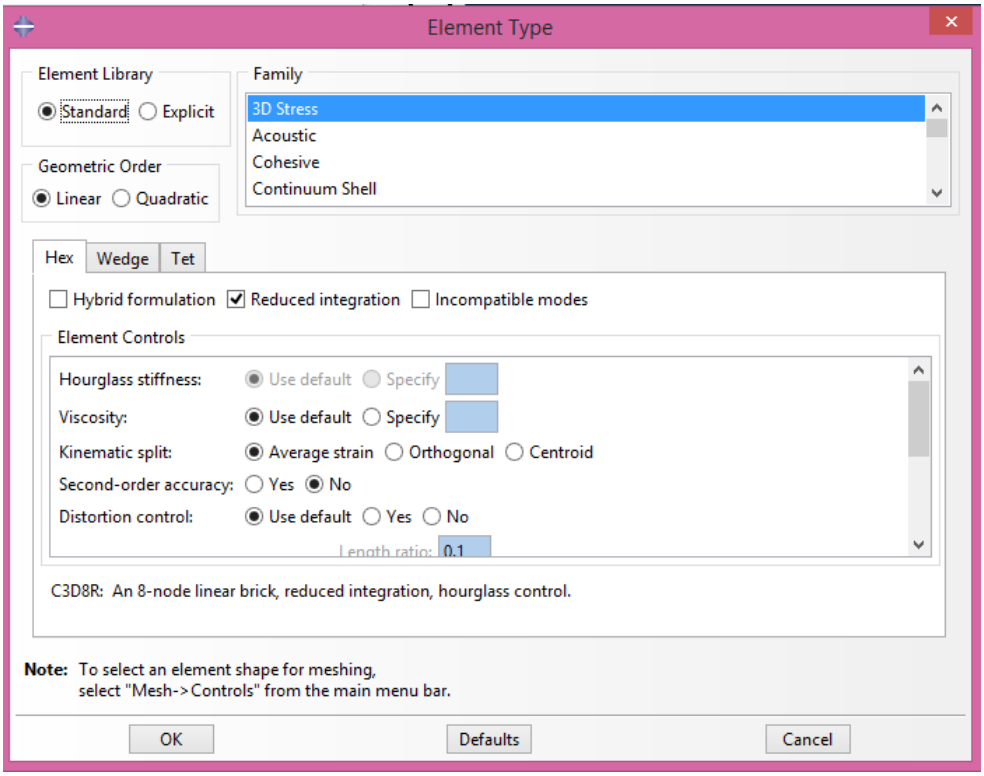

Figure 4.12 The elements properties

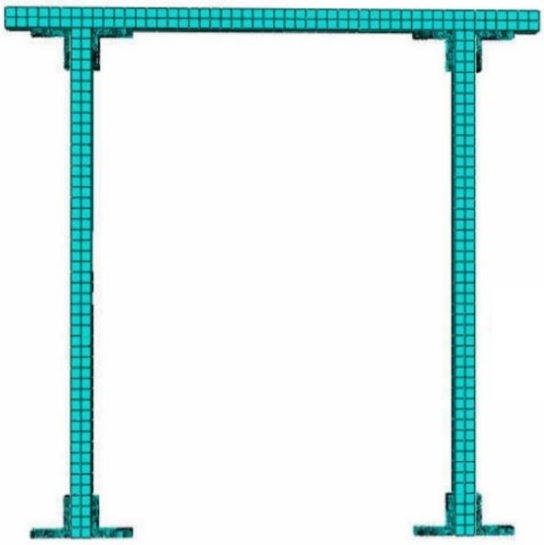

Figure 4.13 Views of the numerical model of structure one (Side view)

Figure 4.14 Views of the numerical model of structure one (Isometric view)

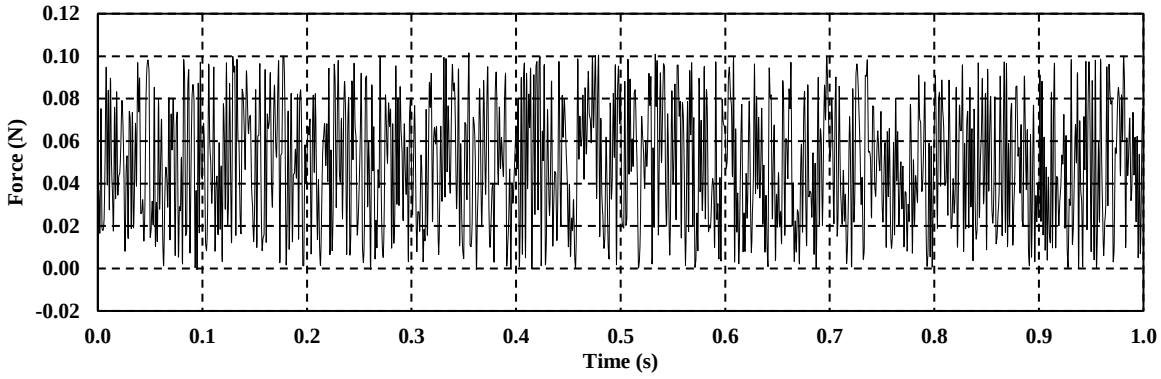

Figure 4.15 An example of the actual random excitations used

After the analysis (as shown in Figure 4.16), the ambient response of the structure will be obtained. Then, the ambient acceleration-time response is used to apply the proposed approach explained in chapter 3 on it to extract the pseudo-free-vibration response of the structure.

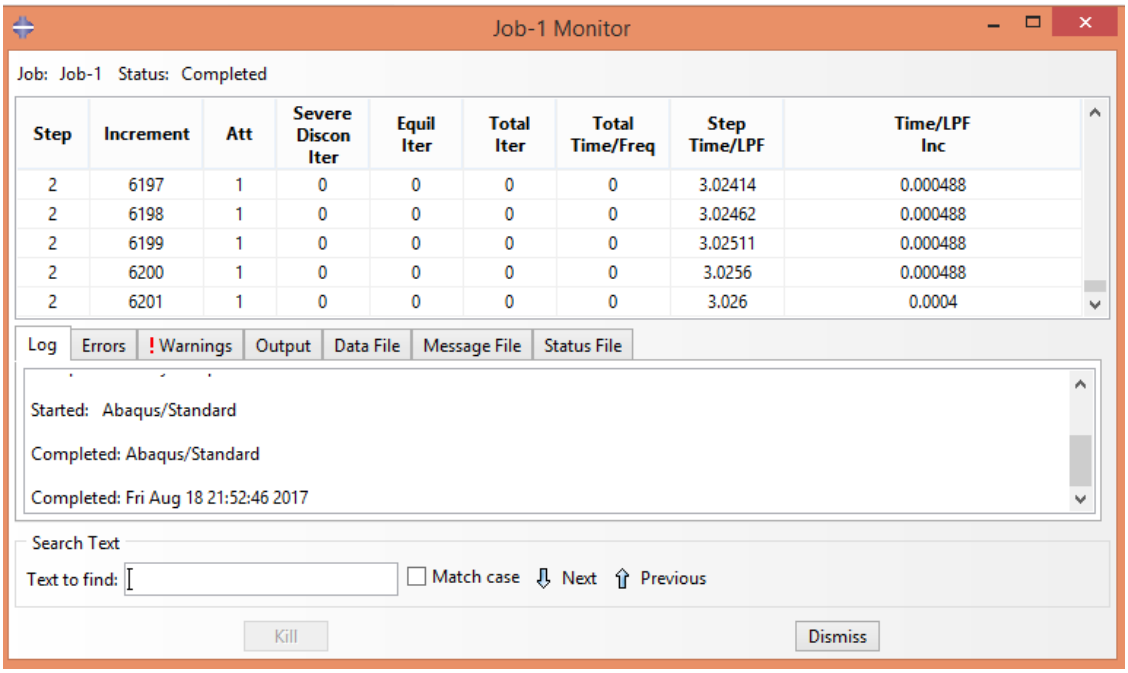

Figure 4.16 Job analysis in ABAQUS

4.4.2 MATLAB Software

Using the MATLAB code provided in Appendix C, the pseudo-free-vibration response of the ambient response obtained from the previous step will be extracted. Then, the pseudo-free-vibration response will be transferred to frequency-domain using FFT. This part of the code is also provided in Appendix C combined with the code provided for obtaining the pseudo-free-vibration response. In order to obtain the pseudo-free-vibration response as well as the diagram in frequency domain, one can simply introduce the acceleration-time response of the structure as matrix D, used in the MATLAB code; then, MATLAB code will automatically extract the pseudo-free-vibration response and FFT diagram. Then, the frequency with the maximum intensity in frequency domain which is fundamental frequency of the structure needs to be traced to detect changes in the stiffness of the structure.

Chapter 5 - Results

This chapter provides the results of the analytical (section 5.1), numerical (section 5.2), and experimental (section 5.5) studies to show the capability of the approach explained in chapter 3. Furthermore, a procedure is proposed to select the accurate values of u_0 and Δt_1 (section 5.3). Also, the effect of different damping ratios is investigated in section 5.4. In the final step (section 5.6), it is shown that the approach works for many different structures with different geometrical characteristics as well.

5.1 Analytical Study

This section, using a simple analytical example introduced in chapter 4, verifies the capability of the proposed novel approach for extracting of the pseudo-free-vibration response of the structures explained in chapter 3 using Newmark's linear acceleration method introduced as the most precise analytical method of linear response of single degree of freedom systems [98]; the free-vibration response of the system was obtained. To extract the free-vibration response using Newmark's linear acceleration method, time steps, p(t), initial displacement and initial velocity are taken as 0.1 sec, 0, 0, and -0.0012 m/sec, respectively. Then, solving the differential equation of the motion (P(t)=0) for the same structure, the exact free-vibration response of the system was also obtained and compared to Newmark's linear acceleration result. Time steps, p(t), initial displacement, and initial velocity are the same as in Newmark's linear acceleration method. Figure 5.1 shows how Newmark's method result is matched with the exact free-vibration response. Thus, in the next step, Newmark's linear acceleration method can be used to obtain the acceleration-time response of the system subjected to different ambient vibrations.

In the next step, using Newmark's linear acceleration method, the acceleration-time response of the structure subjected to five different ambient vibrations were extracted. The ambient vibrations, P(t), were generated using "rand" function in Excel software which can produce random numbers between zero and one. After obtaining the time-acceleration responses of the structures, their pseudo-free-vibrations were extracted using the MATLAB [101] code specially written to execute the 8-step procedure outlined in chapter 3.

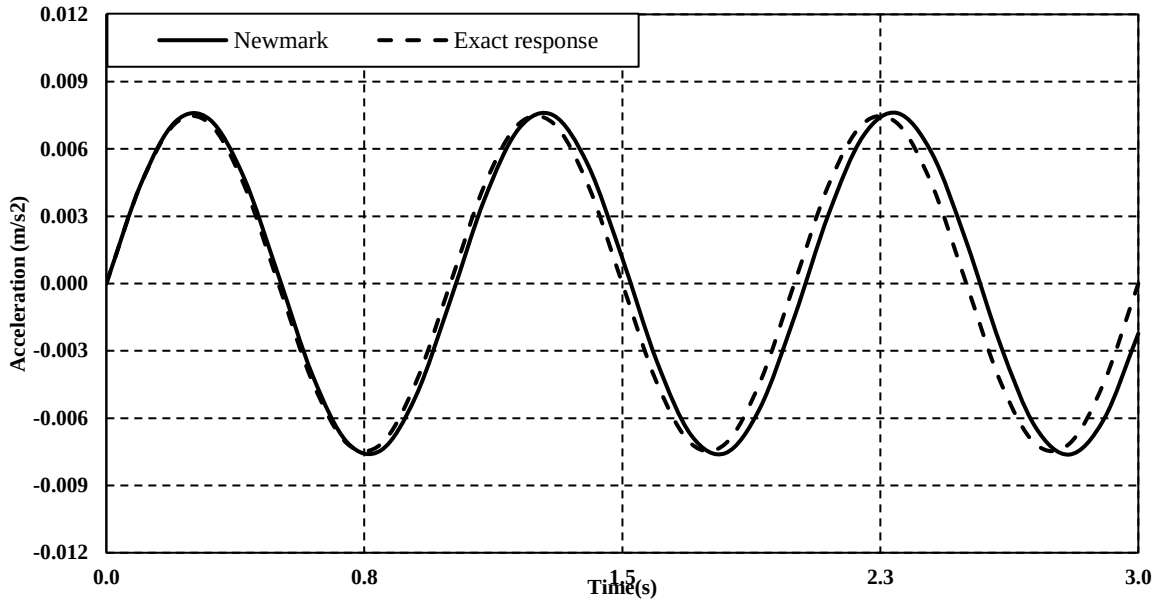

Figure 5.1 Comparing the free-vibration responses of the single degree of freedom system using two different methods namely Newmark's linear acceleration method and exact free-vibration

As Figure 5.2 shows, the pseudo-free-vibration responses are precisely matched with the exact solution shown in Figure 5.1. Meanwhile, Figure 5.2 shows that the proposed method for extracting the pseudo-free-vibration response of the structures works precisely. It should be noted that the magnitude of the pseudo-free-vibration responses depends on the magnitudes of the ambient vibrations applied on the structure such that the larger magnitude of the ambient vibrations, the larger magnitude of the pseudo-free-vibration responses.

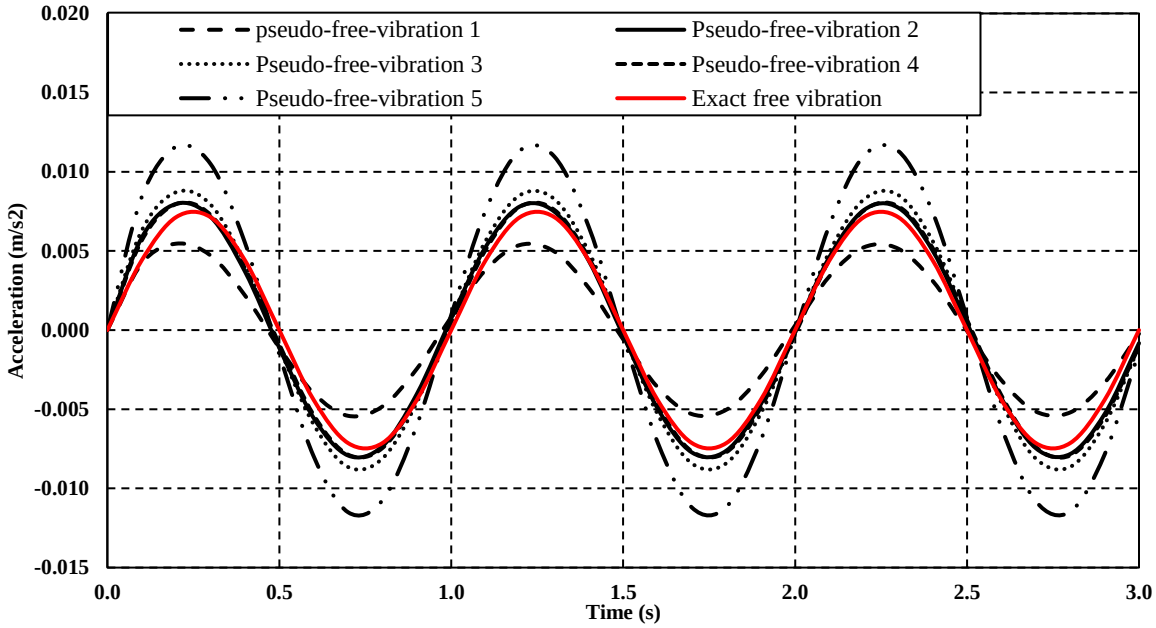

Figure 5.2 Comparing the pseudo-free-vibration responses of the single degree of freedom system with the exact free-vibration response

In the last step, the pseudo-free-vibration responses were transferred to the frequency domain using Fast Fourier Transform, and their fundamental frequencies were extracted. Figure 5.3 shows that although the ambient vibrations applied on the structure have been changed, as expected, the fundamental frequencies remained constant. As a result, regardless of the ambient vibrations applied, using the proposed method for extracting the pseudo-free-vibration response, the fundamental frequency of the single-degree of freedom structure will not be changed because the pseudo-free-vibration responses are perfectly similar to the exact-free-vibration response so that the pseudo-free-vibration responses will keep the fundamental frequency of the structure without any change.

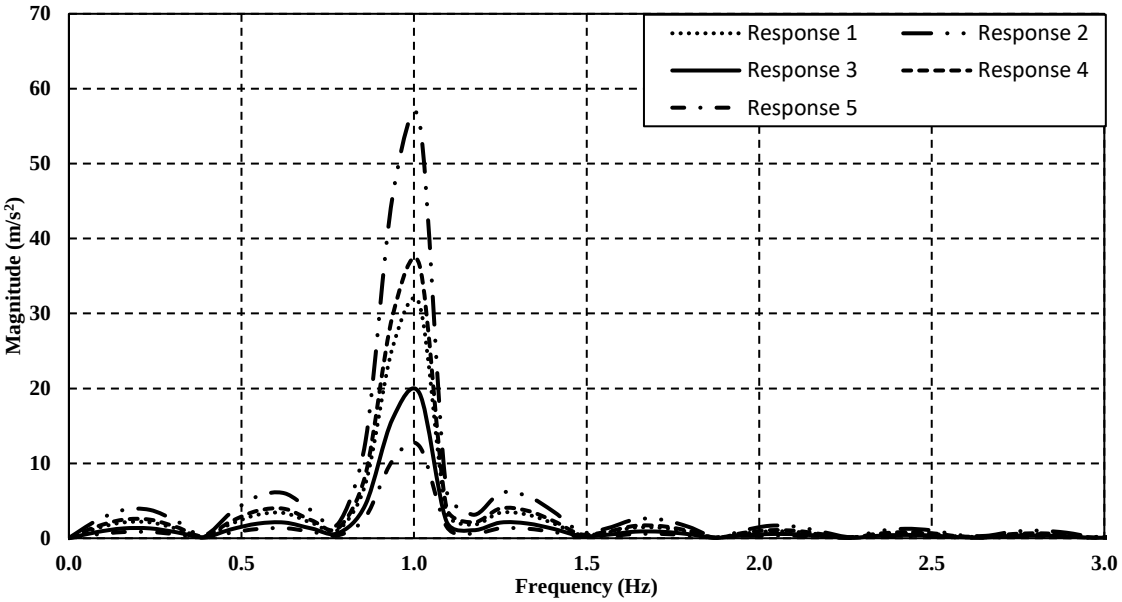

Figure 5.3 The natural frequency of the single degree of freedom system extracted using the 8-step MATLAB code

5.2 Numerical Study

Each structure, introduced in the previous chapter, has been analyzed under three different dynamic loads (denoted dynamic load one, two, and three). These dynamic loads were applied to the base of the structures as a ground acceleration, and the responses of the structures were extracted from a point at the top right of the structures. Meanwhile, the dynamic loads were generated using "rand" function in Excel software which can produce random numbers between zero and one, and the maximum magnitude of each dynamic load is set to be 0.1 Newton. Each of these dynamic loads has a one-second time period with a time step equal to 0.001 second.

Therefore, based on the aforementioned characteristics of the dynamic loads, such excitation can be considered a random vibration. After obtaining the time-acceleration responses of the structures using ABAQUS software with a sampling rate of 2048 times per second, their pseudo-free-vibration responses were extracted using the MATLAB code. Then, the pseudo-free-

vibration responses were transferred to the frequency domain using Fast Fourier Transform by averaging out the random component of the response and removing the particular solution. Both extracted pseudo-free-vibration response and frequency domain responses of structures one and two under dynamic load one are shown in Figures 5.4 through 5.7. As seen in Figures 5.5 and 5.7, the fundamental frequency in frequency domain using FFT for structures one and two are 24.2 and 31.3 Hz, respectively. It then can be concluded that structure two, which is stiffer than structure one, has a higher fundamental frequency. Consequently, if a structure has been damaged its stiffness will decrease and the fundamental frequency can be expected to decrease as well. Therefore, detecting a reduction of the fundamental frequency of a structure can be a sign of loss of stiffness possibly caused by damage. This procedure was repeated for structures one and two after dynamic loads two and three have been applied to them. The results shown in Figure 5.8 reveal that although the dynamic loads have been changed, the fundamental frequencies of the structures one and two remained constant. Indeed, using the proposed random-vibration-based approach, the fundamental frequency in frequency domain obtained using Fast Fourier Transform will remain constant for each single structure with the same geometrical characteristics even if the applied dynamic loads are different. This shows that the procedure proposed for extracting pseudo-free-vibration response works precisely.

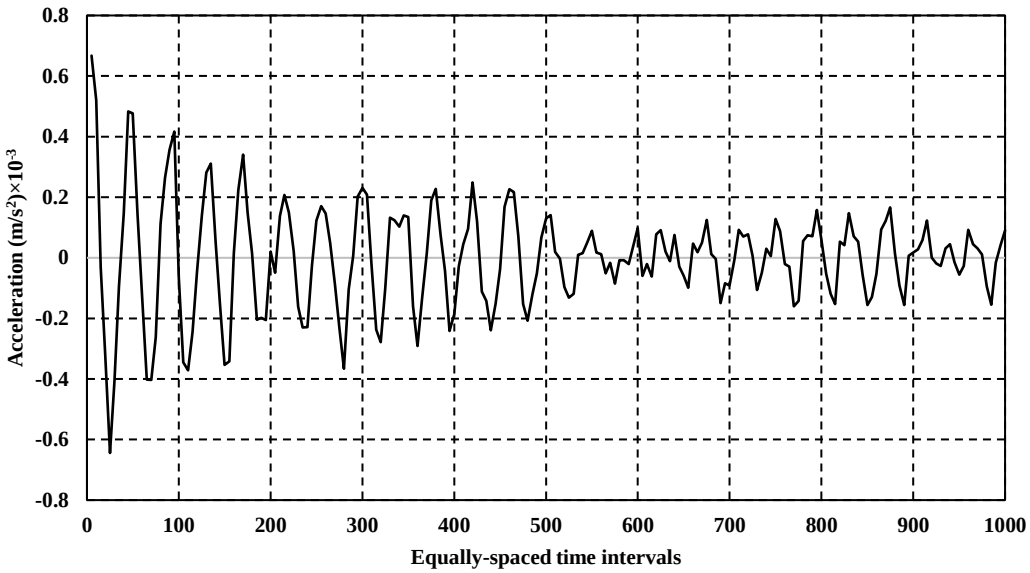

Figure 5.4 Signal processing results of structure one subjected to dynamic load one (pseudo-free-vibration response diagram)

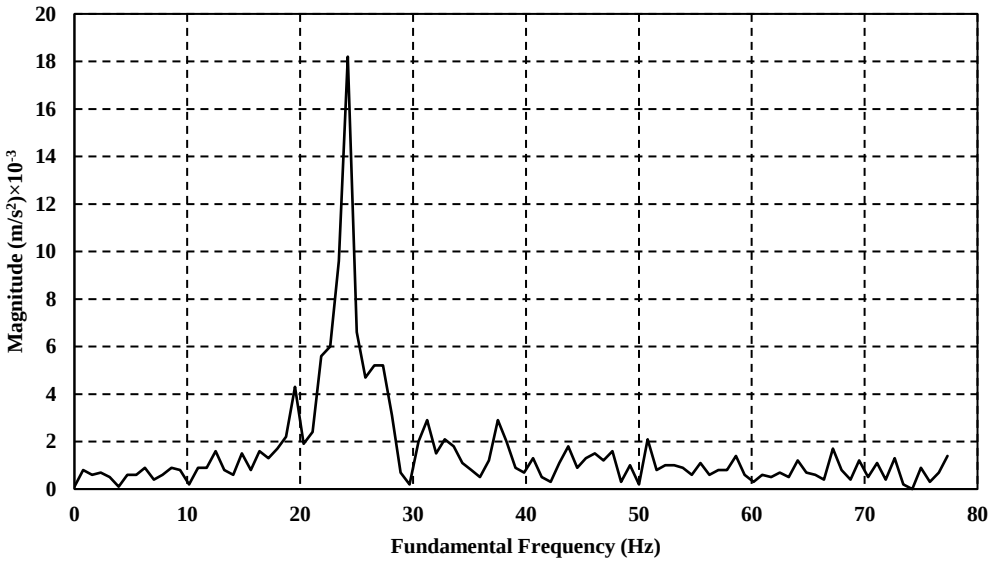

Figure 5.5 Signal processing results of structure one subjected to dynamic load one (FFT diagram)

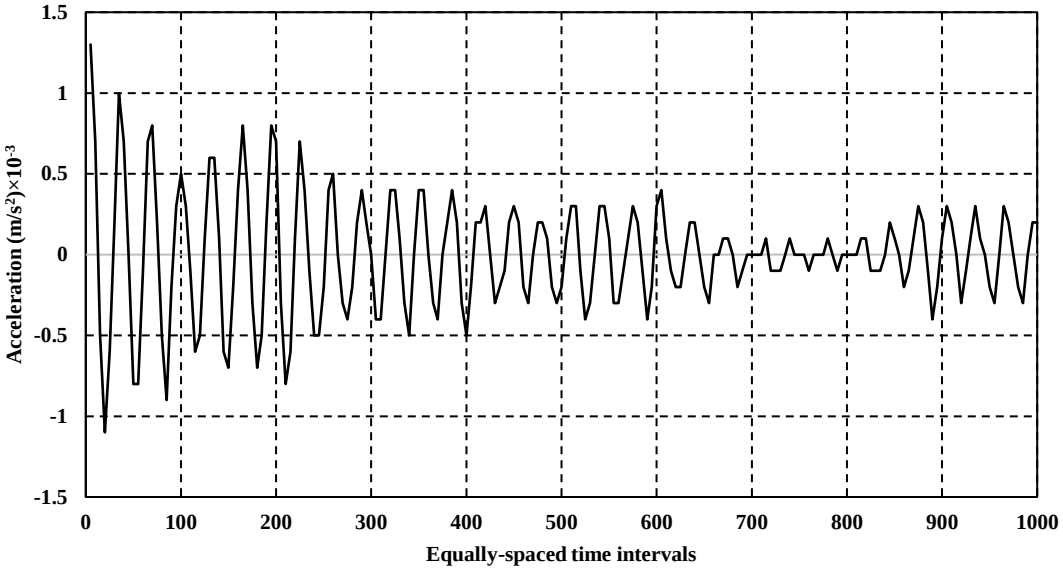

Figure 5.6 Signal processing results of structure two subjected to dynamic load one (pseudo-free-vibration response diagram)

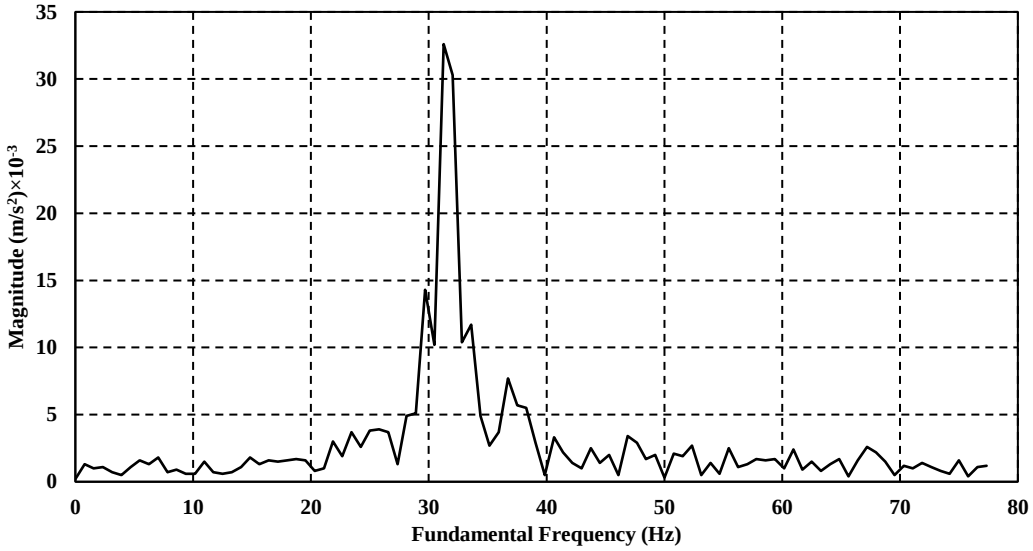

Figure 5.7 Signal processing results of structure two subjected to dynamic load one (FFT diagram)

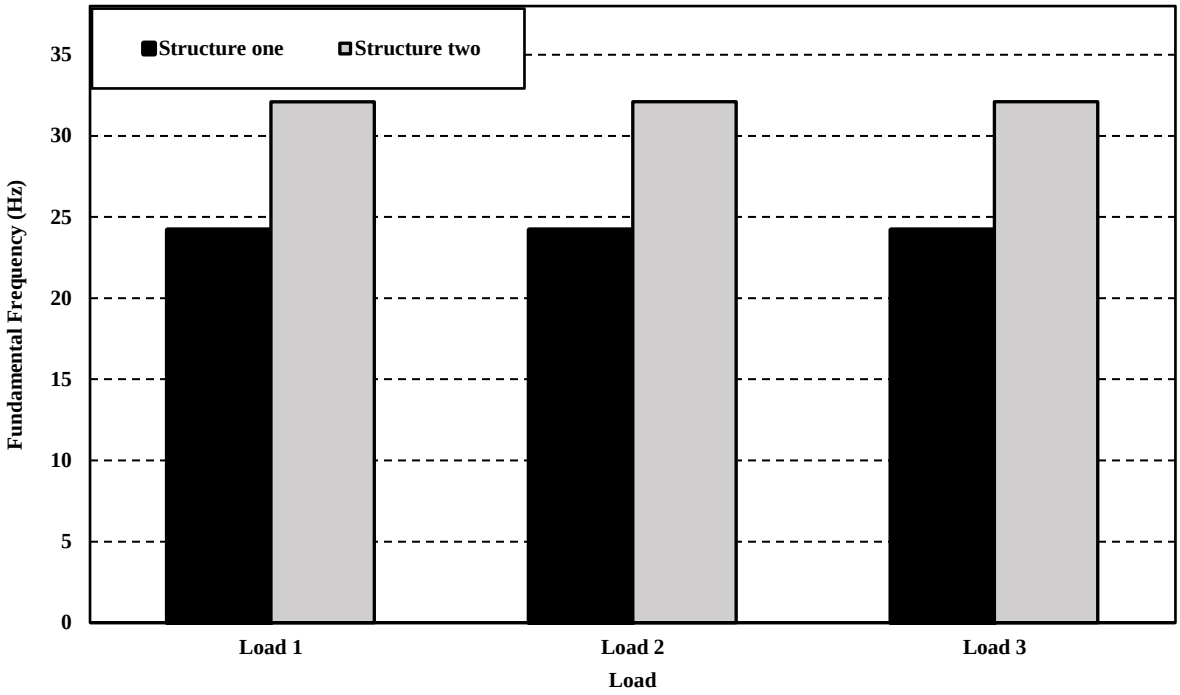

Figure 5.8 Comparison of the fundamental frequency of the numerical results of structures one and two subjected to dynamic loads one, two and three

5.3 A proposed procedure to determine the exact values of u_0 and Δt_1

The values of u_0 and Δt_1 are of utmost importance in obtaining accurate results using the proposed approach explained in chapter 3 such that if large values of u_0 and Δt_1 are selected, one might obtain completely incorrect results. The general approach first used to select the suitable values of u_0 and Δt_1 required to find the accurate results is a trial and error approach. In this regard, for both u_0 and Δt_1, one should start with a random value, and then, this should be gradually decreased until the fundamental frequency converges to a certain value. This approach was followed, and the results are shown in the Figures 5.9 and 5.10. Then, based on the results explained in the following paragraphs, the authors determined specific values of u_0 and Δt_1 to be used in this study.

The value of Δt_1 should be small because according to the proposed approach for extracting the pseudo-free-vibration response, such a small time-step would provide enough points for obtaining the pseudo-free-vibration response of the structure. Besides that, selecting a large value for Δt_1 will cause the approach explained in chapter 3 to filter out some of vital points so that the extracted pseudo-free-vibration response will not be an acceptable representative for the exact free vibration response. As shown in Figure 5.9, the arbitrary value selected for the trial and error approach is 3.5% of the total time duration of acceleration-time response. Then, the fundamental frequency of structure one was obtained for different values of Δt_1 varying from 3.5% to 0.1% of the total time duration of acceleration-time response. As it can be clearly observed, after decreasing the value of Δt_1, the fundamental frequency gradually converged around a certain value (about 24.4 Hz). It should be noted that in Figure 5.9, u_0 is constant and equal to 10% of the maximum acceleration in the acceleration vs. time response. From that figure, a value Δt_1 less or equal to 1% may be suitable as a result of this trial and error approach to obtain the value of fundamental frequency of this structure. In this study Δt_1=0.5% of the total duration of the acceleration signal was used, shown in Figure 5.9 as a gray bar.

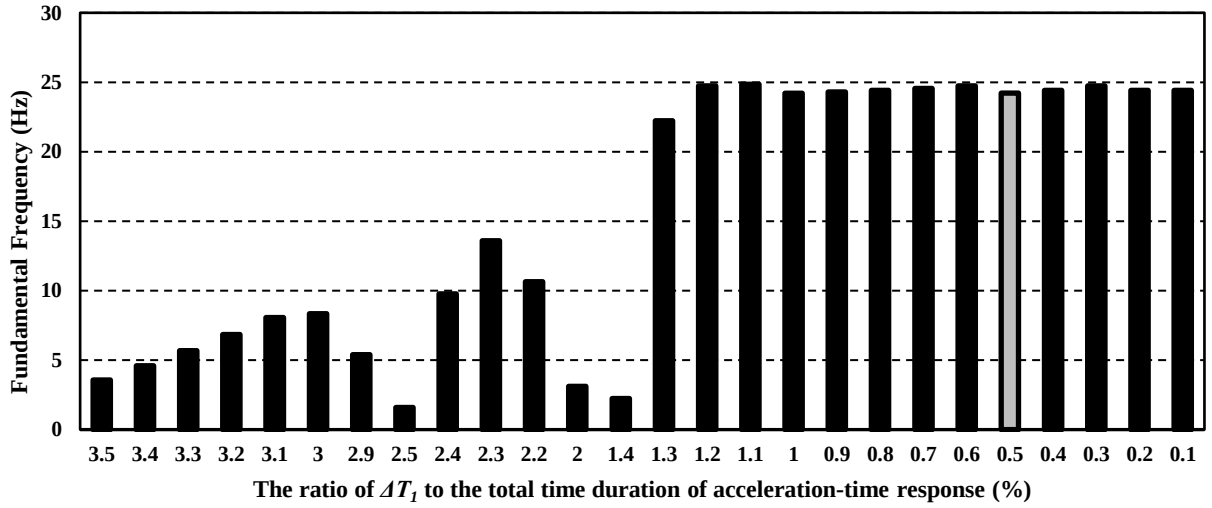

Figure 5.9 Fundamental frequencies of structure one when Δt_1 is varying while u_0 is constant

An initial value for the acceleration (u_0) should also be carefully chosen such that, preferably, the horizontal line from the initial acceleration (u_0) intersects as many points as possible on the signal curve shown in Figure 3.2. As shown in Figure 5.10, the arbitrary value selected for the trial and error approach is 50% of the maximum acceleration in the acceleration-time response. Then, the fundamental frequency of structure one was obtained using different values of u_0 varying from 50% to 0.00001% of the maximum acceleration magnitude in the acceleration-time response. As shown in Figure 5.10, while gradually decreasing the value of u_0, the fundamental frequency remains around 24.22 Hz. It should be noticed that in Figure 5.10, Δt_1 is constant and equal to 0.5% of the total time duration of the acceleration signal. Meanwhile, the results illustrated in Figure 5.10 show that the value of u_0 does not have a considerable effect on the fundamental frequency. Thus, in the current study, it was found that a value of u_0 equal to 10% of the maximum acceleration magnitude in the acceleration vs. time response, shown in Figure 5.10 as a gray bar, is an acceptable value to obtain accurate results.

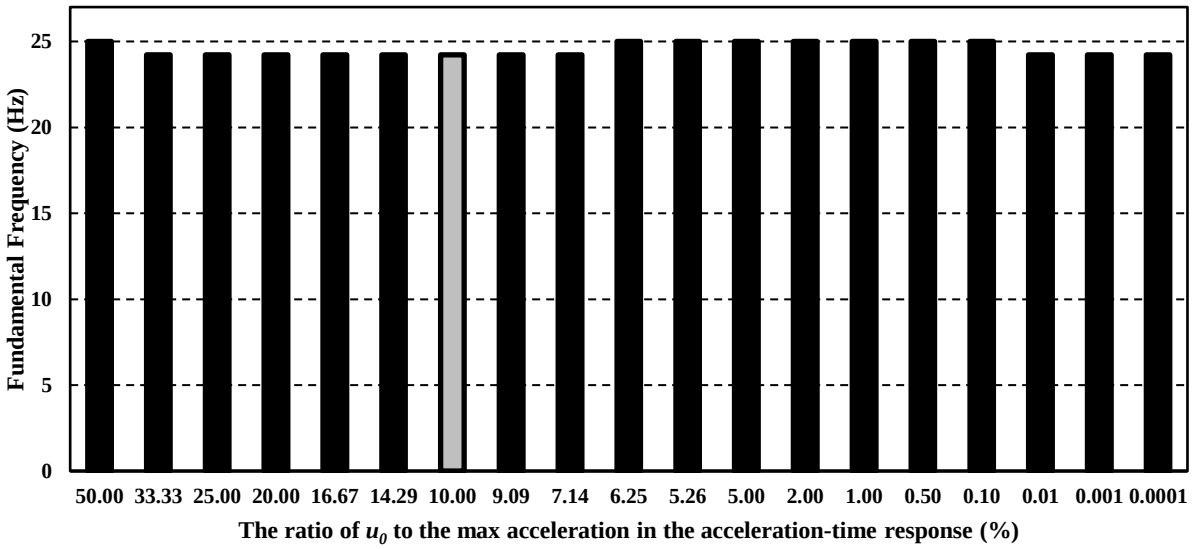

Figure 5.10 Fundamental frequencies of structure one when u_0 is varying while Δt_1 is constant

5.4 Evaluation of the effects of damping ratio on the results

This section evaluates the effects of different damping ratios on the results of the approach discussed in the preceding sections. In this regard, using different values of damping ratio including 0%, 3%, 4%, 6%, and 7%, structure one shown in Figure 4.2 was analyzed in ABAQUS software, and the acceleration versus time responses were obtained. (It should be noted that Section 5.2 provides the results shown in Figures 5.4 to 5.8 for structure one with damping ratio of 5%). Then, using the approach explained in chapter 3, the pseudo-free-vibration responses were obtained and transferred to frequency domain using FFT. The pseudo-free-vibration responses along with their corresponding FFT diagrams are provided in Figures 5.11 to 5.16 for damping ratios of 0%, 4%, and 7%. In the following, the authors explain how the approach discussed in chapter 3 can extract the pseudo-free-vibration response which can be a suitable representative of the exact free vibration response even when the structure is analyzed with different damping ratios. The results are consistent with simple concepts of structural dynamics.

Figure 5.11 shows an undamped pseudo-free-vibration response obtained using the proposed approach delineated in chapter 3. Figure 5.12 shows the FFT diagram, and as shown, the undamped fundamental frequency and its intensity are 24.2 Hz and 0.93, respectively. Figures 5.13 through 5.16 show the damped pseudo-free-vibration responses of structure one with damping ratios of 4% and 7% and that the larger the damping ratio, the less the acceleration magnitudes are. Figures 5.14 and 5.16 show that the fundamental frequencies of structure one for damping ratios of 4% and 7% are equal and also the same as for damping ratios of 0% and 5%. However, more damping produces less undamped fundamental frequencies magnitudes. The bar chart shown in Figure 5.17 compares the fundamental frequencies, and as it can be observed they are all equal, which shows that this approach for extracting pseudo-free-vibration response can extract the

undamped fundamental frequency (f_n) not the damped fundamental frequency (f_D) otherwise they would not be the same.

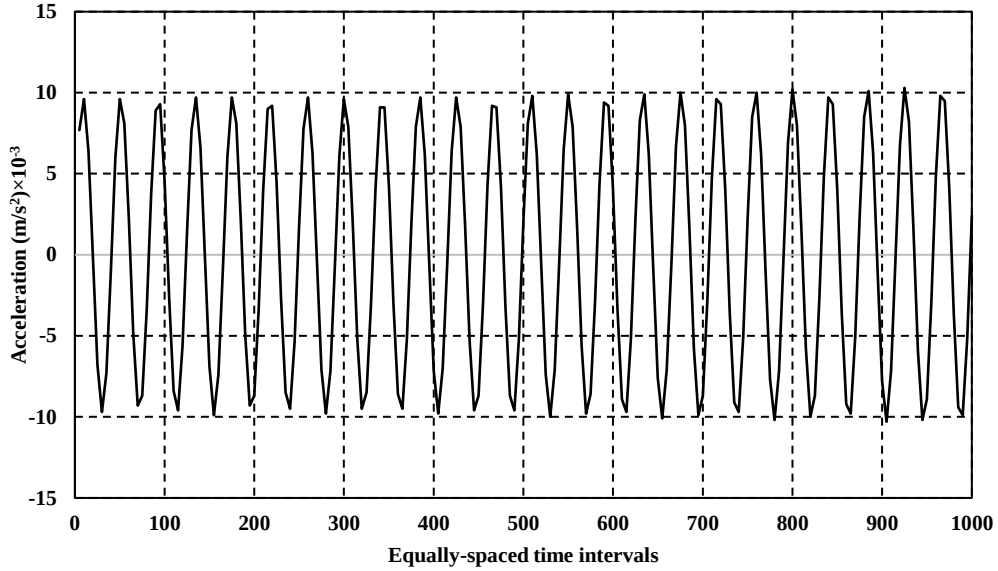

Figure 5.11 Pseudo-free-vibration response diagram of structure one subjected to dynamic load one (damping ratio=0%)

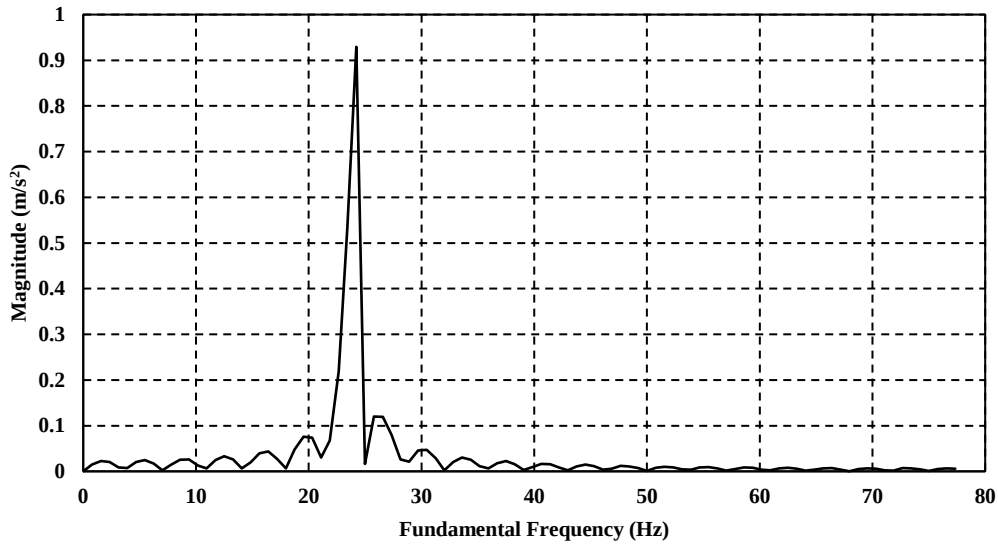

Figure 5.12 FFT diagram of structure one subjected to dynamic load one (damping ratio=0%)

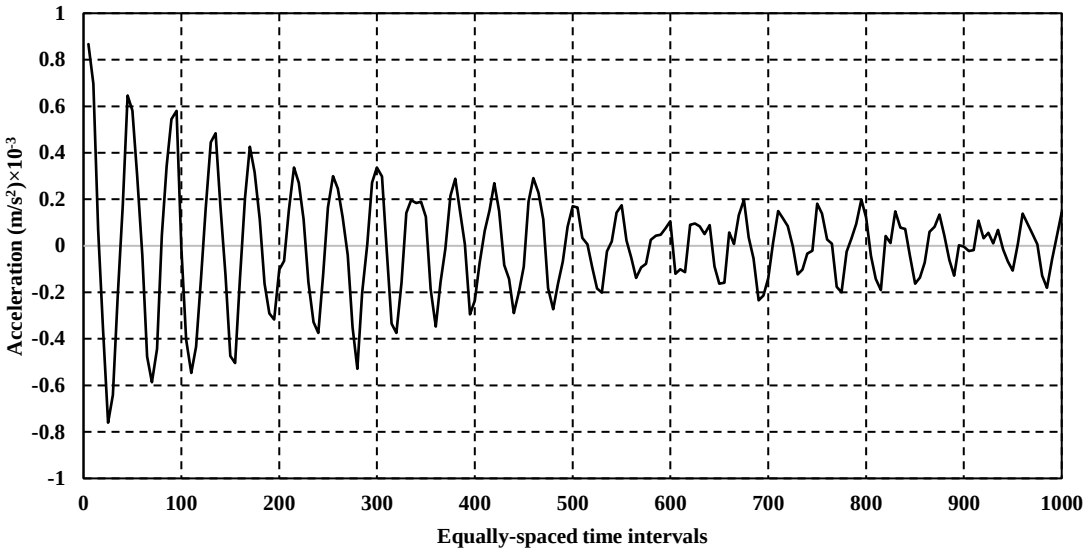

Figure 5.13 Pseudo-free-vibration response diagram of structure one subjected to dynamic load one (damping ratio=4%)

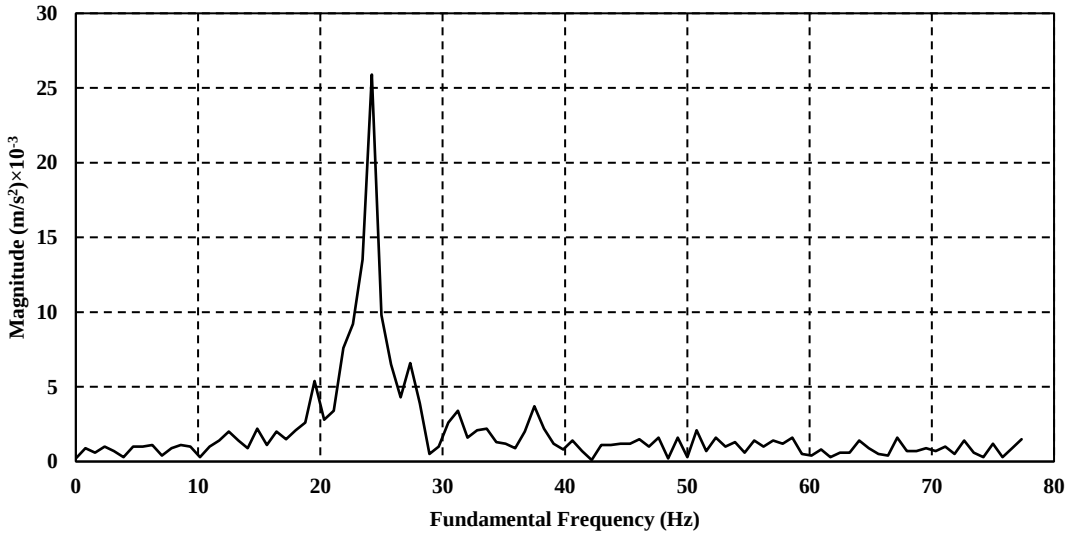

Figure 5.14 FFT diagram of structure one subjected to dynamic load one (damping ratio=4%)

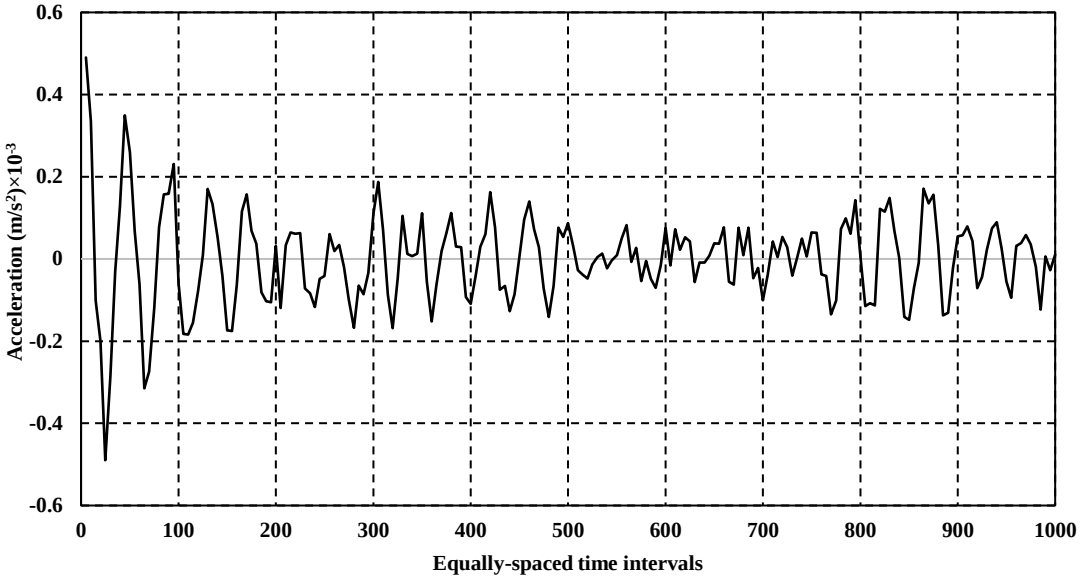

Figure 5.15 Pseudo-free-vibration response diagram of structure one subjected to dynamic load one (damping ratio=7%)

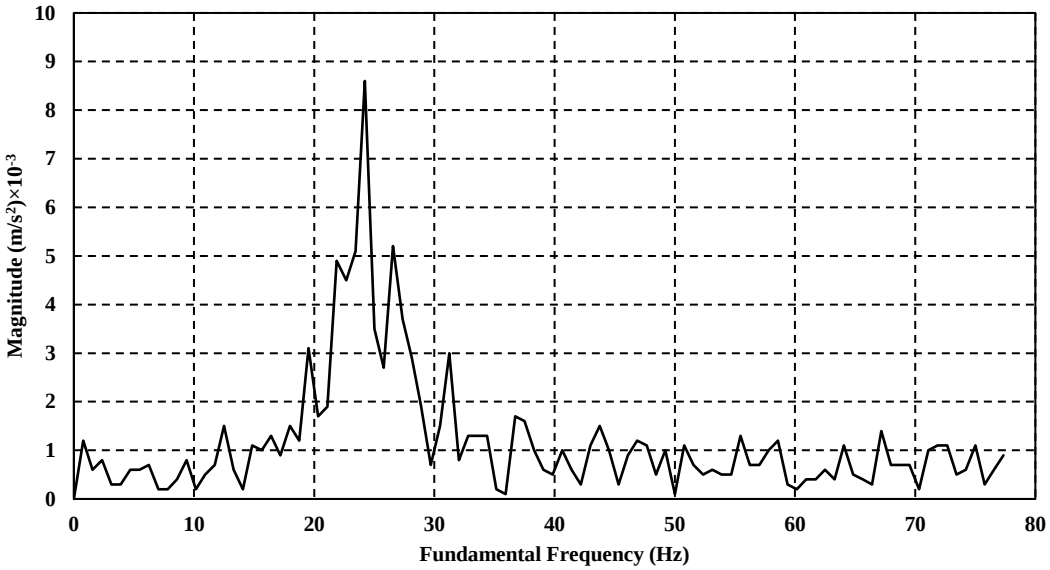

Figure 5.16 FFT diagram of structure one subjected to dynamic load one (damping ratio=7%)

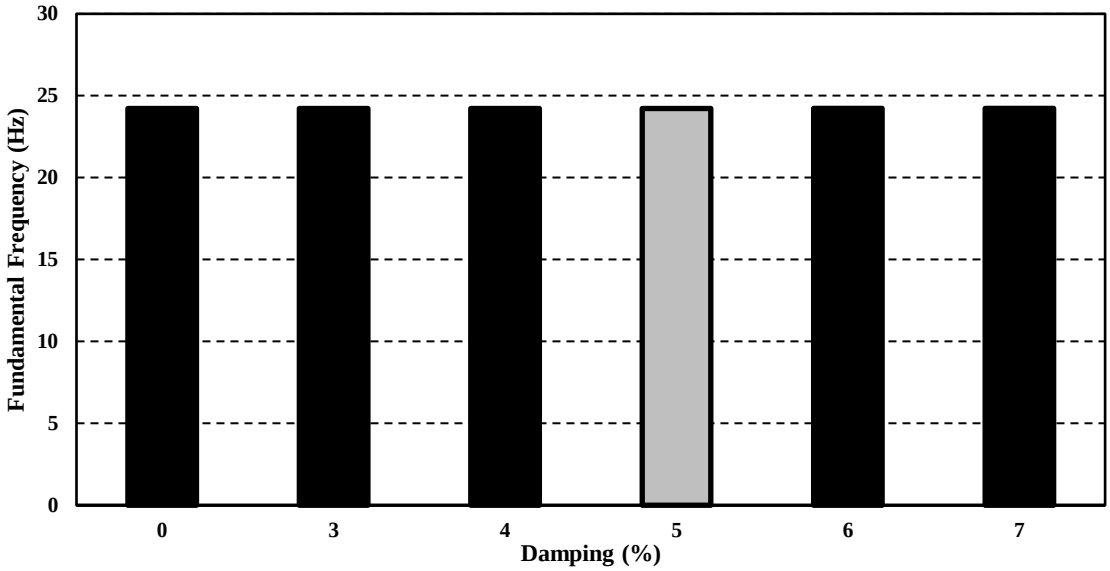

Figure 5.17 The fundamental frequency of structure one subjected to dynamic load one for different damping ratios varying from 0 to 7 percent

5.5 Experimental Study

According to the procedure explained in chapter 3 and based on the extracted acceleration-time records from the experimental models explained in previous chapter, the pseudo-free-vibration responses were extracted using the MATLAB code. Then, their pseudo-free-vibration responses shown in Figures 5.18 and 5.20 were transferred to the frequency domain using Fast Fourier Transform. The results shown in Figures 5.19 and 5.21 illustrate that the fundamental frequency in frequency domain using Fast Fourier Transform for structures one and two are 25.8 and 32.8 Hz, respectively. These results are consistent with the conclusion drawn from the numerical models.

Repeating the procedure for structures one and two subjected to applying dynamic loads two and three shows that by using the proposed random-vibration-based approach, the fundamental frequency in frequency domain using Fast Fourier Transform will remain constant while the applied dynamic loads are different. According to Figures 5.22, 5.23, the results based on

numerical and experimental samples are very close so that the simulated numerical models would be reliably used for the remainder of this study.

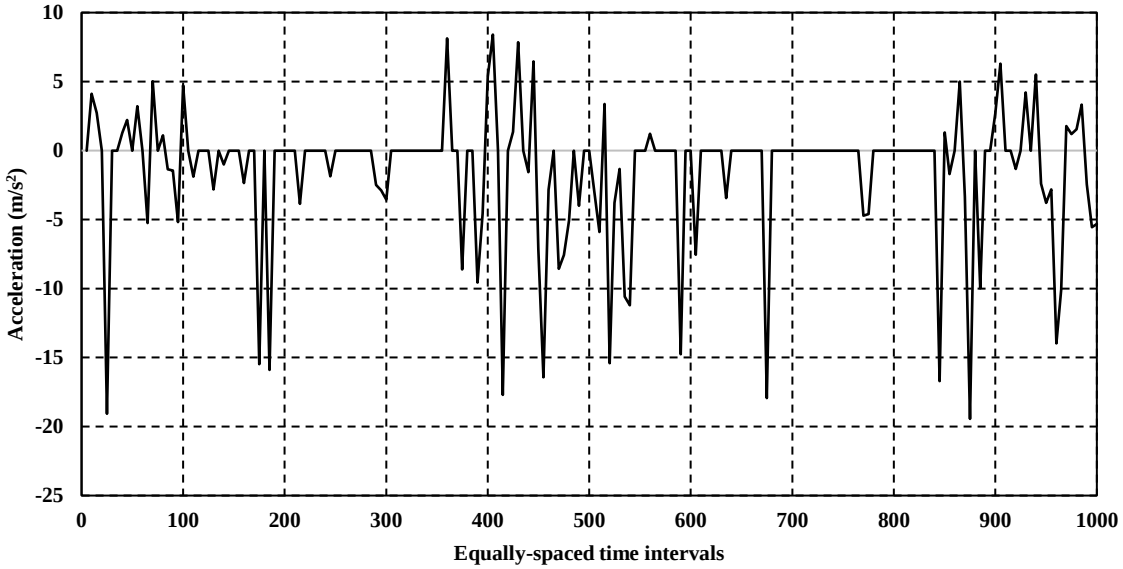

Figure 5.18 Signal processing results of experimental model one subjected to dynamic load one (pseudo-free-vibration response diagram)

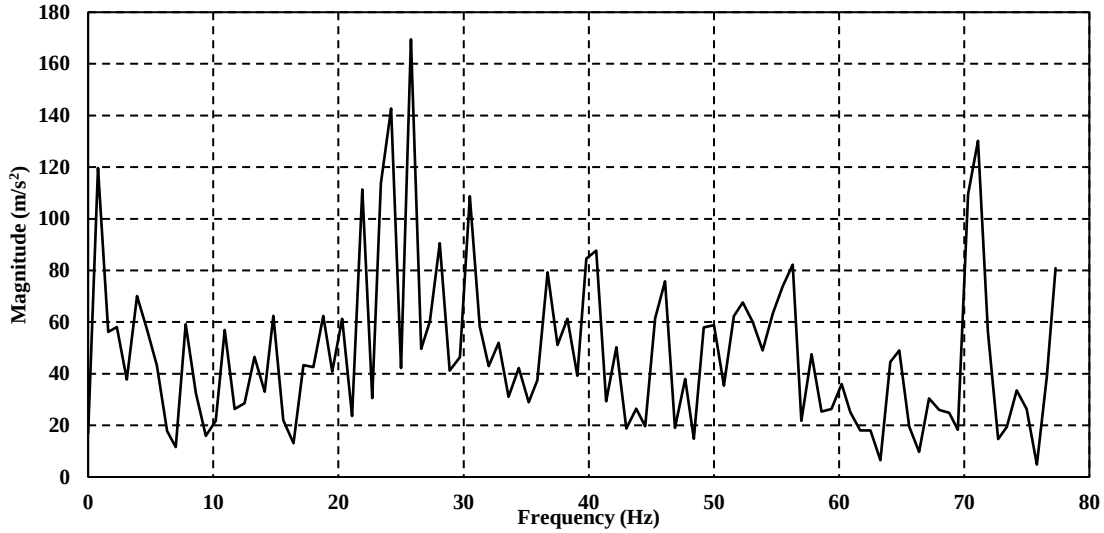

Figure 5.19 Signal processing results of experimental model one subjected to dynamic load one (FFT diagram)

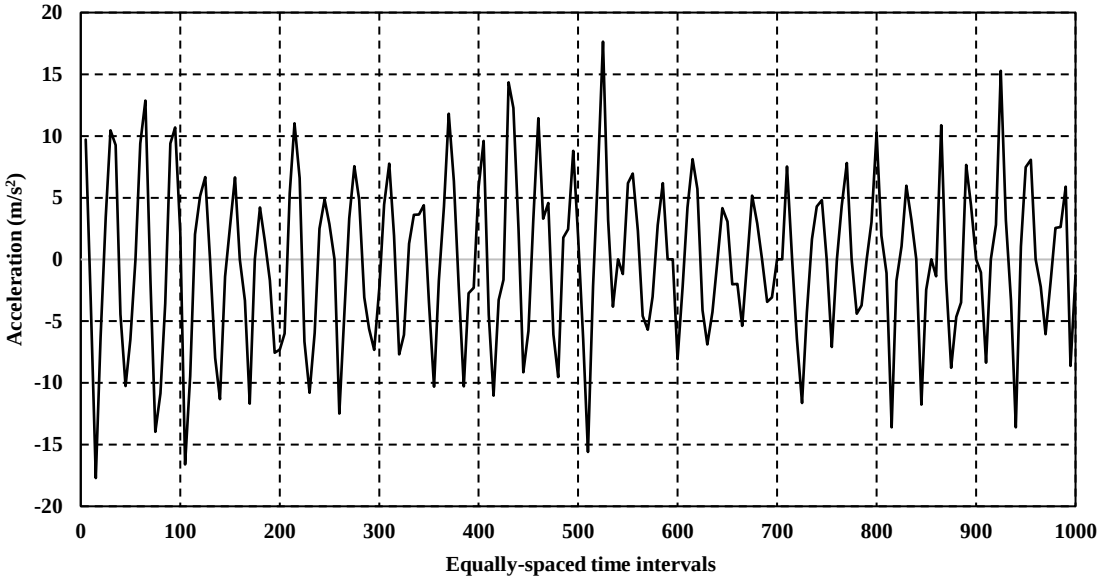

Figure 5.20 Signal processing results of experimental model two subjected to dynamic load one (pseudo-free-vibration response diagram)

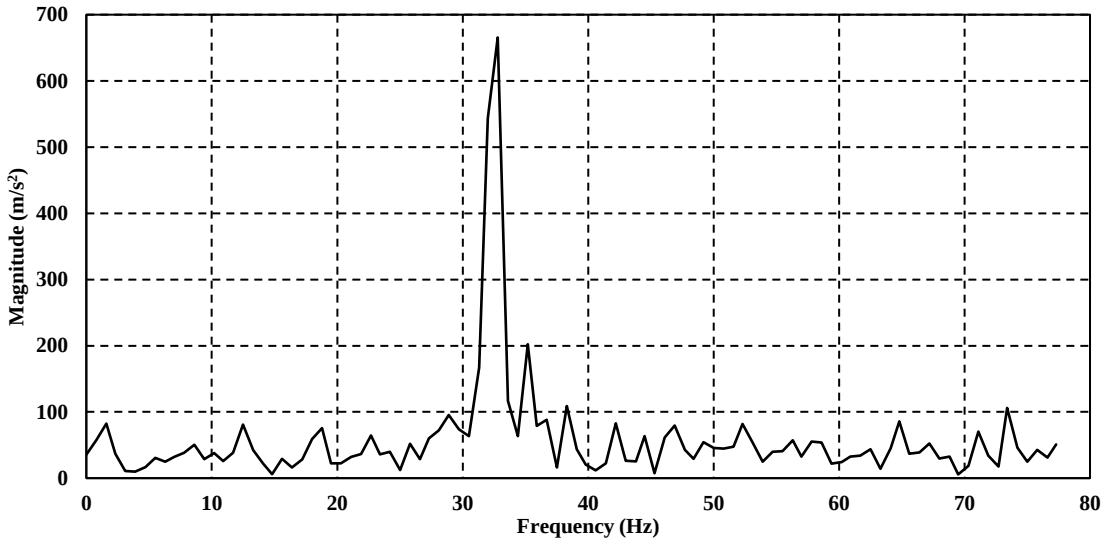

Figure 5.21 Signal processing results of experimental model two subjected to dynamic load one (FFT diagram)

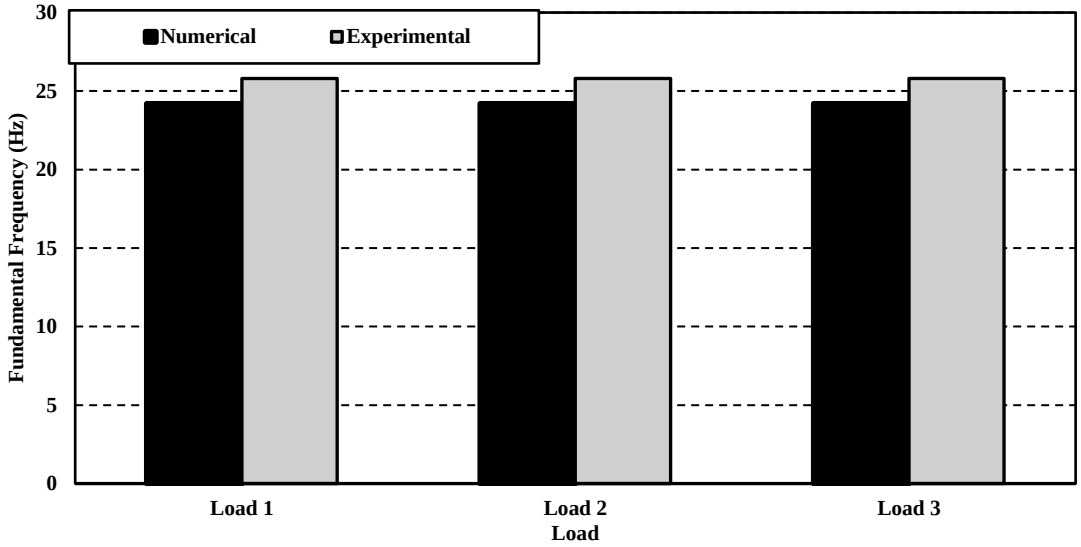

Figure 5.22 Comparing of the fundamental frequencies of the experimental and numerical results of structures one and two subjected to dynamic loads one, two and three (structure one)

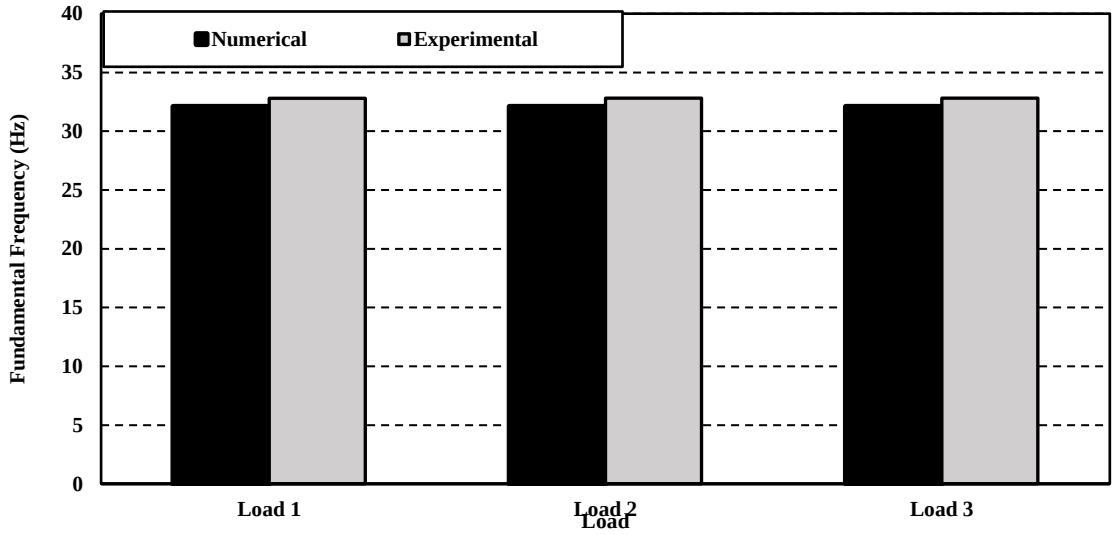

Figure 5.23 Comparing of the fundamental frequencies of the experimental and numerical results of structures one and two subjected to dynamic loads one, two and three (structure two)

5.6 Thirty different numerical models

Detecting a reduction of the fundamental frequency of a structure can be an indication of loss of stiffness possibly caused by damage. This approach makes changes in the structure fundamental frequency easy to detect without the need to apply forced vibration nor the use of complex equipment and instrumentation.

So far, it has been proved that the random-vibration-based approach works, and the results of the numerical models match those of the experimental models. In the following, it is shown that the approach works on a large number of different structures with different geometrical characteristics as well. Thus, 15 structures were selected to be analyzed under two different dynamic loads. In these structures, only the columns heights have been changed (For example, C250 refers to a structure for which all geometrical characteristics are the same as Figures 4.2 and 4.3 except that the column height is 250 mm). It can be observed in Figure 5.24 that the larger the stiffness is, the larger the fundamental frequency becomes such that the highest and lowest fundamental frequencies correspond to C250 and C690, respectively. Moreover, according to Figure 5.25, although the dynamic load applied on the structures has been changed, the fundamental frequencies are very close to those in Figure 5.24. Therefore, using 30 different analyses, the conclusions which had been drawn through the numerical and experimental models in sections 5.2 and 5.5 were confirmed.

Meanwhile, another result based on this study is that detecting a reduction of the fundamental frequency of a structure can be an indication of loss of stiffness possibly caused by damage. This approach makes changes in the structure fundamental frequency easy to detect without the need to apply forced vibration nor the use of complex equipment and instrumentation.

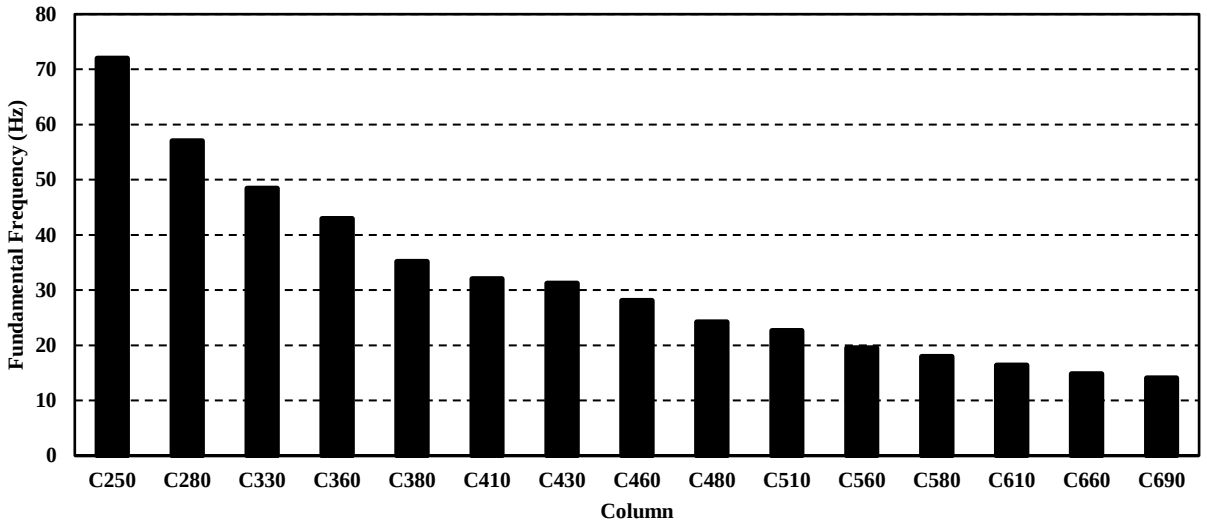

Figure 5.24 The fundamental frequency of the signal processing results of different models with different column heights under dynamic load one (For example, C250 refers to a structure for which all geometrical characteristics are the same as Figures 4.2 and 4.3 except that the column height is 250 mm)

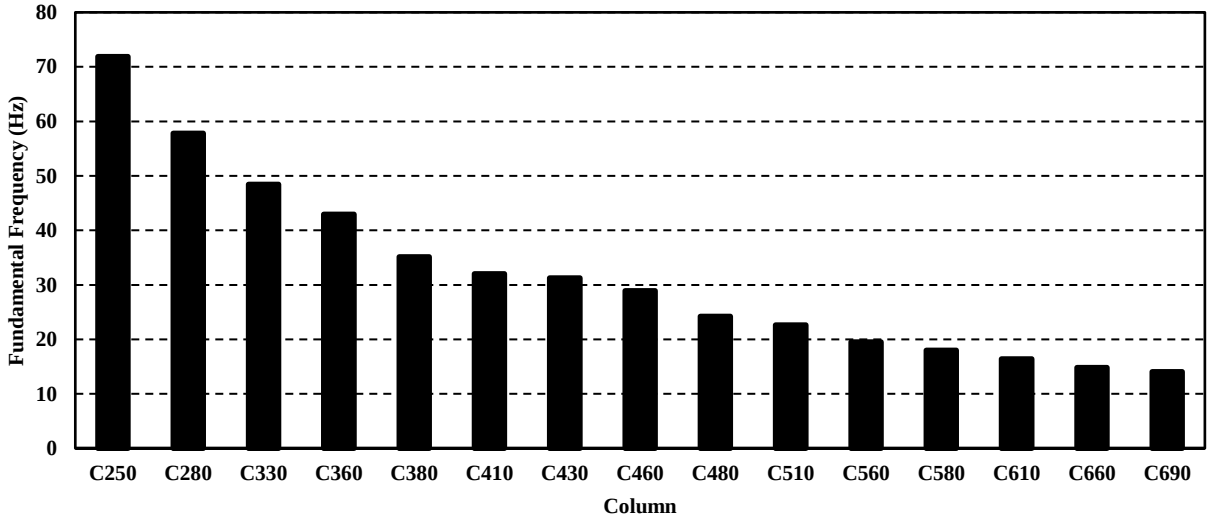

Figure 5.25 The fundamental frequency of the signal processing results of different models with different column heights under dynamic load two (For example, C250 refers to a structure for which all geometrical characteristics are the same as Figures 4.2 and 4.3 except that the column height is 250 mm

Chapter 6 - Conclusion and Future Study

6.1 Conclusions

This study is a report on a novel ambient-vibration-based approach proposed for steel structures for extracting the pseudo-free-vibration response that can be used to detect any change in the dynamic properties of a structure which may be caused by damage. Based on the results from the analytical verification as well as the numerical and experimental models, the following conclusions are made.

The response (acceleration-time) is the sum of the free vibration solution and the particular solution which depends on the load. The particular solution and the initial condition, are removed by taking the average of many sub-records of same length Δt and same u_0. The result is a free vibration solution, which can then be used. The trigger value u_0 and the length Δt must be carefully chosen. One through a trial and error procedure should start with an arbitrary value, and then it should be gradually decreased until the fundamental frequency converges to a certain value. In this study, Δt_1 equal to 0.5% of the total duration of the acceleration signal and u_0 equal to 10% of the maximum acceleration in the acceleration vs. time response were used. The approach is applicable when a structure is subject to an ambient vibration, and its frequencies can be uniquely detected regardless of the excitation.

Validity of the method in extracting the pseudo-free-vibration response has been verified analytically. In this study, the pseudo-free-vibration response could be extracted for the physical and numerical models, and as expected, changing the stiffness of the structures will change the fundamental frequencies in the frequency domain using Fast Fourier Transform such that when a structure loses some of its stiffness, it will produce a lower fundamental frequency.

If different arbitrary vibrations are applied to a structure while its flexural stiffness has not changed, using this proposed method to extract the pseudo-free-vibration response and exploring its frequency content show that the fundamental frequencies in frequency-domain will remain the same. This validates the approach further.

The results show that the procedure proposed for obtaining the pseudo-free-vibration response is insensitive to the damping ratio.

Detecting a reduction of the fundamental frequency of a structure can be an indication of loss of stiffness possibly caused by damage. This approach makes changes in the structure fundamental frequency easy to detect without the need to apply forced vibration nor the use of complex equipment and instrumentation.

6.1 Future Study

In the following, some of the areas are suggested as future research:

- This project is a proof of concept study to show the capability of the approach for obtaining the pseudo-free-vibration as a tool used for damage identification. The physical model used in this research is simple because it provides the possibility of verification using simple concepts explained in the preceding chapters. As a future study, further research on more complex structures with a larger number of degrees of freedom and damage locations are needed. Meanwhile, for better correlation of the collected data of full-size structures, several sensors should be placed at different locations. The ideal accelerometer positions are another step for future study.
- An actual damage scenario needs to be performed in the structure with different intensities to see how sensitive the approach is to different damage intensities and scenarios. For instance, the stiffness of the beam-to-column connections can be gradually decreased from

a full-fixed connection to a full-pinned connection. In each step, the procedure explained in chapter 3 would be repeated to see the sensitivity of the approach to small stiffness changes.

A signal-processing-based approach for damage detection of steel structures

by

Amin Moghadam

B.S., University of Qom, 2012
M.S., Sharif University of Technology, 2014

A THESIS

submitted in partial fulfillment of the requirements for the degree

MASTER OF SCIENCE

Department of Civil Engineering
College of Engineering

KANSAS STATE UNIVERSITY
Manhattan, Kansas

2019

Approved by:

Major Professor
Professor Hani Melhem

References

[1] L. Qiao, A. Esmaeily, and H. G. Melhem, “Structural damage detection using signal pattern-recognition,” in *Key Engineering Materials*, 2009, vol. 400, pp. 465–470.

[2] M. Shariati, N. H. Ramli-Sulong, M. M. A. KH, P. Shafigh, and H. Sinaei, “Assessing the strength of reinforced concrete structures through Ultrasonic Pulse Velocity and Schmidt Rebound Hammer tests,” *Sci. Res. Essays*, vol. 6, no. 1, pp. 213–220, 2011.

[3] P. A. Doyle and C. M. Scala, “Crack depth measurement by ultrasonics: a review,” *Ultrasonics*, vol. 16, no. 4, pp. 164–170, 1978.

[4] X. Xu, T. Xia, A. Venkatachalam, and D. Huston, “Development of high-speed ultrawideband ground-penetrating radar for rebar detection,” *J. Eng. Mech.*, vol. 139, no. 3, pp. 272–285, 2012.

[5] F. J. Koch, L. C. Vandervalk, and D. J. Beamish, “High resolution ultrasonic coating thickness gauge,” Mar-1998.

[6] P. C. Chang and S. C. Liu, “Recent research in nondestructive evaluation of civil infrastructures,” *J. Mater. Civ. Eng.*, vol. 15, no. 3, pp. 298–304, 2003.

[7] L. Qiao, “Structural damage detection using signal-based pattern recognition,” PhD Thesis, Kansas State University, 2009.

[8] J. M. Brownjohn, “Ambient vibration studies for system identification of tall buildings,” *Earthq. Eng. Struct. Dyn.*, vol. 32, no. 1, pp. 71–95, 2003.

[9] D. E. Hudson, *Dynamic Tests of Full-Scale Structures. Chapter 7 in “Earthquake Engineering”, edited by R. Wiegel*. Prentice Hall, 1970.

[10] C. Williams and W. F. Tsang, “Determination of structural parameters from full-scale vibration tests.,” in *CIVIL ENGINEERING DYNAMICS*, Thomas Telford Publishing, 1989, pp. 43–59.

[11] D. S. Carder, “Observed vibrations of bridges,” *Bull. Seismol. Soc. Am.*, vol. 27, no. 4, pp. 267–303, 1937.

[12] S. Doebling, C. Farrar, M. Primee, and D. Shevitz, “Damage identification and health monitoring of structural and mechanical systems from changes in their vibration characteristics,” Los Alamos National Laboratory, New Mexico, a literature review Report LA-13070-MS, UC-900, 1996.

[13] J. M. Lifshitz and A. Rotem, “Determination of Reinforcement Unbonding of Composites by a Vibration Technique,” *J. Compos. Mater.*, vol. 3, no. 3, pp. 412–423, Mar. 1969.

[14] Hearn George and Testa Rene B., “Modal Analysis for Damage Detection in Structures,” *J. Struct. Eng.*, vol. 117, no. 10, pp. 3042–3063, Oct. 1991.

[15] J. A. Loya, L. Rubio, and J. Fernández-Sáez, “Natural frequencies for bending vibrations of Timoshenko cracked beams,” *J. Sound Vib.*, vol. 290, no. 3, pp. 640–653, Mar. 2006.

[16] H. Nahvi and M. Jabbari, “Crack detection in beams using experimental modal data and finite element model,” *Int. J. Mech. Sci.*, vol. 47, no. 10, pp. 1477–1497, Oct. 2005.

[17] T. G. Chondros, “Variational formulation of a rod under torsional vibration for crack identification,” *Theor. Appl. Fract. Mech.*, vol. 44, no. 1, pp. 95–104, Sep. 2005.

[18] D. Y. Zheng and N. J. Kessissoglou, “Free vibration analysis of a cracked beam by finite element method,” *J. Sound Vib.*, vol. 273, no. 3, pp. 457–475, Jun. 2004.

[19] A. Morassi, “IDENTIFICATION OF A CRACK IN A ROD BASED ON CHANGES IN A PAIR OF NATURAL FREQUENCIES,” *J. Sound Vib.*, vol. 242, no. 4, pp. 577–596, May 2001.

[20] T. D. Chaudhari and S. K. Maiti, “A study of vibration of geometrically segmented beams with and without crack,” *Int. J. Solids Struct.*, vol. 37, no. 5, pp. 761–779, Feb. 2000.

[21] J. Fernandez-Saez, L. Rubio, and C. Navarro, “Approximate calculation of the fundamental frequency for bending vibrations of cracked beams,” *J. Sound Vib.*, vol. 225, no. 2, pp. 345–352, 1999.

[22] E. I. Shifrin and R. Ruotolo, “NATURAL FREQUENCIES OF A BEAM WITH AN ARBITRARY NUMBER OF CRACKS,” *J. Sound Vib.*, vol. 222, no. 3, pp. 409–423, May 1999.

[23] M. Boltezar, B. Strancar, and A. Kuhelj, “IDENTIFICATION OF TRANSVERSE CRACK LOCATION IN FLEXURAL VIBRATIONS OF FREE–FREE BEAMS,” *J. Sound Vib.*, vol. 211, no. 5, pp. 729–734, Apr. 1998.

[24] M. H. Dado, “A comprehensive crack identification algorithm for beams under different end conditions,” *Appl. Acoust.*, vol. 51, no. 4, pp. 381–398, Aug. 1997.

[25] C. Davini, A. Morassi, and N. Rovere, “Modal analysis of notched bars: tests and comments on the sensitivity of an identification technique,” *J. Sound Vib.*, vol. 179, no. 3, pp. 513–527, Jan. 1995.

[26] J.-J. Sinou and A. W. Lees, “The influence of cracks in rotating shafts,” *J. Sound Vib.*, vol. 285, no. 4, pp. 1015–1037, Aug. 2005.

[27] Y.-S. Lee and M.-J. Chung, “A study on crack detection using eigenfrequency test data,” *Comput. Struct.*, vol. 77, no. 3, pp. 327–342, Jun. 2000.

[28] Y. Narkis and E. Elmalah, “Crack identification in a cantilever beam under uncertain end conditions,” *Int. J. Mech. Sci.*, vol. 38, no. 5, pp. 499–507, May 1996.

[29] Y. Narkis, “Identification of Crack Location in Vibrating Simply Supported Beams,” *J. Sound Vib.*, vol. 172, no. 4, pp. 549–558, May 1994.

[30] J. J. Sinou, “Numerical investigations of a robust identification of crack location and size in beams using only changes in ratio pulsations of the cracked beams,” *Struct. Eng. Mech.*, vol. 25, no. 6, pp. 691–716, 2007.

[31] A. Messina, I. A. Jones, and E. J. Williams, “Damage detection and localization using natural frequency changes,” in *Proceedings of conference on Identification in Engineering Systems*, 1996, pp. 67–76.

[32] A. Messina, E. J. Williams, and T. Contursi, “STRUCTURAL DAMAGE DETECTION BY A SENSITIVITY AND STATISTICAL-BASED METHOD,” *J. Sound Vib.*, vol. 216, no. 5, pp. 791–808, Oct. 1998.

[33] B. H. Koh and S. J. Dyke, “Structural health monitoring for flexible bridge structures using correlation and sensitivity of modal data,” *Comput. Struct.*, vol. 85, no. 3, pp. 117–130, Feb. 2007.

[34] P. G. Nikolakopoulos, D. E. Katsareas, and C. A. Papadopoulos, “Crack identification in frame structures,” *Comput. Struct.*, vol. 64, no. 1, pp. 389–406, Jul. 1997.

[35] X. F. Yang, A. S. J. Swamidas, and R. Seshadri, “CRACK IDENTIFICATION IN VIBRATING BEAMS USING THE ENERGY METHOD,” *J. Sound Vib.*, vol. 244, no. 2, pp. 339–357, Jul. 2001.

[36] G. M. Dong, J. Chen, and J. Zou, “Parameter identification of a rotor with an open crack,” *Eur. J. Mech. - ASolids*, vol. 23, no. 2, pp. 325–333, Mar. 2004.

[37] Swamidas A. S. J., Yang X., and Seshadri R., “Identification of Cracking in Beam Structures Using Timoshenko and Euler Formulations,” *J. Eng. Mech.*, vol. 130, no. 11, pp. 1297–1308, Nov. 2004.

[38] S. P. Lele and S. K. Maiti, “MODELLING OF TRANSVERSE VIBRATION OF SHORT BEAMS FOR CRACK DETECTION AND MEASUREMENT OF CRACK EXTENSION,” *J. Sound Vib.*, vol. 257, no. 3, pp. 559–583, Oct. 2002.

[39] B. Li, X. F. Chen, J. X. Ma, and Z. J. He, “Detection of crack location and size in structures using wavelet finite element methods,” *J. Sound Vib.*, vol. 285, no. 4, pp. 767–782, Aug. 2005.

[40] M. Dilena and A. Morassi, “The use of antiresonances for crack detection in beams,” *J. Sound Vib.*, vol. 276, no. 1, pp. 195–214, Sep. 2004.

[41] J.-J. Sinou, “Damage Assessment Based on the Frequencies’ Ratio Surfaces Intersection Method for the Identification of the Crack Depth, Location and Orientation,” *Struct. Durab. Health Monit.*, vol. 3, no. 3, pp. 134–162, 2007.

[42] C. Modena, D. Sonda, and D. Zonta, “Damage Localization in Reinforced Concrete Structures by Using Damping Measurements,” *Key Engineering Materials*, 1999. [Online]. Available: https://www.scientific.net/KEM.167-168.132. [Accessed: 02-Oct-2018].

[43] A. P. Bovsunovsky, “The mechanisms of energy dissipation in the non-propagating fatigue cracks in metallic materials,” *Eng. Fract. Mech.*, vol. 71, no. 16, pp. 2271–2281, Nov. 2004.

[44] C. Kyriazoglou, B. H. Le Page, and F. J. Guild, “Vibration damping for crack detection in composite laminates,” *Compos. Part Appl. Sci. Manuf.*, vol. 35, no. 7, pp. 945–953, Jul. 2004.

[45] S. D. Panteliou, T. G. Chondros, V. C. Argyrakis, and A. D. Dimarogonas, “DAMPING FACTOR AS AN INDICATOR OF CRACK SEVERITY,” *J. Sound Vib.*, vol. 241, no. 2, pp. 235–245, Mar. 2001.

[46] F. Léonard, J. Lanteigne, S. Lalonde, and Y. Turcotte, “FREE-VIBRATION BEHAVIOUR OF A CRACKED CANTILEVER BEAM AND CRACK DETECTION,” *Mech. Syst. Signal Process.*, vol. 15, no. 3, pp. 529–548, May 2001.

[47] J.-J. Sinou, *A review of damage detection and health monitoring of mechanical systems from changes in the measurement of linear and non-linear vibrations*. Nova Science Publishers, Inc., 2009.

[48] A. Morassi, “Identification of a crack in a rod based on changes in a pair of natural frequencies,” *J. Sound Vib.*, vol. 242, no. 4, pp. 577–596, 2001.

[49] M. Dilena and A. Morassi, “The use of antiresonances for crack detection in beams,” *J. Sound Vib.*, vol. 276, no. 1–2, pp. 195–214, 2004.

[50] R. D. Adams, P. Cawley, C. J. Pye, B. J. Stone, and W. G. R. Davies, “A vibration technique for nondestructively assessing the integrity of structures,” *J Mech Eng Sci*, vol. 21, no. 1, p. 57, 1979.

[51] P. Cawley and R. D. Adams, “The location of defects in structures from measurements of natural frequencies,” *J. Strain Anal. Eng. Des.*, vol. 14, no. 2, pp. 49–57, 1979.

[52] M. M. F. Yuen, “A numerical study of the eigenparameters of a damaged cantilever,” *J. Sound Vib.*, vol. 103, no. 3, pp. 301–310, 1985.

[53] H. G. Natke and C. Cempel, “Model-aided diagnosis based on symptoms,” in *Proceedings of DAMAS*, 1997, vol. 97, pp. 363–375.

[54] J. Kullaa, “Damage detection of the Z24 bridge using control charts,” *Mech. Syst. Signal Process.*, vol. 17, no. 1, pp. 163–170, 2003.

[55] J. Maeck and G. De Roeck, “Damage assessment using vibration analysis on the Z24-bridge,” *Mech. Syst. Signal Process.*, vol. 17, no. 1, pp. 133–142, 2003.

[56] S. S. Law and X. Q. Zhu, “Dynamic behavior of damaged concrete bridge structures under moving vehicular loads,” *Eng. Struct.*, vol. 26, no. 9, pp. 1279–1293, 2004.

[57] S. W. Doebling, C. R. Farrar, and M. B. Prime, “A summary review of vibration-based damage identification methods,” *Shock Vib. Dig.*, vol. 30, no. 2, pp. 91–105, 1998.

[58] S. W. Doebling, C. R. Farrar, M. B. Prime, and D. W. Shevitz, “Damage identification and health monitoring of structural and mechanical systems from changes in their vibration characteristics: a literature review,” 1996.

[59] W. M. West, “Illustration of the use of modal assurance criterion to detect structural changes in an orbiter test specimen,” 1986.

[60] M. G. Srinivasan and C. A. Kot, “Effect of damage on the modal parameters of a cylindrical shell,” Argonne National Lab., IL (United States), 1992.

[61] M. Palacz and M. Krawczuk, “Vibration parameters for damage detection in structures,” *J. Sound Vib.*, vol. 249, no. 5, pp. 999–1010, 2002.

[62] R. J. Allemang, “The modal assurance criterion–twenty years of use and abuse,” *Sound Vib.*, vol. 37, no. 8, pp. 14–23, 2003.

[63] E. Parloo, P. Guillaume, and M. Van Overmeire, “Damage assessment using mode shape sensitivities,” *Mech. Syst. Signal Process.*, vol. 17, no. 3, pp. 499–518, 2003.

[64] A. K. Pandey, M. Biswas, and M. M. Samman, “Damage detection from changes in curvature mode shapes,” *J. Sound Vib.*, vol. 145, no. 2, pp. 321–332, 1991.

[65] Y. K. Ho and D. J. Ewins, “On the structural damage identification with mode shapes,” in *International Conference on System Identification and Structural Health Monitoring*, 2000, pp. 677–686.

[66] M. A. Wahab and G. De Roeck, “Damage detection in bridges using modal curvatures: application to a real damage scenario,” *J. Sound Vib.*, vol. 226, no. 2, pp. 217–235, 1999.

[67] A. Dutta and S. Talukdar, “Damage detection in bridges using accurate modal parameters,” *Finite Elem. Anal. Des.*, vol. 40, no. 3, pp. 287–304, 2004.

[68] N. Stubbs, J. T. Kim, and K. Topole, “An efficient and robust algorithm for damage localization in offshore platforms,” in *Proceedings of the ASCE 10th Structures Congress*, 1992, vol. 1, pp. 543–546.

[69] N. Stubbs, J.-T. Kim, and C. R. Farrar, “Field verification of a nondestructive damage localization and severity estimation algorithm,” in *Proceedings-SPIE the international society for optical engineering*, 1995, pp. 210–210.

[70] A. Alvandi and C. Cremona, “Assessment of vibration-based damage identification techniques,” *J. Sound Vib.*, vol. 292, no. 1–2, pp. 179–202, 2006.

[71] J.-J. Sinou, *A review of damage detection and health monitoring of mechanical systems from changes in the measurement of linear and non-linear vibrations*. Nova Science Publishers, Inc., 2009.

[72] C. Lin, “Unity check method for structural damage detection,” in *Dynamics Specialists Conference*, 1994, p. 1717.

[73] C. S. Lin, “Location of modeling errors using modal test data,” *AIAA J.*, vol. 28, no. 9, pp. 1650–1654, 1990.

[74] H. P. Gysin, “Critical application of an error matrix method for location of finite element modeling inaccuracies,” in *Proc. of the 4th International Modal Analysis Conference*, 1986, pp. 1339–1351.

[75] Y. S. Park, “Weighted-Error-Matrix Application to Detect Stiffness Damage by Dynamic Characteristics Measurement,” *J. Modal Anal.*, vol. 6, no. 2, pp. 101–107, 1988.

[76] A. E. Aktan, K. L. Lee, C. Chuntavan, and T. Aksel, “Modal testing for structural identification and condition assessment of constructed facilities,” in *Proceedings-spie the International Society for Optical Engineering*, 1994, pp. 462–462.

[77] R. L. Mayes, “Experimental algorithm for detecting damage applied to the I-40 bridge over the Rio Grande,” in *Smart Structures and Materials 1995: Smart Systems for Bridges, Structures, and Highways*, 1995, vol. 2446, pp. 204–215.

[78] K. C. Park, G. W. Reich, and K. F. Alvin, “Structural damage detection using localized flexibilities,” *J. Intell. Mater. Syst. Struct.*, vol. 9, no. 11, pp. 911–919, 1998.

[79] W. Heylen and P. Sas, *Modal analysis theory and testing*. Katholieke Universteit Leuven, Departement Werktuigkunde, 2006.

[80] D. J. Ewins, *Modal testing: theory and practice*, vol. 15. Research studies press Letchworth, 1984.

[81] F. Wahl, G. Schmidt, and L. Forrai, “On the significance of antiresonance frequencies in experimental structural analysis,” *J. Sound Vib.*, vol. 219, no. 3, pp. 379–394, 1999.

[82] E. Douka, G. Bamnios, and A. Trochidis, “A method for determining the location and depth of cracks in double-cracked beams,” *Appl. Acoust.*, vol. 65, no. 10, pp. 997–1008, 2004.

[83] N. Dharmaraju and J. K. Sinha, “Some comments on use of antiresonance for crack identification in beams,” *J. Sound Vib.*, vol. 286, pp. 669–671, 2005.

[84] W. Heylen and S. Lammens, “FRAC: a consistent way of comparing frequency response functions,” in *Proceedings of the Conference on Identification in Engineering Systems*, 1996, pp. 48–57.

[85] C. Zang and M. Imregun, “Structural damage detection using artificial neural networks and measured FRF data reduced via principal component projection,” *J. Sound Vib.*, vol. 242, no. 5, pp. 813–827, 2001.

[86] C. Zang, M. I. Friswell, and M. Imregun, “Structural health monitoring and damage assessment using measured FRFs from multiple sensors, part I: The indicator of correlation criteria,” in *Key Engineering Materials*, 2003, vol. 245, pp. 131–140.

[87] G. D. Gounaris, C. A. Papadopoulos, and A. D. Dimarogonas, “Crack identification in beams by coupled response measurements,” *Comput. Struct.*, vol. 58, no. 2, pp. 299–305, 1996.

[88] D. Liu, H. Gurgenci, and M. Veidt, “Crack detection in hollow section structures through coupled response measurements,” *J. Sound Vib.*, vol. 261, no. 1, pp. 17–29, 2003.

[89] A. C. Chasalevris and C. A. Papadopoulos, “Coupled horizontal and vertical bending vibrations of a stationary shaft with two cracks,” *J. Sound Vib.*, vol. 309, no. 3–5, pp. 507–528, 2008.

[90] J. W. Lee, J. D. Kim, C. B. Yun, J. H. Yi, and J. M. Shim, “Health-monitoring method for bridges under ordinary traffic loadings,” *J. Sound Vib.*, vol. 257, no. 2, pp. 247–264, 2002.

[91] C. A. Papadopoulos and A. D. Dimarogonas, “Coupled longitudinal and bending vibrations of a rotating shaft with an open crack,” *J. Sound Vib.*, vol. 117, no. 1, pp. 81–93, 1987.

[92] C. A. Papadopoulos and A. D. Dimarogonas, “Coupling of bending and torsional vibration of a cracked Timoshenko shaft,” *Ing.-Arch.*, vol. 57, no. 4, pp. 257–266, 1987.

[93] C. A. Papadopoulos and A. D. Dimarogonas, “Coupled vibration of cracked shafts,” *J. Vib. Acoust.*, vol. 114, no. 4, pp. 461–467, 1992.

[94] W. M. Ostachowicz and M. Krawczuk, “Coupled torsional and bending vibrations of a rotor with an open crack,” *Arch. Appl. Mech.*, vol. 62, no. 3, pp. 191–201, 1992.

[95] K. R. Collins, R. H. Plaut, and J. Wauer, “Detection of cracks in rotating Timoshenko shafts using axial impulses,” *J. Vib. Acoust.*, vol. 113, no. 1, pp. 74–78, 1991.

[96] Moghadam, A. and Melhem, H., “Analytical and Experimental Verification of a Proposed Ambient Vibration-Based Approach to Extract Pseudo-Free-Vibration Response,” presented at the Society for Experimental Mechanics, Orlando, Florida, USA, 2019.

[97] Moghadam A., Esmaeily A., and Melhem H., “A numerical study on a proposed signal processing-based approach for damage detection of steel structures,” presented at the Engineering Mechanics Institute (EMI), Massachusetts Institute of Technology, Boston, USA, 2018.

[98] A. K. Chopra and A. K. Chopra, *Dynamics of structures: theory and applications to earthquake engineering*, vol. 3. Pearson/Prentice Hall Upper Saddle River, NJ, 2007.

[99] H. Abaqus, "Karlsson and Sorensen," *Inc Pawtuck. RI*, vol. 2860, 1998.

[100] A. Moghadam, H. E. Estekanchi, and M. Yekrangnia, "Evaluation of PR steel frame connection with torsional plate and its optimal placement," *Sci. Iran.*, vol. 25, no. 3, pp. 1025–1038, Jun. 2018.

[101] I. Mathworks, "MATLAB: R2014a," *Mathworks Inc Natick*, 2014.

Appendix A - Pseudo-Free-Vibration and FFT Diagrams for Changing Δt_1 while u_0 is constant

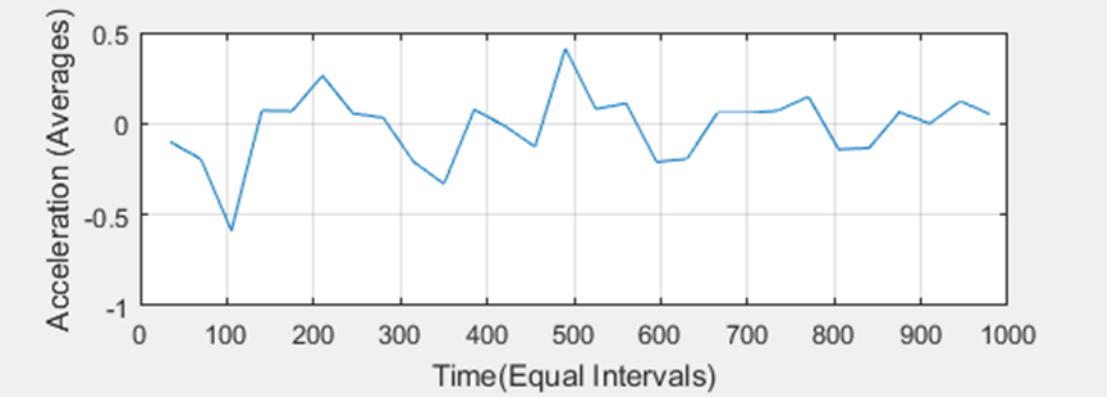

Figure A.1 Signal processing results of structure one subjected to dynamic load one (pseudo-free-vibration response diagram-Δt_1= 3.5%, u_0= 0.1D_{max})

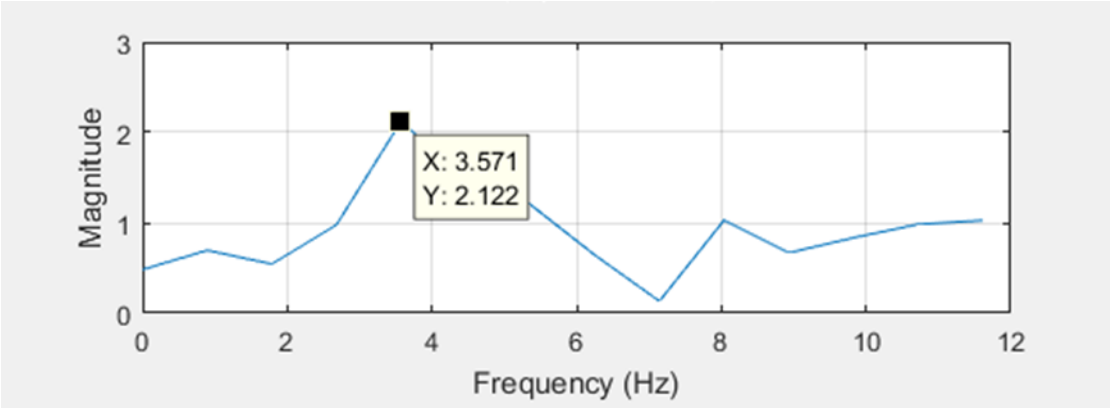

Figure A.2 Signal processing results of structure one subjected to dynamic load one (FFT diagram- Δt_1= 3.5%, u_0= 0.1D_{max})

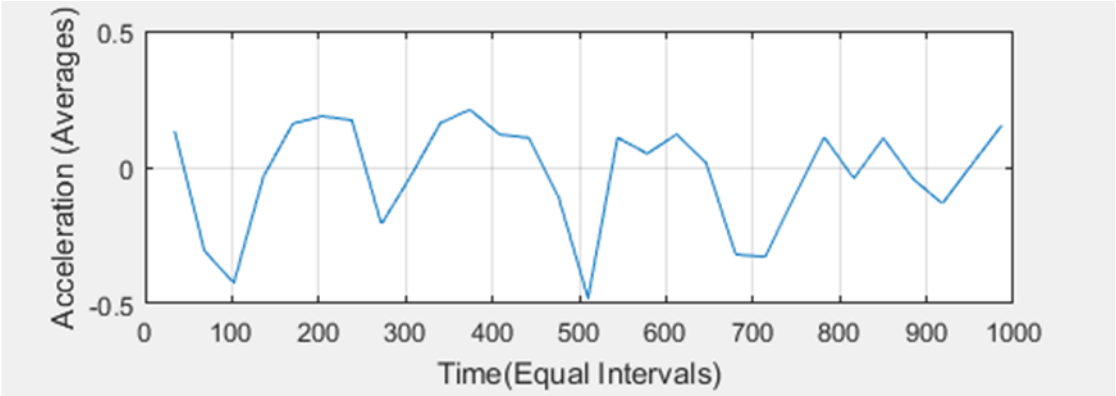

Figure A.3 Signal processing results of structure one subjected to dynamic load one (pseudo-free-vibration response diagram- Δt_1= 3.4%, u_0= 0.1D_{max})

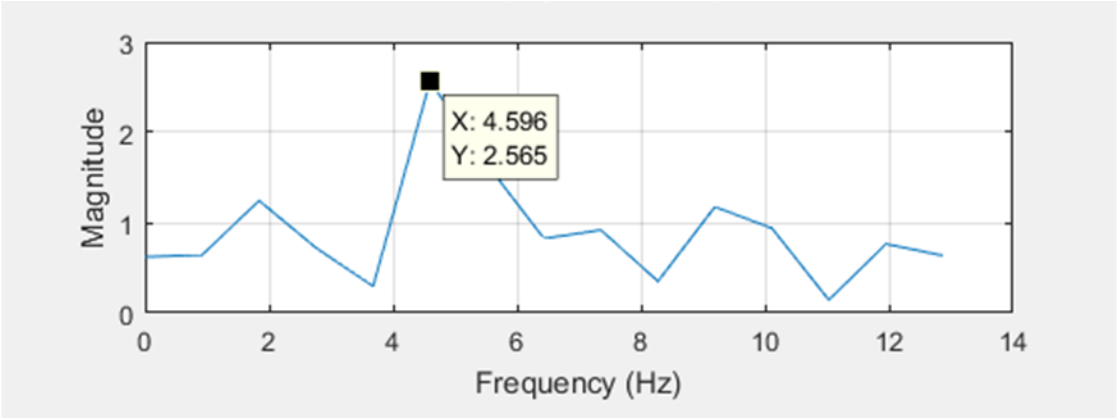

Figure A.4 Signal processing results of structure one subjected to dynamic load one (FFT diagram- Δt_1= 3.4%, u_0= 0.1D_{max})

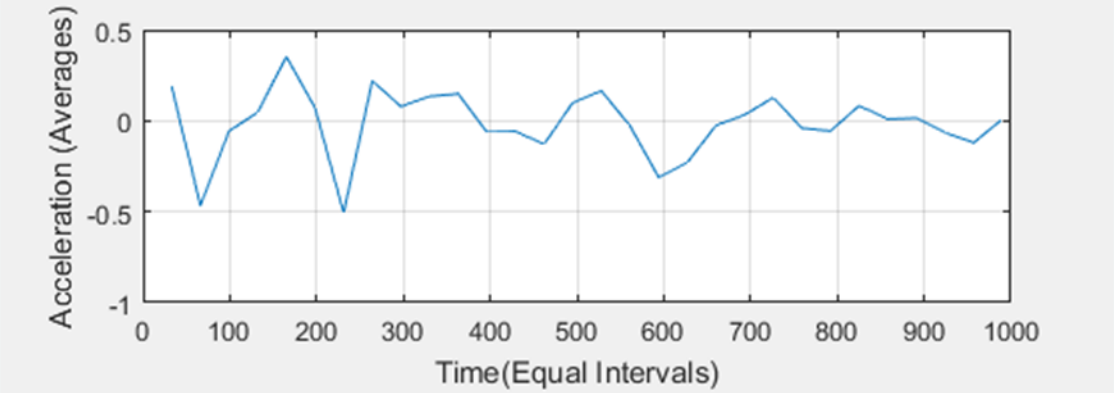

Figure A.5 Signal processing results of structure one subjected to dynamic load one (pseudo-free-vibration response diagram- Δt_1= 3.3%, u_0= 0.1D_{max})

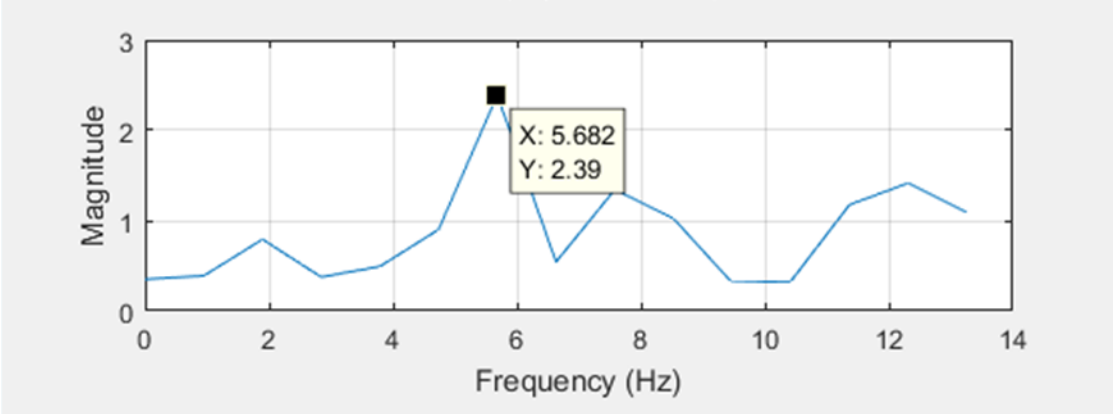

Figure A.6 Signal processing results of structure one subjected to dynamic load one (FFT diagram- Δt_1= 3.3%, u_0= 0.1D_{max})

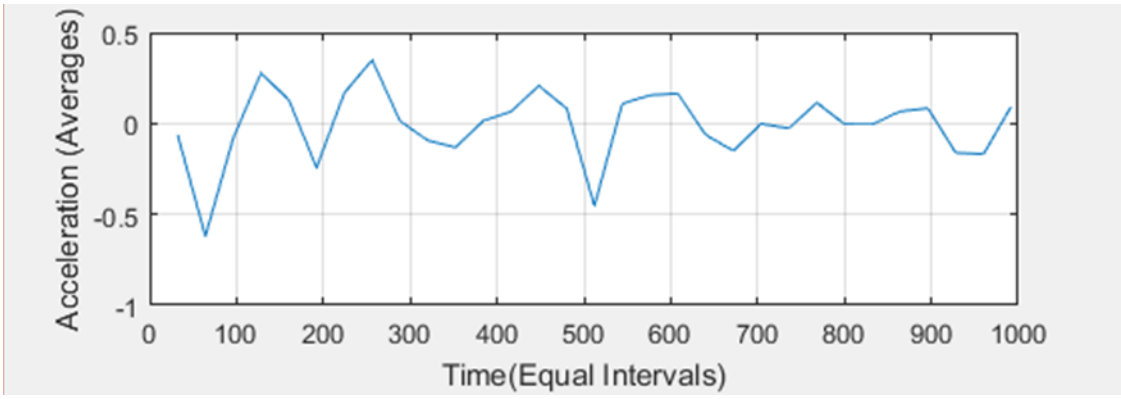

Figure A.7 Signal processing results of structure one subjected to dynamic load one (pseudo-free-vibration response diagram- Δt_1= 3.2%, u_0= 0.1D_{max})

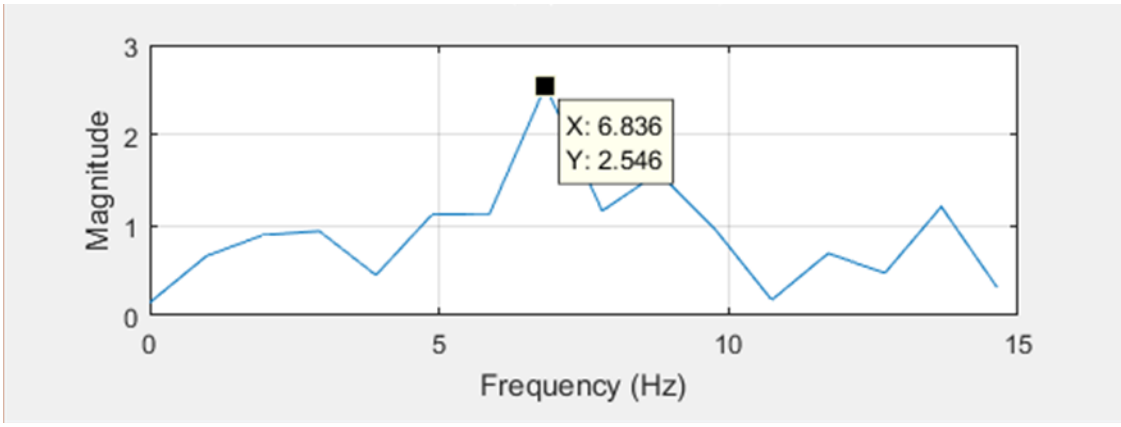

Figure A.8 Signal processing results of structure one subjected to dynamic load one (FFT diagram- Δt_1= 3.2%, u_0= 0.1D_{max})

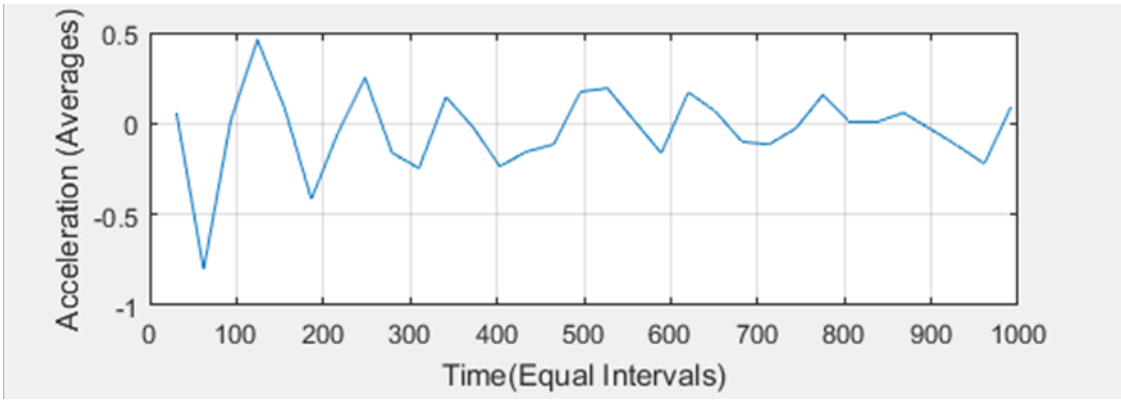

Figure A.9 Signal processing results of structure one subjected to dynamic load one (pseudo-free-vibration response diagram- Δt_1= 3.1%, u_0= 0.1D_{max})

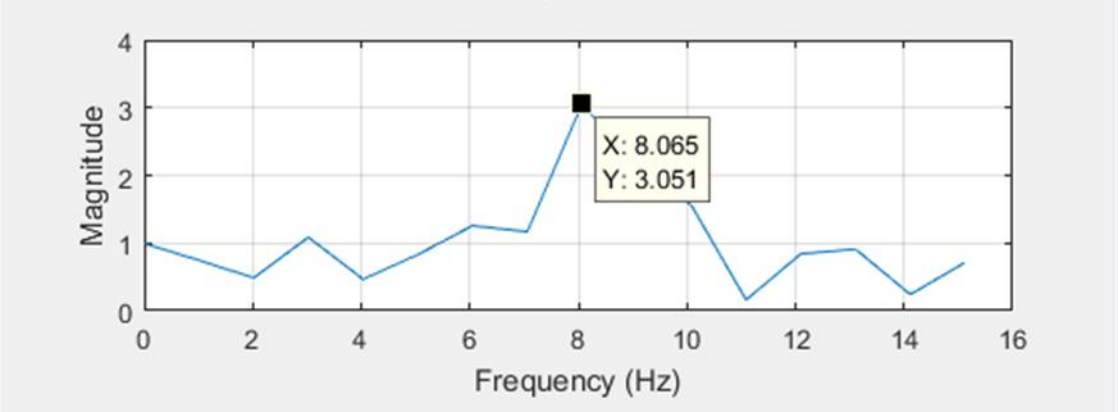

Figure A.10 Signal processing results of structure one subjected to dynamic load one (FFT diagram- Δt_1= 3.1%, u_0= 0.1D_{max})

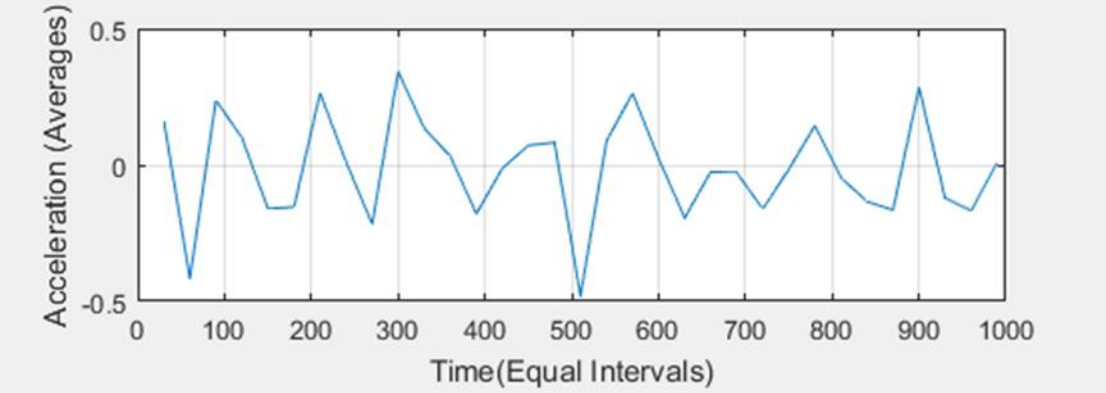

Figure A.11 Signal processing results of structure one subjected to dynamic load one (pseudo-free-vibration response diagram- Δt_1= 3.0%, u_0= 0.1D_{max})

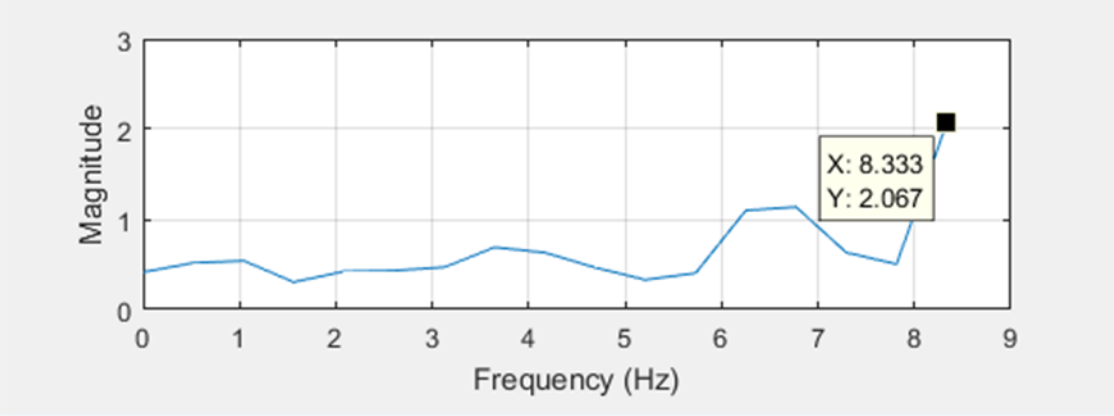

Figure A.12 Signal processing results of structure one subjected to dynamic load one (FFT diagram- Δt_1= 3.0%, u_0= 0.1D_{max})

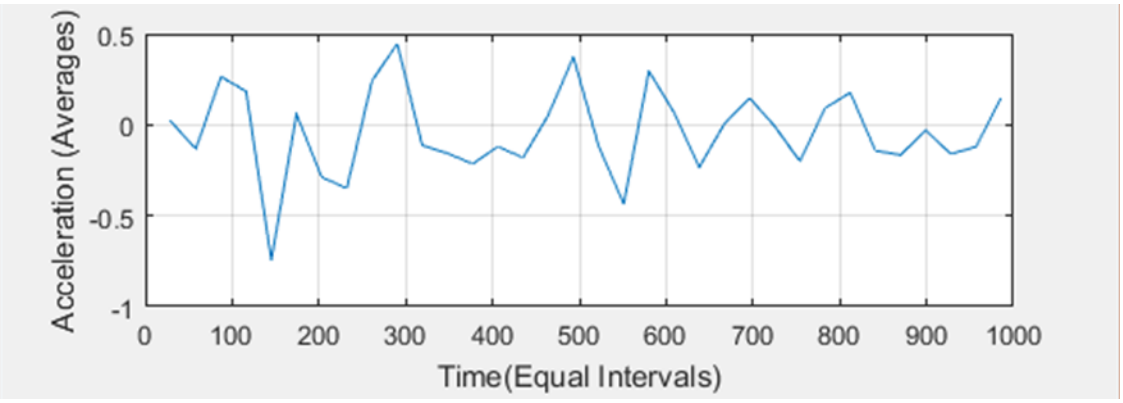

Figure A.13 Signal processing results of structure one subjected to dynamic load one (pseudo-free-vibration response diagram- Δt_1= 2.9%, u_0= 0.1D_{max})

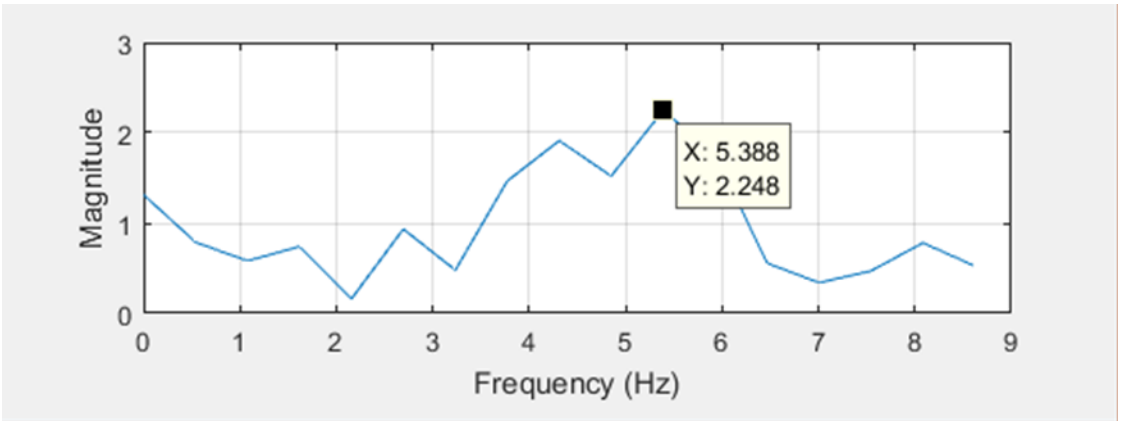

Figure A.14 Signal processing results of structure one subjected to dynamic load one (FFT diagram- Δt_1= 2.9%, u_0= 0.1D_{max})

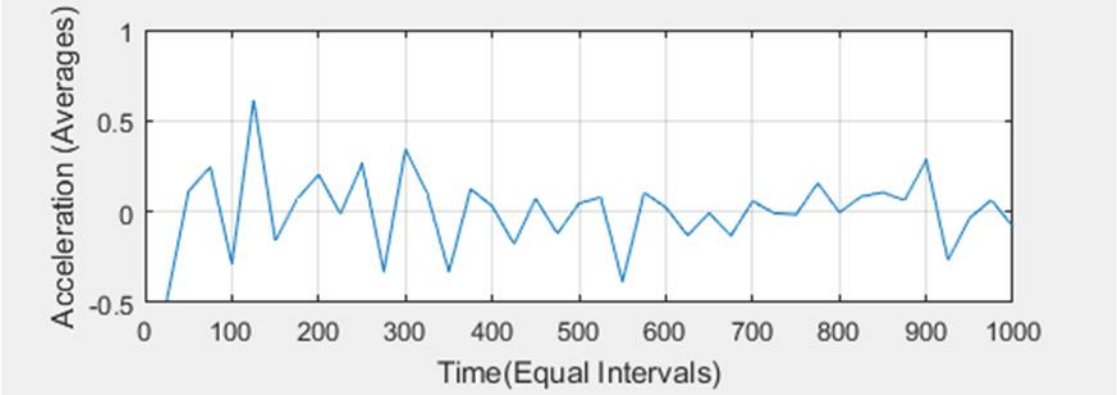

Figure A.15 Signal processing results of structure one subjected to dynamic load one (pseudo-free-vibration response diagram- Δt_1= 2.5%, u_0= 0.1D_{max})

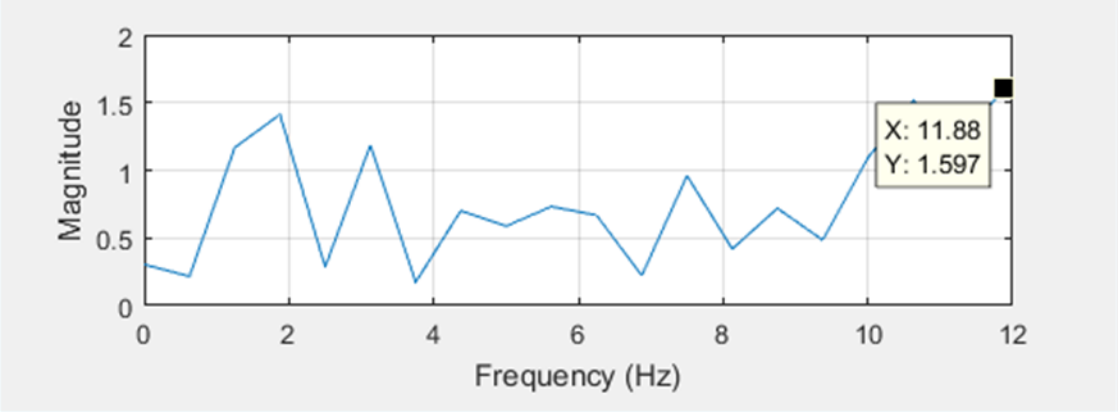

Figure A.16 Signal processing results of structure one subjected to dynamic load one (FFT diagram- Δt_1= 2.5%, u_0= 0.1D_{max})

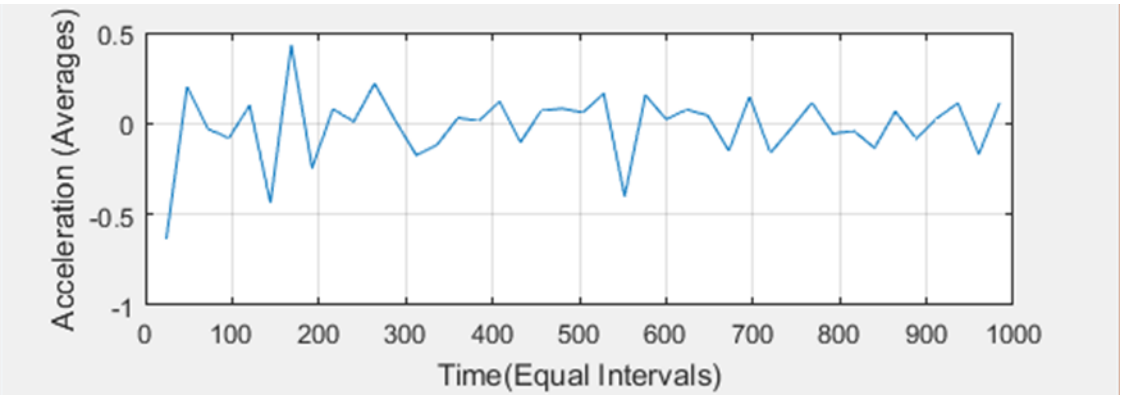

Figure A.17 Signal processing results of structure one subjected to dynamic load one (pseudo-free-vibration response diagram- Δt_1= 2.4%, u_0= 0.1D_{max})

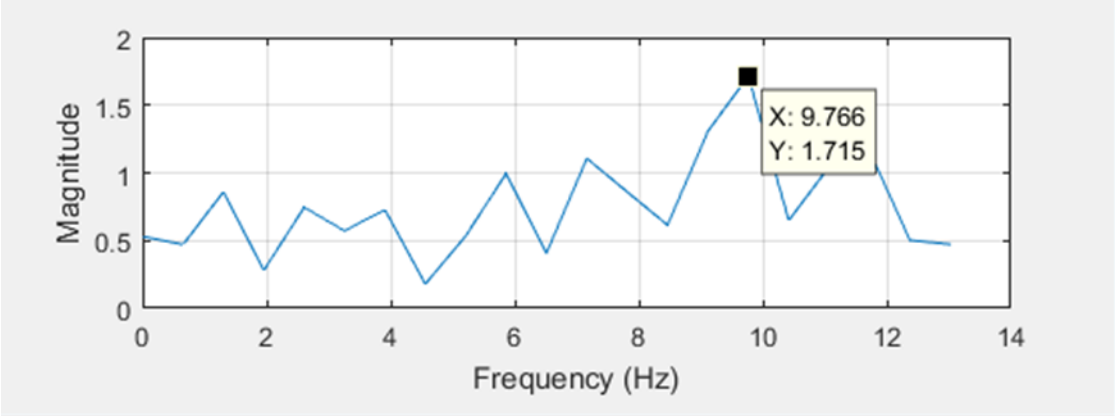

Figure A.18 Signal processing results of structure one subjected to dynamic load one (FFT diagram- Δt_1= 2.4%, u_0= 0.1D_{max})

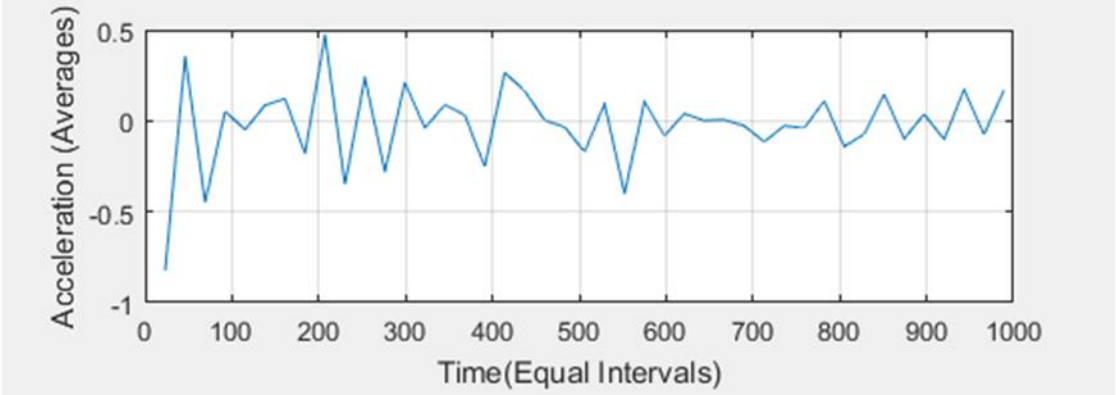

Figure A.19 Signal processing results of structure one subjected to dynamic load one (pseudo-free-vibration response diagram- Δt_1= 2.3%, u_0= 0.1D_{max})

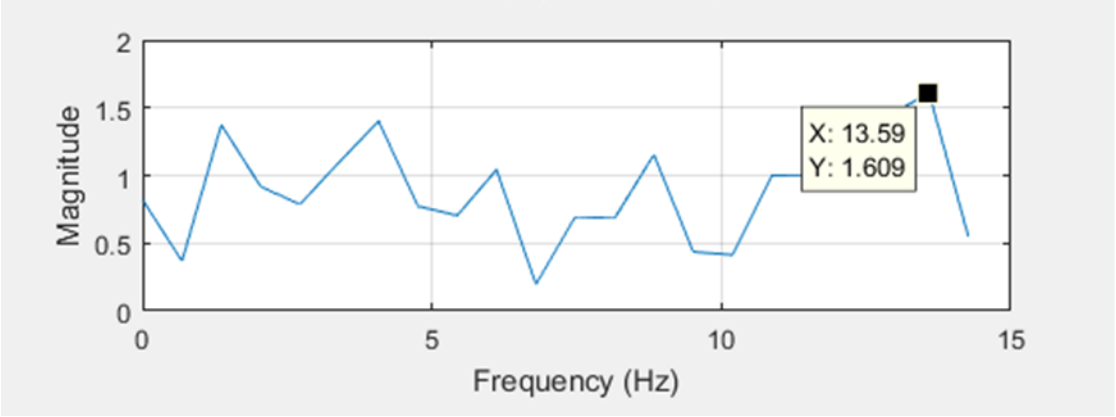

Figure A.20 Signal processing results of structure one subjected to dynamic load one (FFT diagram- Δt_1= 2.3%, u_0= 0.1D_{max})

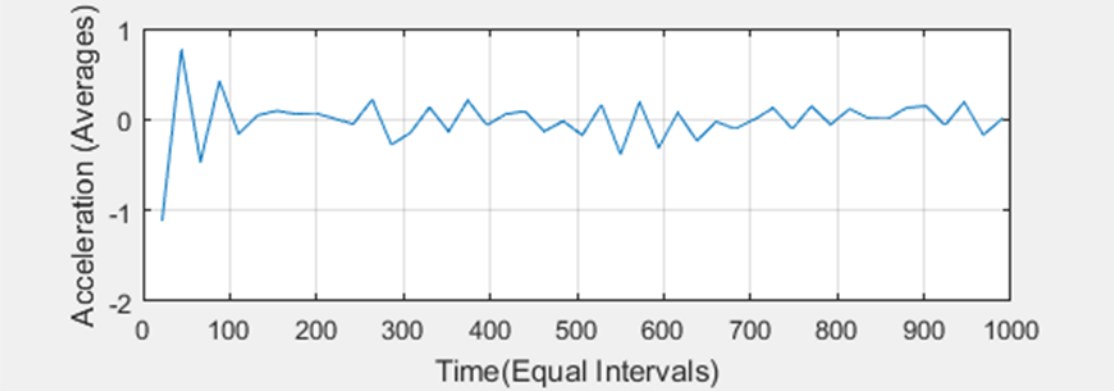

Figure A.21 Signal processing results of structure one subjected to dynamic load one (pseudo-free-vibration response diagram- Δt_1= 2.2%, u_0= 0.1D_{max})

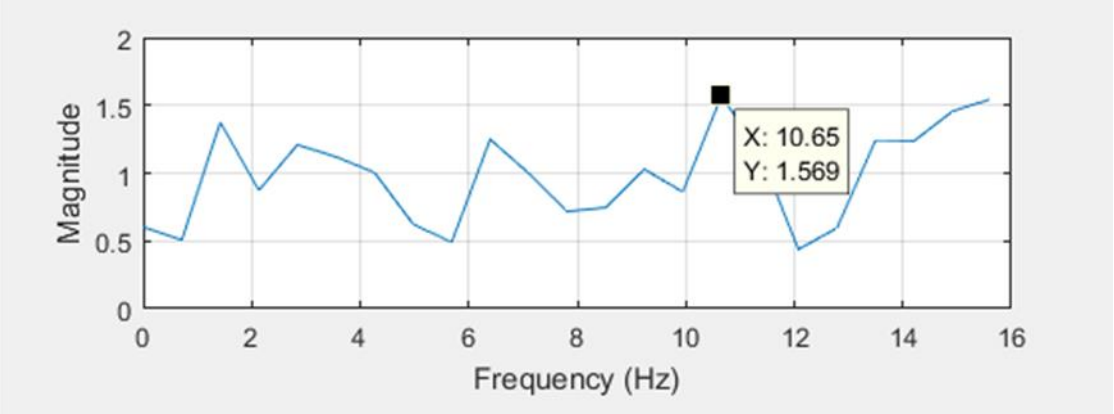

Figure A.22 Signal processing results of structure one subjected to dynamic load one (FFT diagram- Δt_1= 2.2%, u_0= 0.1D_{max})

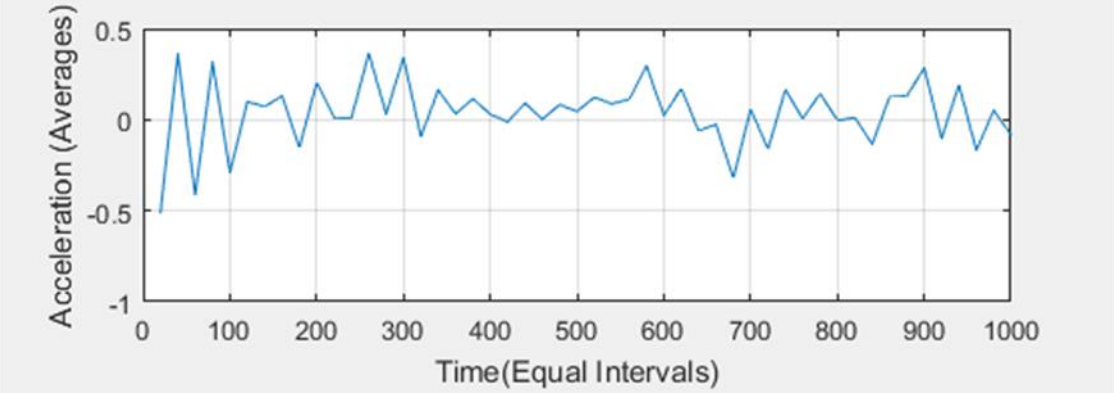

Figure A.23 Signal processing results of structure one subjected to dynamic load one (pseudo-free-vibration response diagram- Δt_1= 2.0%, u_0= 0.1D_{max})

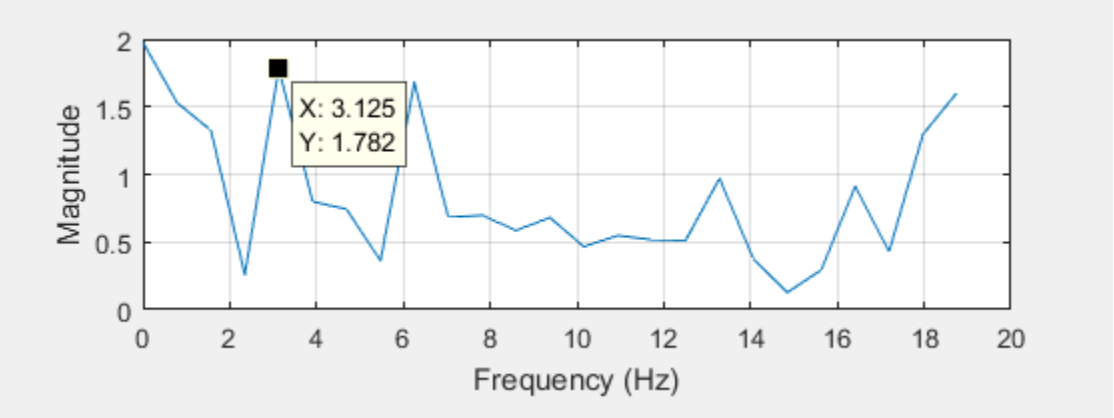

Figure A.24 Signal processing results of structure one subjected to dynamic load one (FFT diagram- Δt_1= 2.0%, u_0= 0.1D_{max})

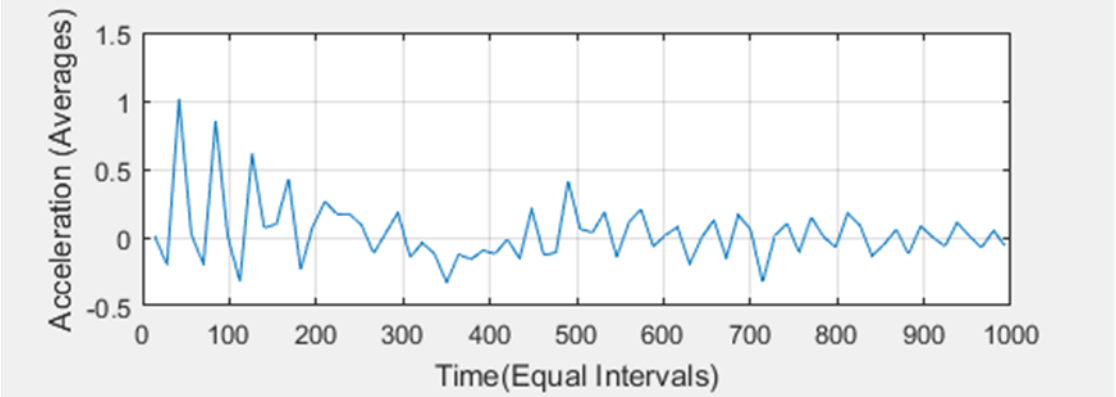

Figure A.25 Signal processing results of structure one subjected to dynamic load one (pseudo-free-vibration response diagram- Δt_1= 1.4%, u_0= 0.1D_{max})

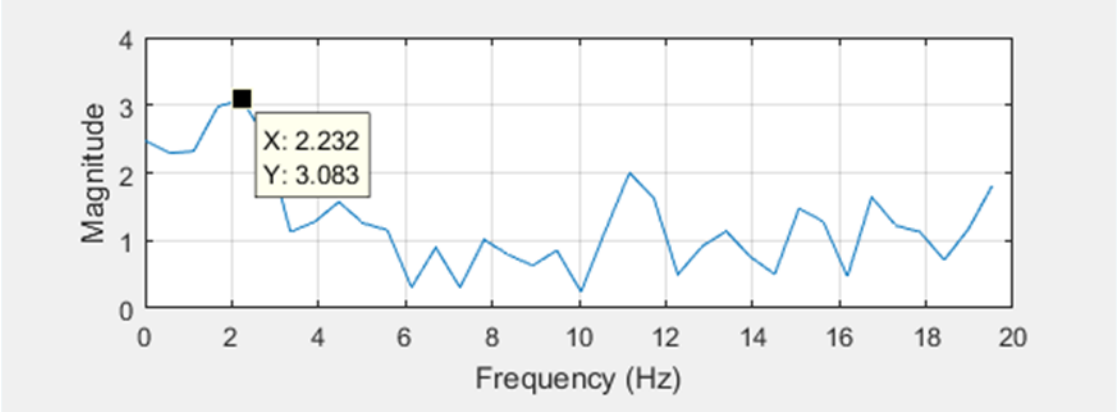

Figure A.26 Signal processing results of structure one subjected to dynamic load one (FFT diagram- Δt_1= 1.4%, u_0= 0.1D_{max})

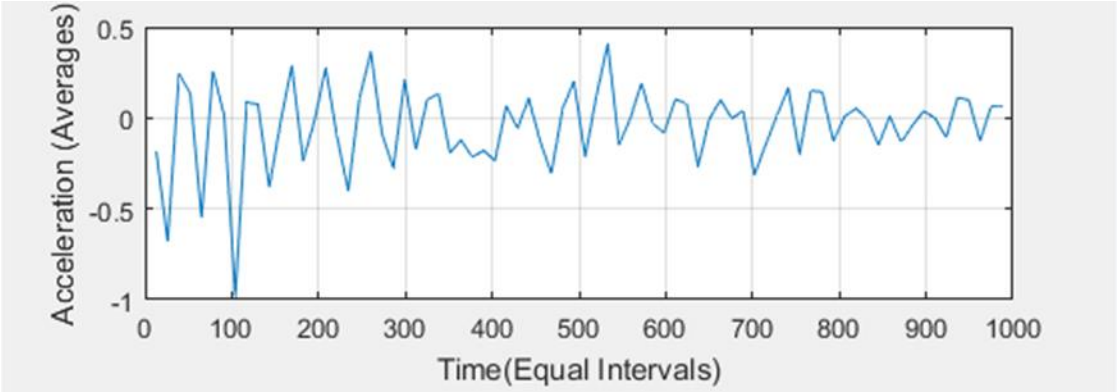

Figure A.27 Signal processing results of structure one subjected to dynamic load one (pseudo-free-vibration response diagram- Δt_1= 1.3%, u_0= 0.1D_{max})

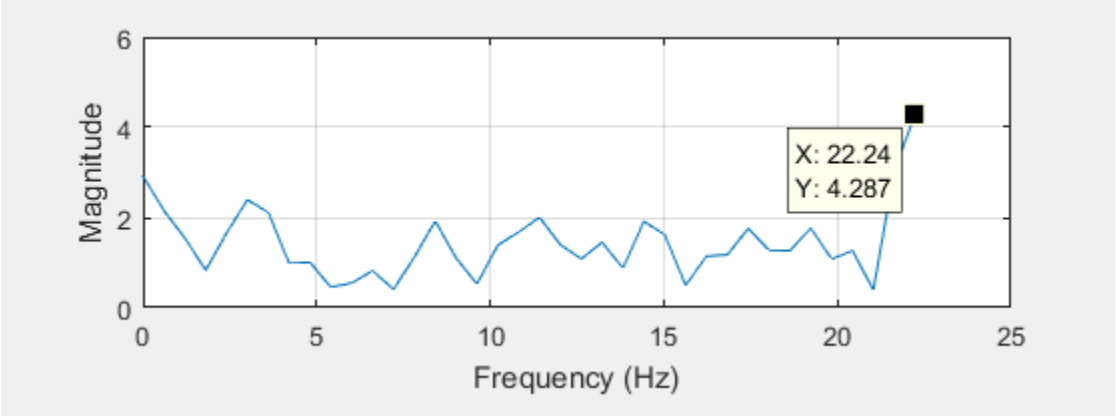

Figure A.28 Signal processing results of structure one subjected to dynamic load one (FFT diagram- Δt_1= 1.3%, u_0= 0.1D_{max})

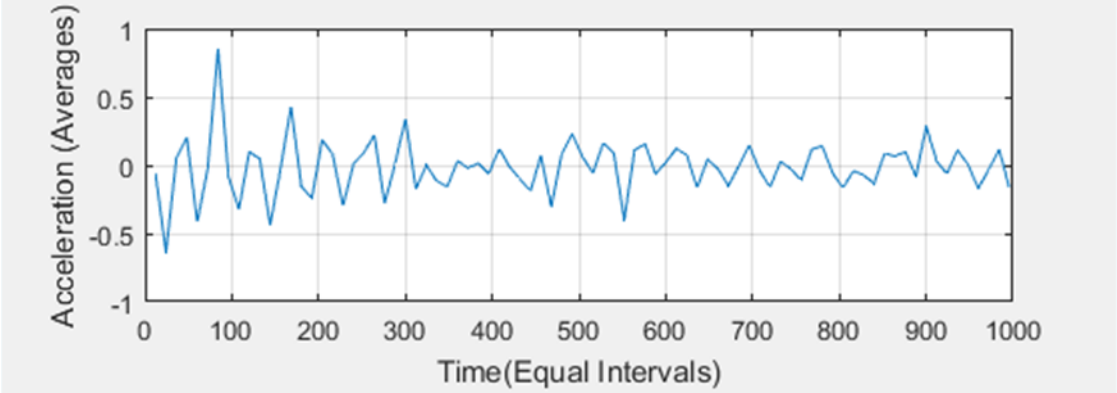

Figure A.29 Signal processing results of structure one subjected to dynamic load one (pseudo-free-vibration response diagram- Δt_1= 1.2%, u_0= 0.1D_{max})

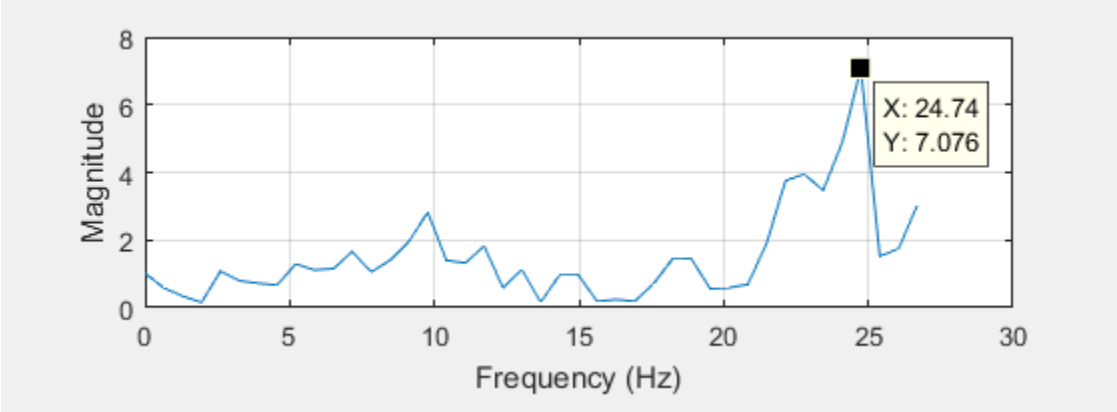

Figure A.30 Signal processing results of structure one subjected to dynamic load one (FFT diagram- Δt_1= 1.2%, u_0= 0.1D_{max})

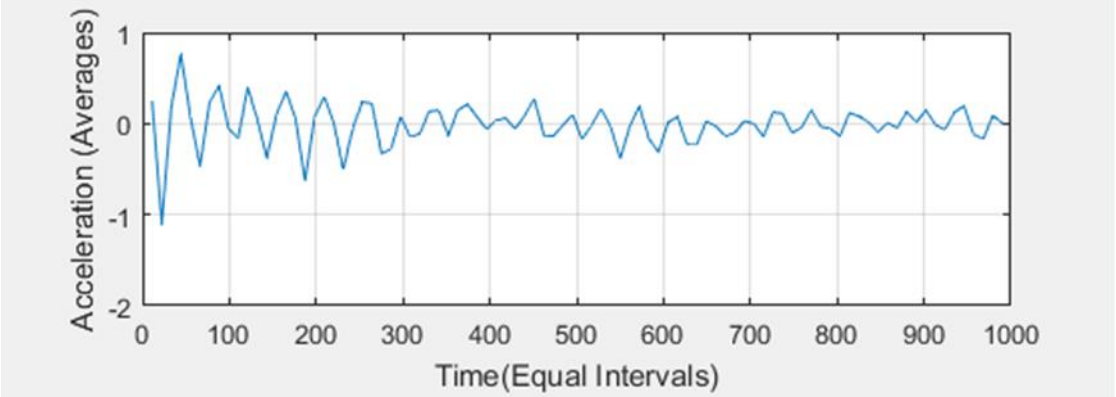

Figure A.31 Signal processing results of structure one subjected to dynamic load one (pseudo-free-vibration response diagram- Δt_1= 1.1%, u_0= 0.1D_{max})

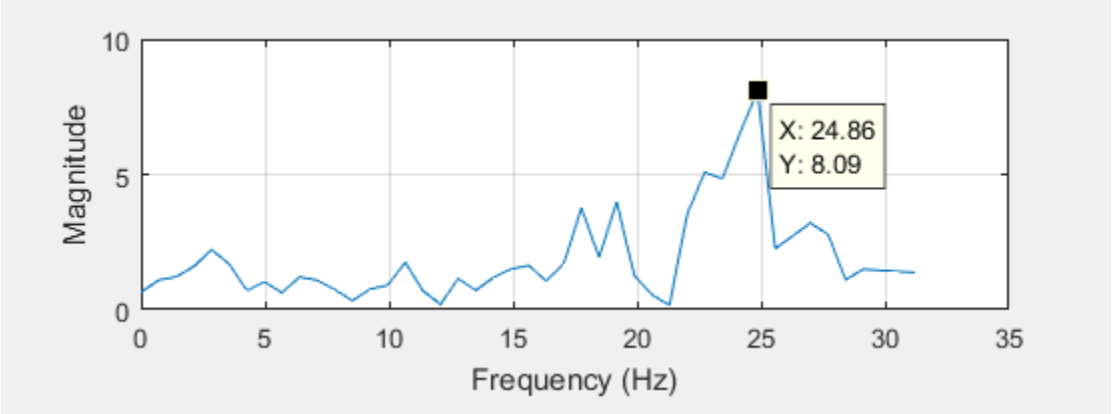

Figure A.32 Signal processing results of structure one subjected to dynamic load one (FFT diagram- Δt_1= 1.1%, u_0= 0.1D_{max})

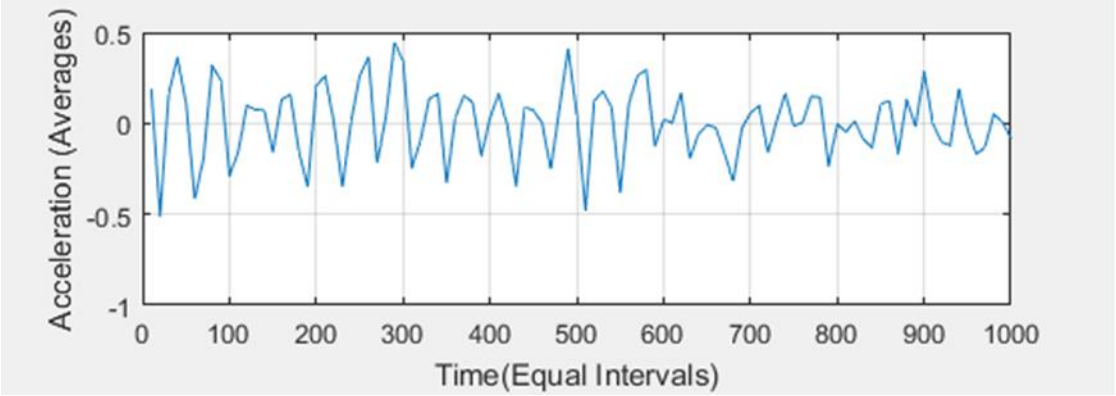

Figure A.33 Signal processing results of structure one subjected to dynamic load one (pseudo-free-vibration response diagram- Δt_1= 1.0%, u_0= 0.1D_{max})

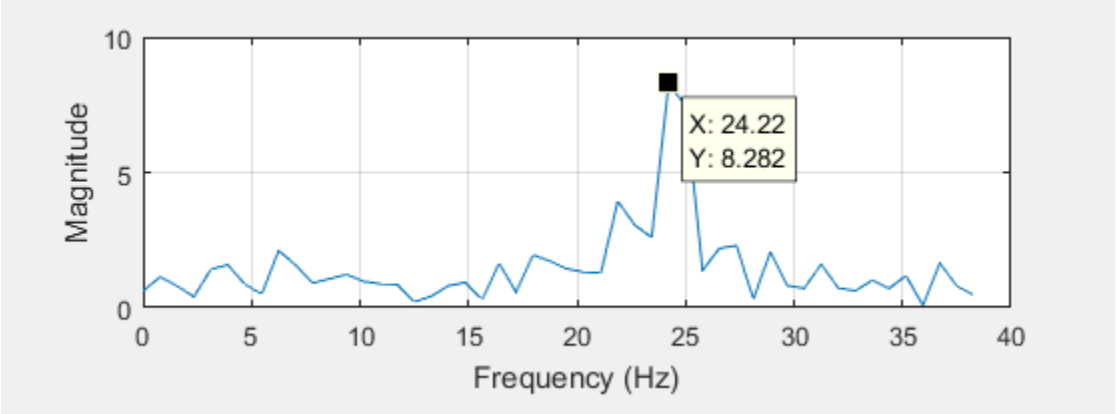

Figure A.34 Signal processing results of structure one subjected to dynamic load one (FFT diagram- Δt_1= 1.0%, u_0= 0.1D_{max})

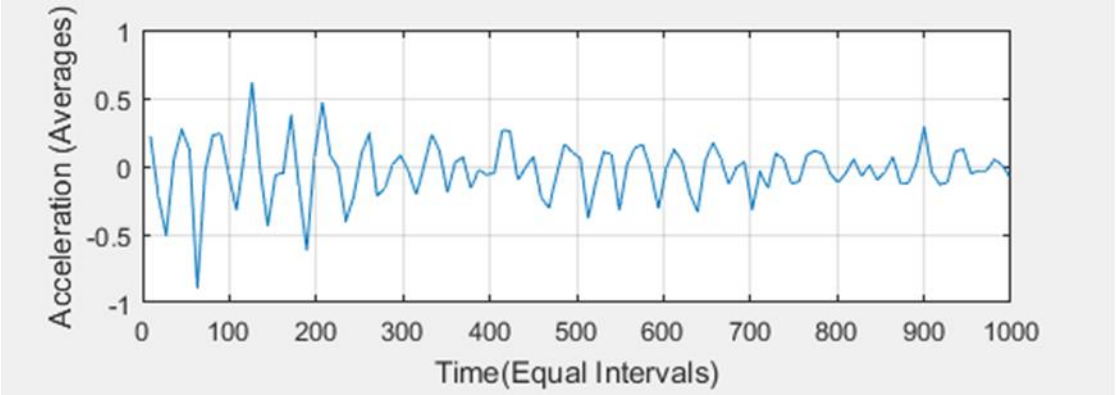

Figure A.35 Signal processing results of structure one subjected to dynamic load one (pseudo-free-vibration response diagram- Δt_1= 0.9%, u_0= 0.1D_{max})

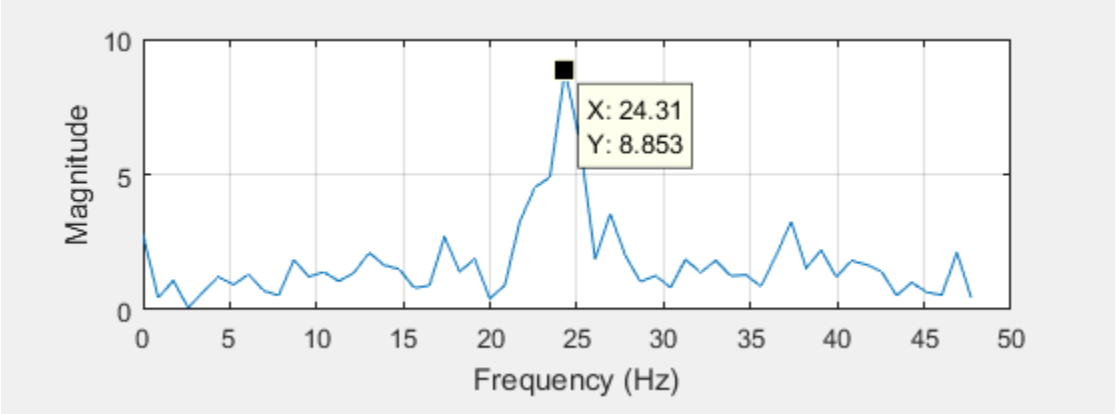

Figure A.36 Signal processing results of structure one subjected to dynamic load one (FFT diagram- Δt_1= 0.9%, u_0= 0.1D_{max})

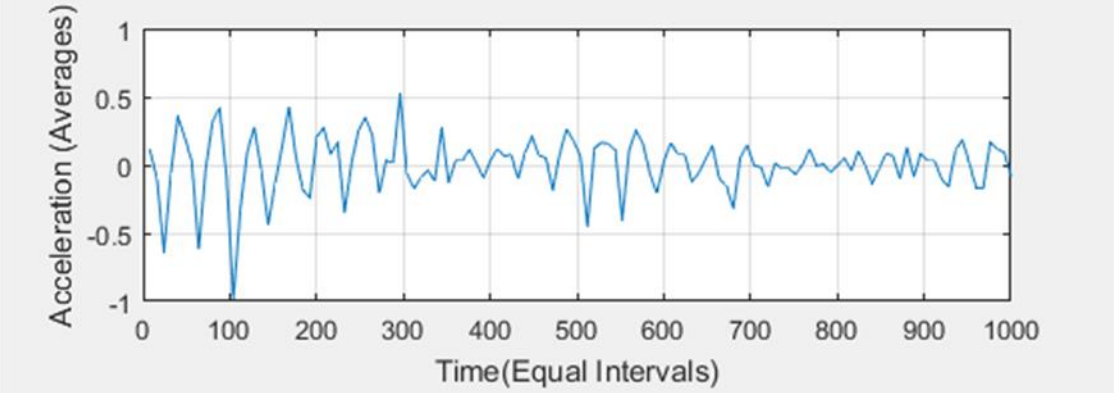

Figure A.37 Signal processing results of structure one subjected to dynamic load one (pseudo-free-vibration response diagram- Δt_1= 0.8%, u_0= 0.1D_{max})

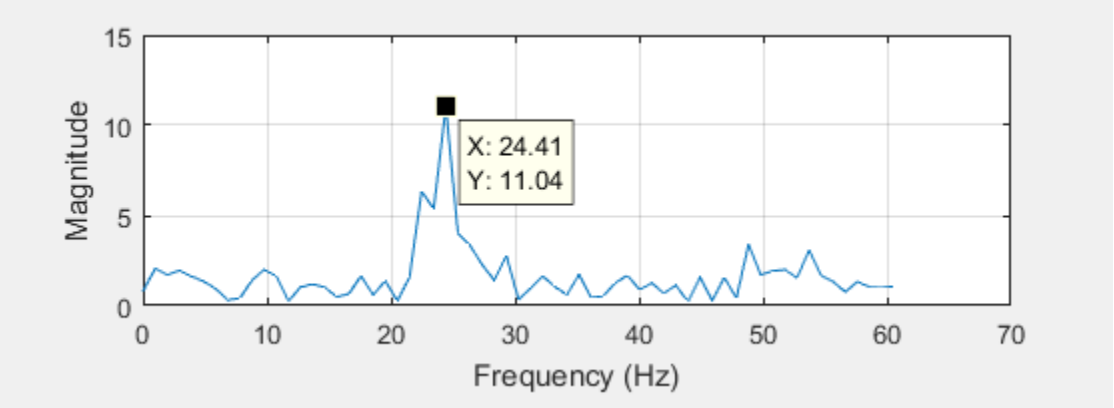

Figure A.38 Signal processing results of structure one subjected to dynamic load one (FFT diagram- Δt_1= 0.8%, u_0= 0.1D_{max})

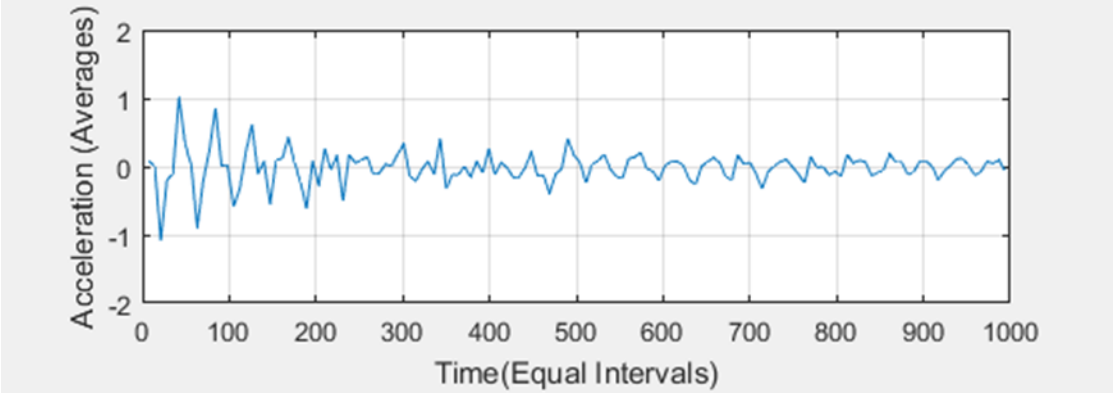

Figure A.39 Signal processing results of structure one subjected to dynamic load one (pseudo-free-vibration response diagram- Δt_1= 0.7%, u_0= 0.1D_{max})

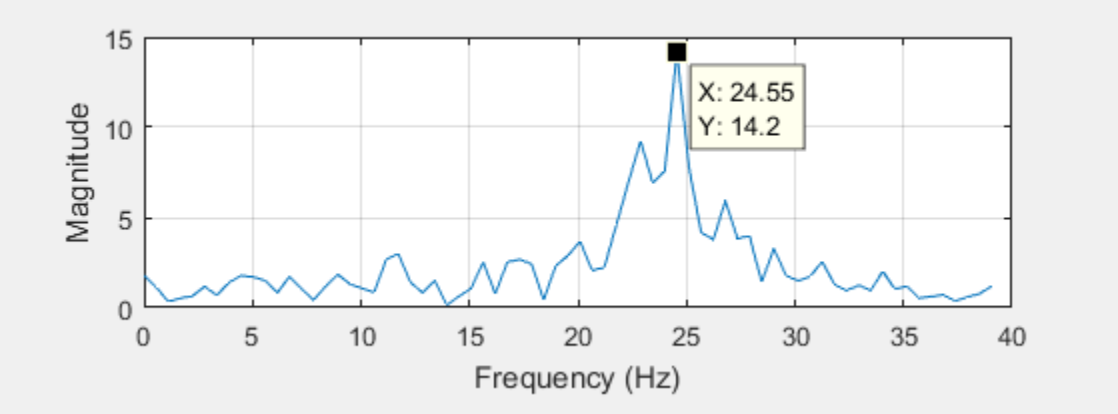

Figure A.40 Signal processing results of structure one subjected to dynamic load one (FFT diagram- Δt_1= 0.7%, u_0= 0.1D_{max})

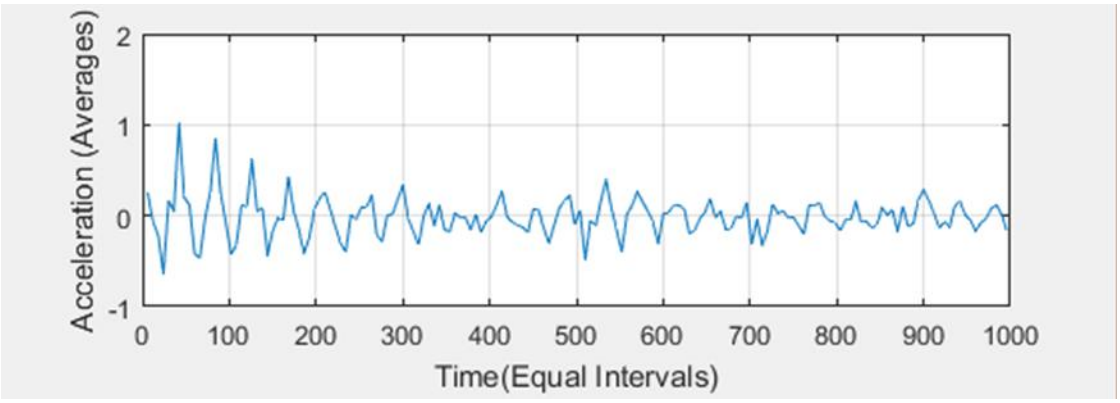

Figure A.41 Signal processing results of structure one subjected to dynamic load one (pseudo-free-vibration response diagram- Δt_1= 0.6%, u_0= 0.1D_{max})

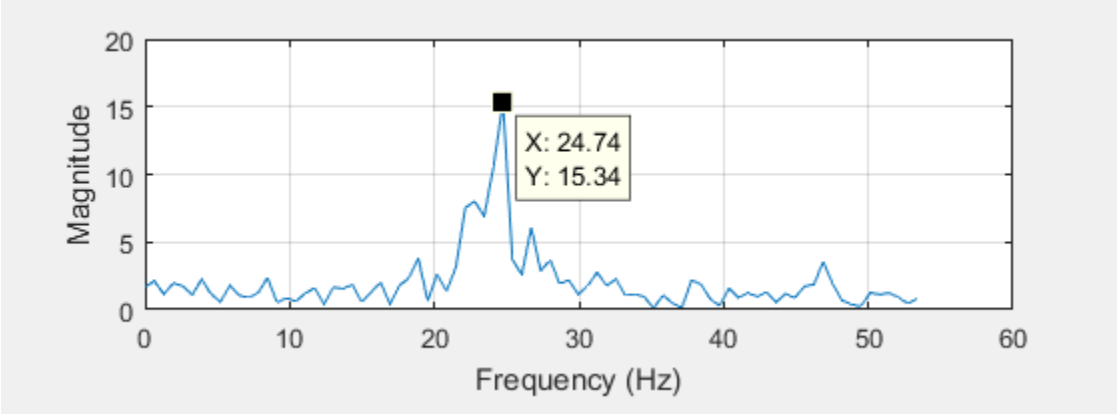

Figure A.42 Signal processing results of structure one subjected to dynamic load one (FFT diagram- Δt_1= 0.6%, u_0= 0.1D_{max})

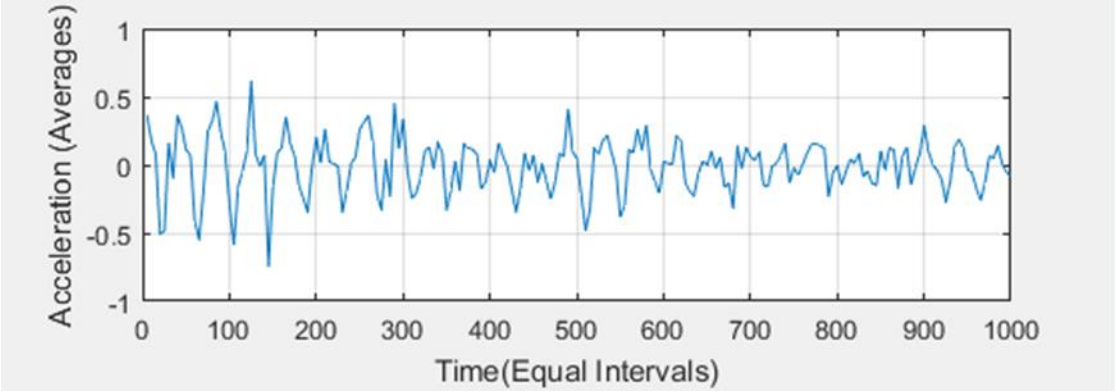

Figure A.43 Signal processing results of structure one subjected to dynamic load one (pseudo-free-vibration response diagram- Δt_1= 0.5%, u_0= 0.1D_{max})

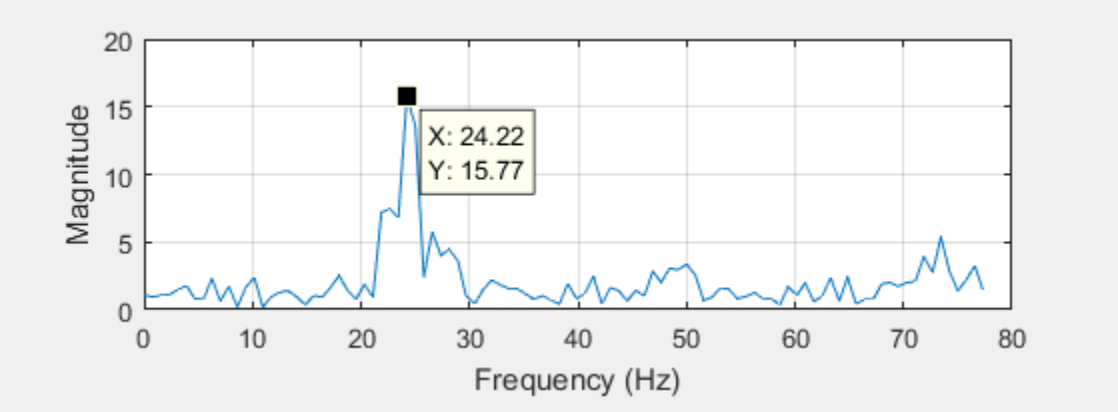

Figure A.44 Signal processing results of structure one subjected to dynamic load one (FFT diagram- Δt_1= 0.5%, u_0= 0.1D_{max})

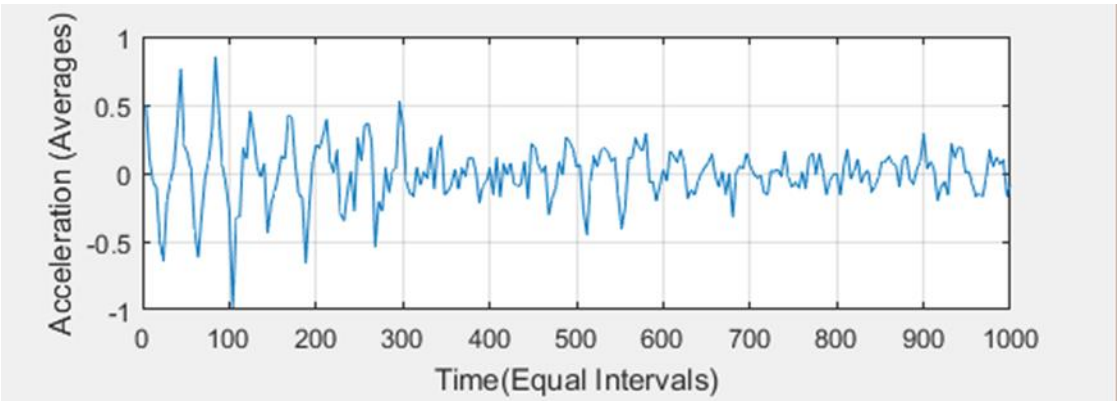

Figure A.45 Signal processing results of structure one subjected to dynamic load one (pseudo-free-vibration response diagram- Δt_1= 0.4%, u_0= 0.1D_{max})

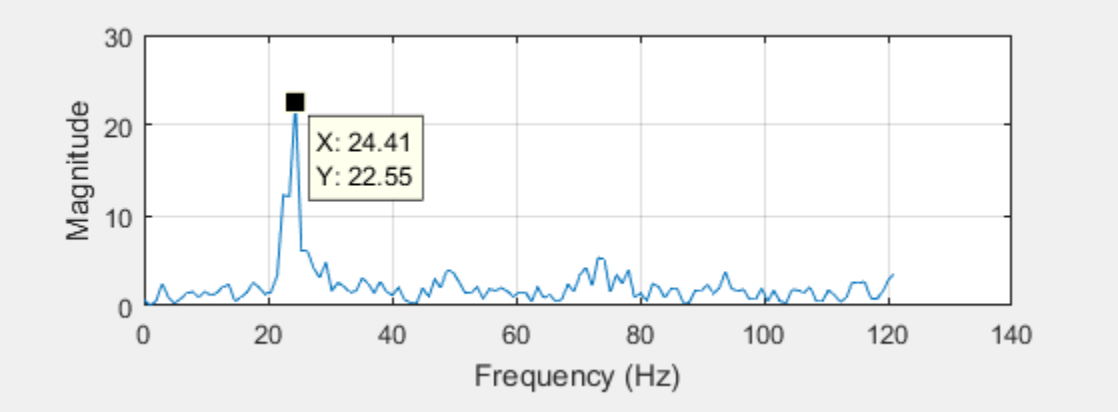

Figure A.46 Signal processing results of structure one subjected to dynamic load one (FFT diagram- Δt_1= 0.4%, u_0= 0.1D_{max})

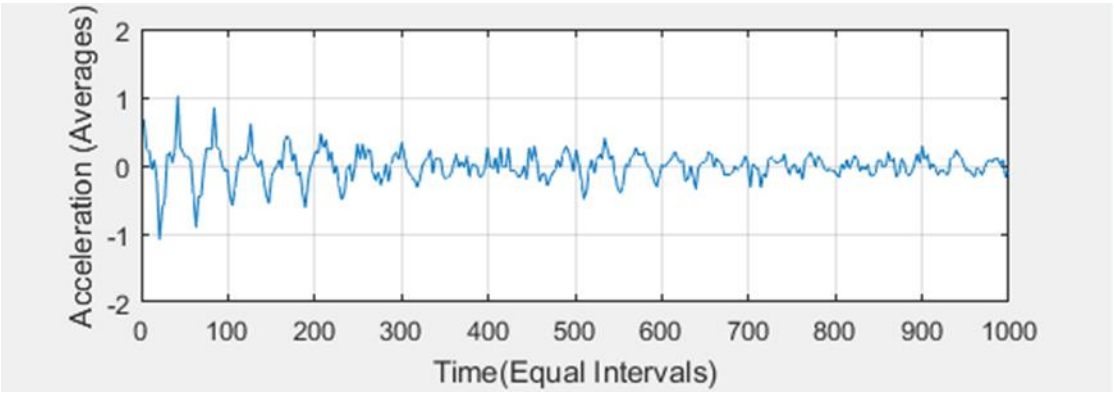

Figure A.47 Signal processing results of structure one subjected to dynamic load one (pseudo-free-vibration response diagram- Δt_1= 0.3%, u_0= 0.1D_{max})

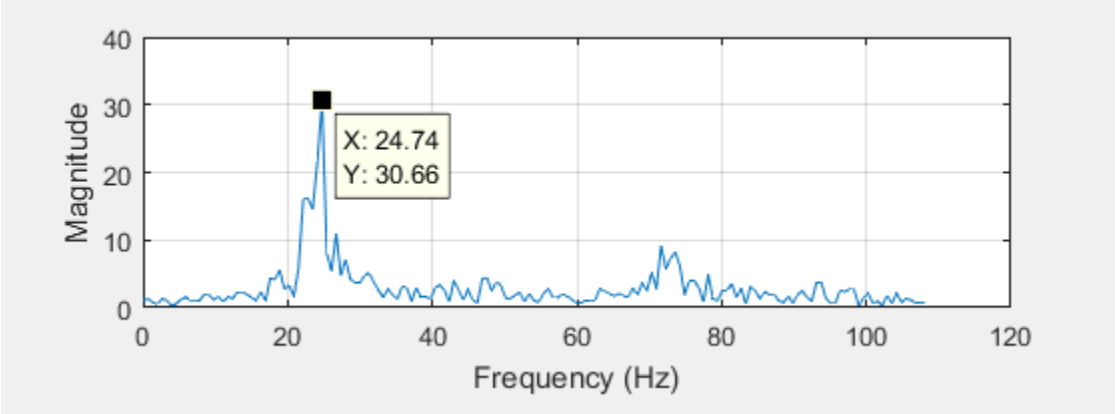

Figure A.48 Signal processing results of structure one subjected to dynamic load one (FFT diagram- Δt_1= 0.3%, u_0= 0.1D_{max})

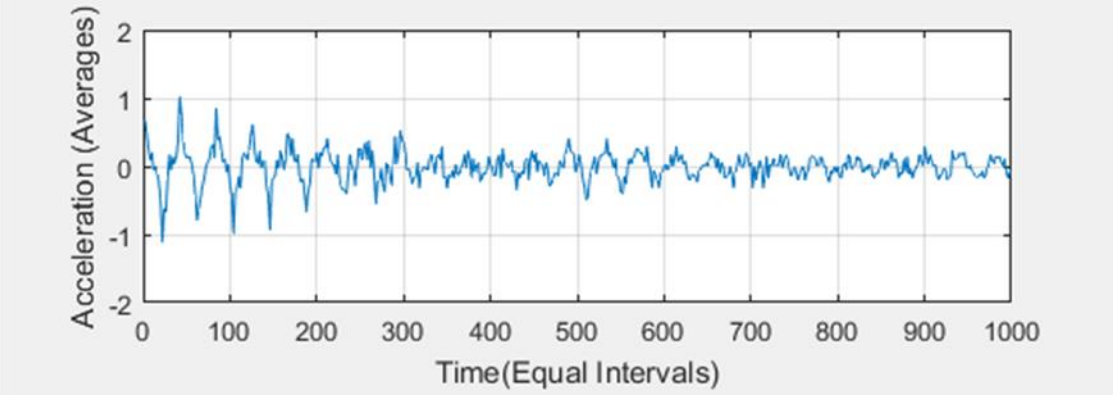

Figure A.49 Signal processing results of structure one subjected to dynamic load one (pseudo-free-vibration response diagram- Δt_1= 0.2%, u_0= 0.1D_{max})

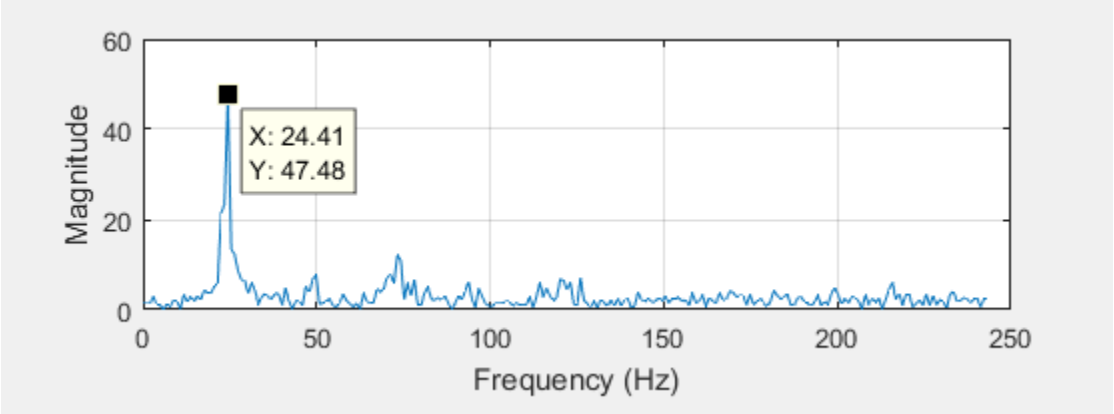

Figure A.50 Signal processing results of structure one subjected to dynamic load one (FFT diagram- Δt_1= 0.2%, u_0= 0.1D_{max})

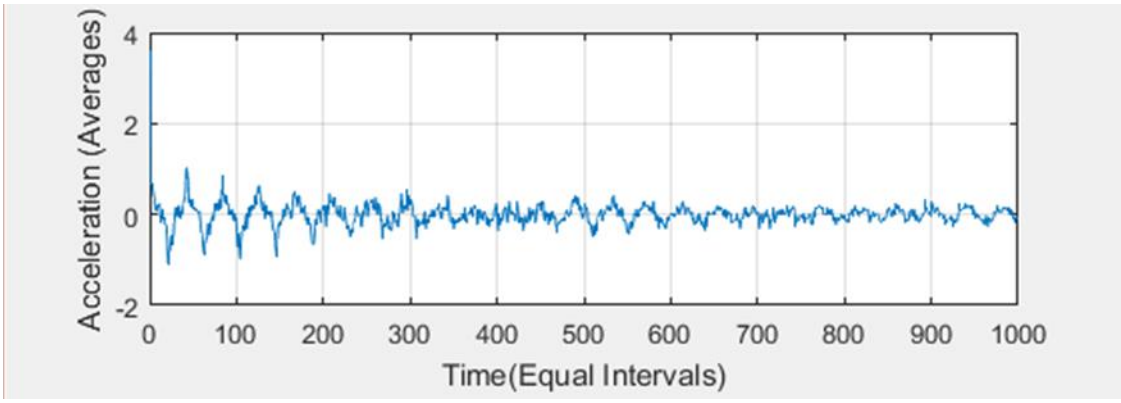

Figure A.51 Signal processing results of structure one subjected to dynamic load one (pseudo-free-vibration response diagram- Δt_1= 0.1%, u_0= 0.1D_{max})

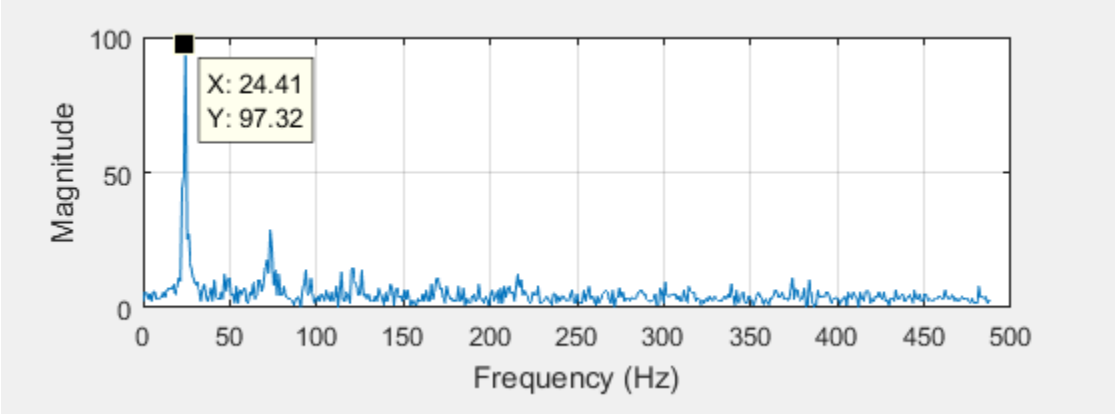

Figure A.52 Signal processing results of structure one subjected to dynamic load one (FFT diagram- Δt_1= 0.1%, u_0= 0.1D_{max})

Appendix B - Pseudo-free-vibration and FFT Diagrams for changing u_0 while Δt_1 is constant

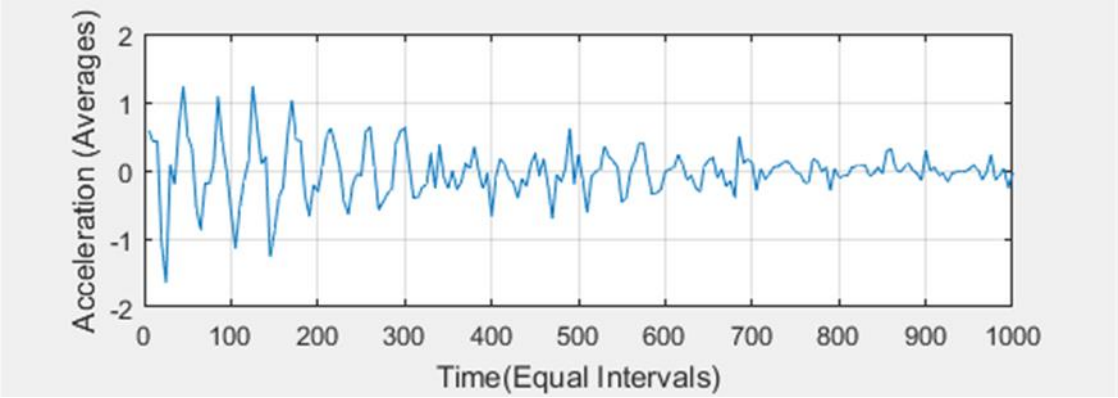

Figure B.1 Signal processing results of structure one subjected to dynamic load one (pseudo-free-vibration response diagram- Δt_1= 0.5%, u_0= (1/2)*D_{max})

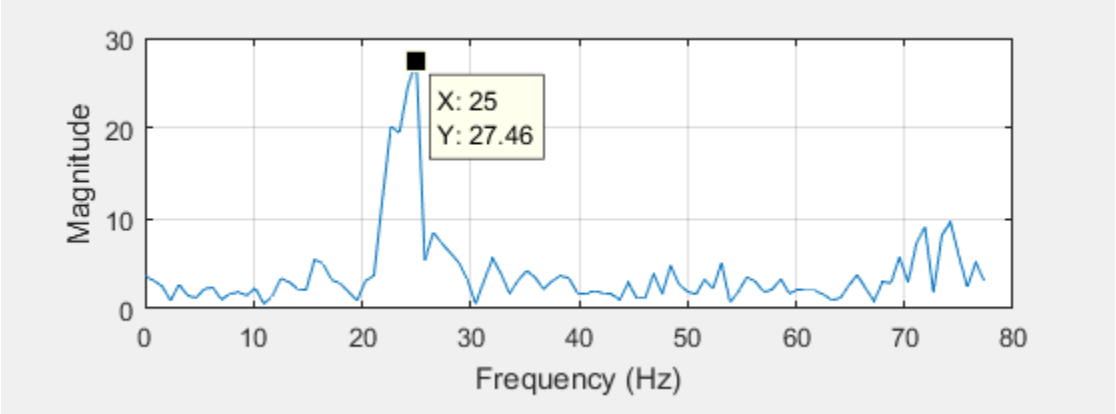

Figure B.2 Signal processing results of structure one subjected to dynamic load one (FFT diagram- Δt_1= 0.5%, u_0= (1/2)*D_{max})

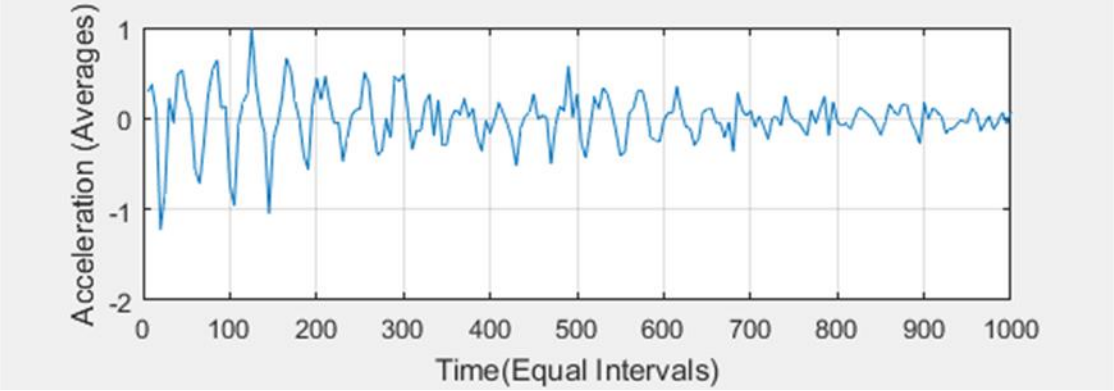

Figure B.3 Signal processing results of structure one subjected to dynamic load one (pseudo-free-vibration response diagram- Δt_1= 0.5%, u_0= (1/3)*D_{max})

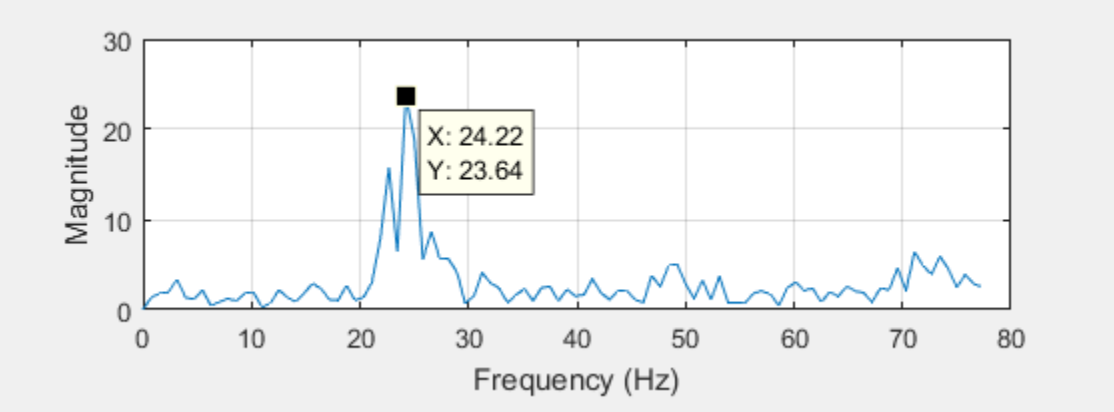

Figure B.4 Signal processing results of structure one subjected to dynamic load one (FFT diagram- Δt_1= 0.5%, u_0= (1/3)*D_{max})

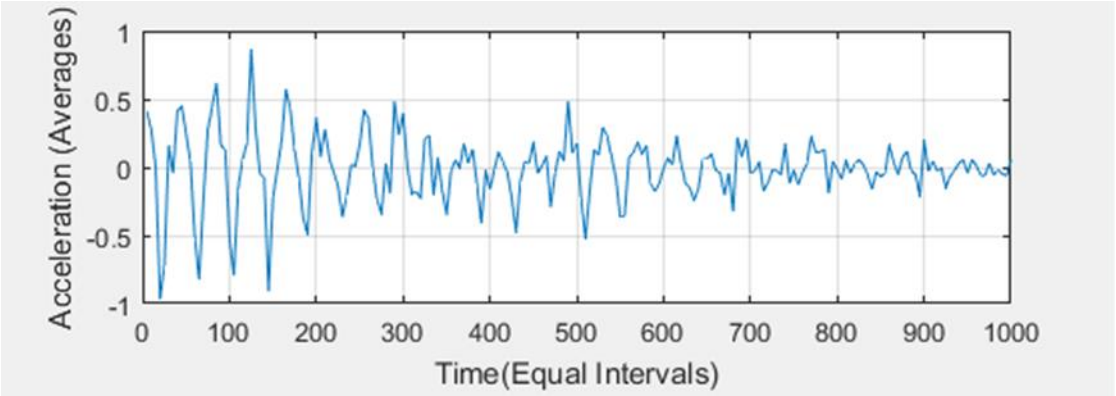

Figure B.5 Signal processing results of structure one subjected to dynamic load one (pseudo-free-vibration response diagram- Δt_1= 0.5%, u_0= (1/4)*D_{max})

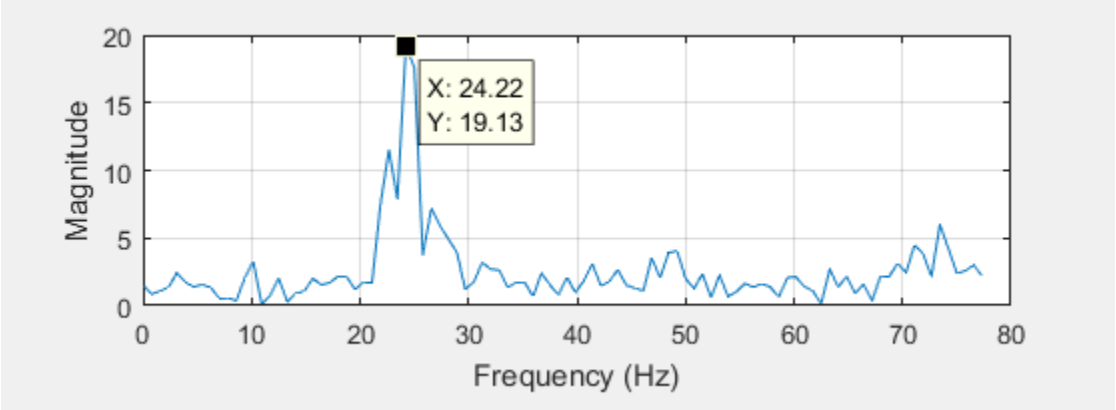

Figure B.6 Signal processing results of structure one subjected to dynamic load one (FFT diagram- Δt_1= 0.5%, u_0= (1/4)*D_{max})

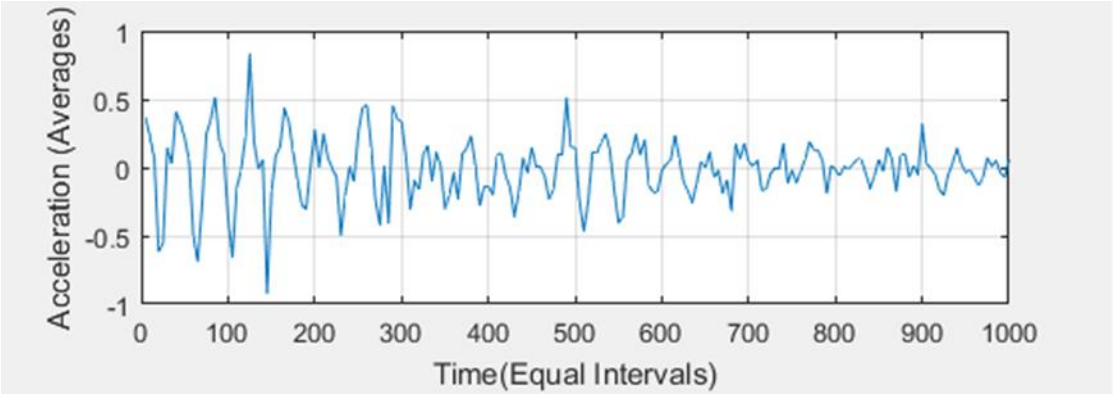

Figure B.7 Signal processing results of structure one subjected to dynamic load one (pseudo-free-vibration response diagram- Δt_1= 0.5%, u_0= (1/5)*D_{max})

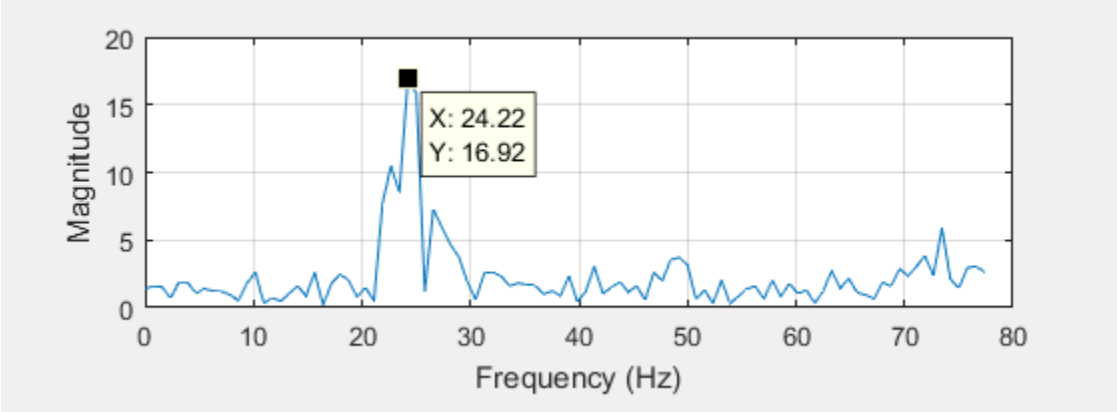

Figure B.8 Signal processing results of structure one subjected to dynamic load one (FFT diagram- Δt_1= 0.5%, u_0= (1/5)*D_{max})

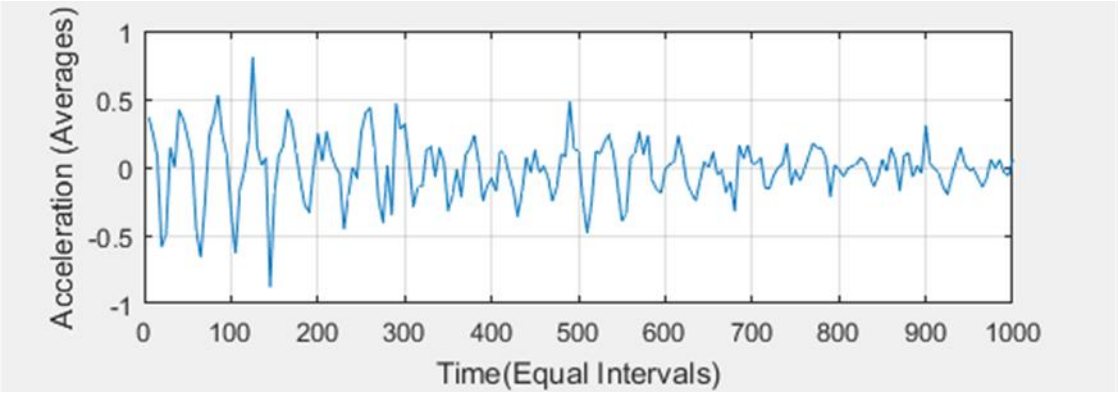

Figure B.9 Signal processing results of structure one subjected to dynamic load one (pseudo-free-vibration response diagram- Δt_1= 0.5%, u_0= (1/6)*D_{max})

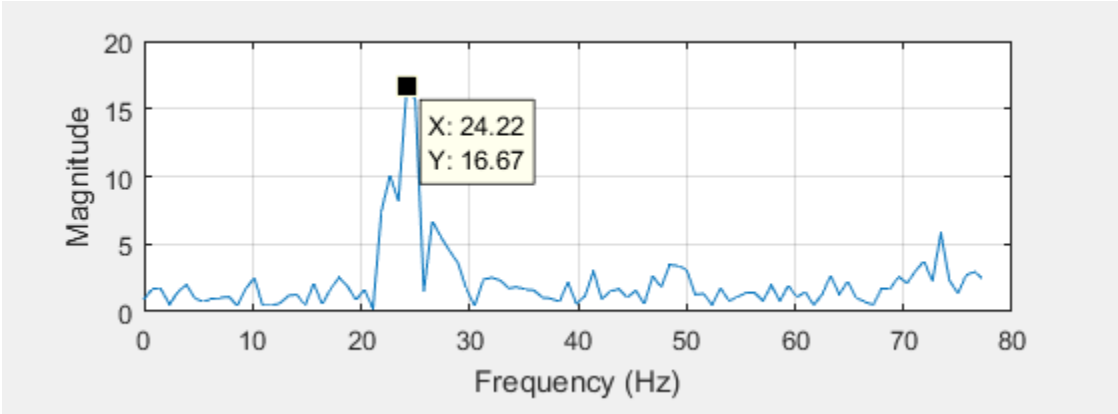

Figure B.10 Signal processing results of structure one subjected to dynamic load one (FFT diagram- Δt_1= 0.5%, u_0= (1/6)*D_{max})

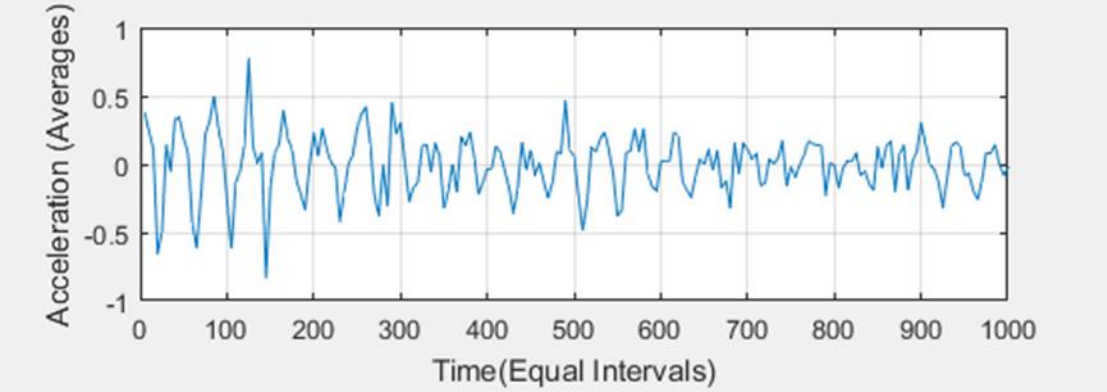

Figure B.11 Signal processing results of structure one subjected to dynamic load one (pseudo-free-vibration response diagram- Δt_1= 0.5%, u_0= (1/7)*D_{max})

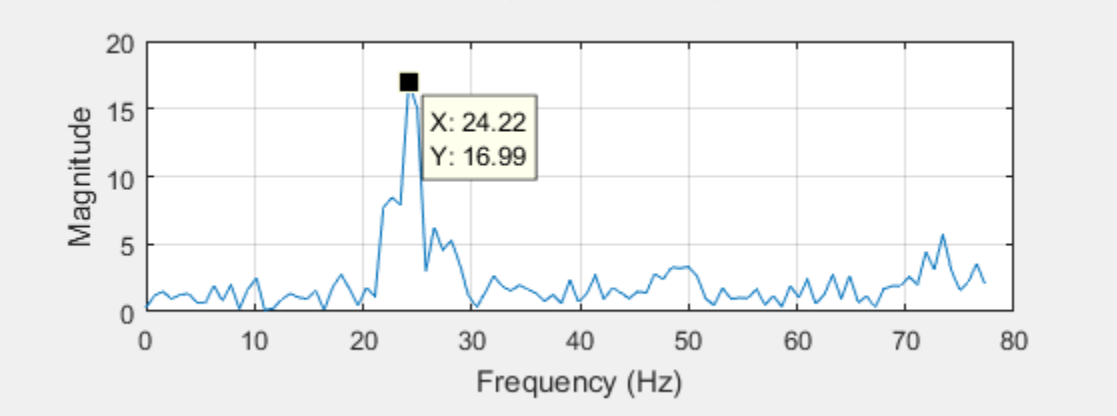

Figure B.12 Signal processing results of structure one subjected to dynamic load one (FFT diagram- Δt_1= 0.5%, u_0= (1/7)*D_{max})

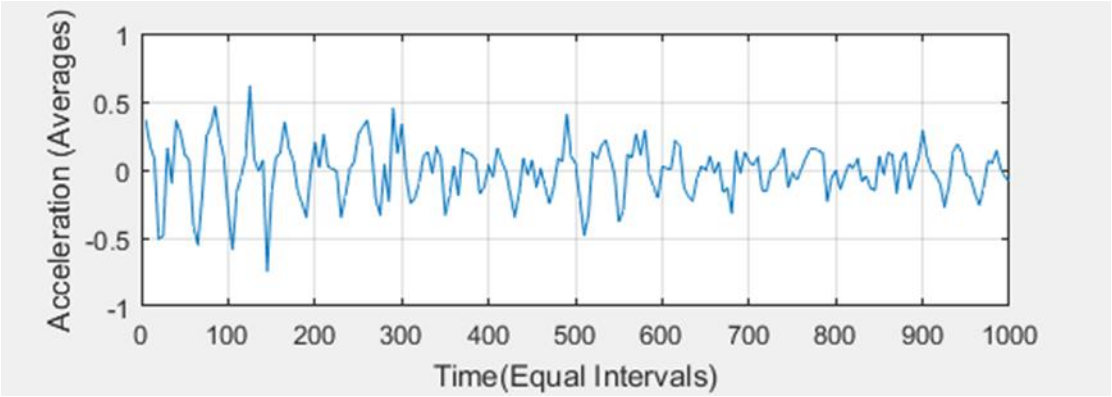

Figure B.13 Signal processing results of structure one subjected to dynamic load one (pseudo-free-vibration response diagram- Δt_1= 0.5%, u_0= (1/10)*D_{max})

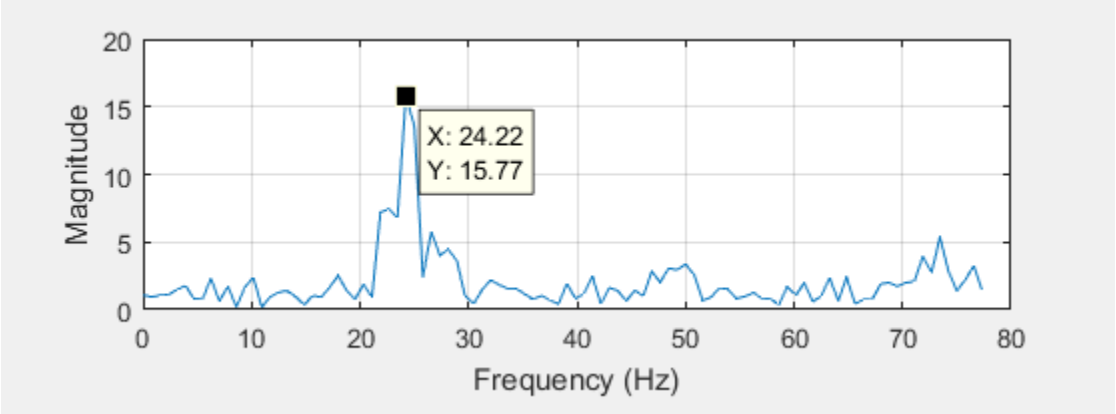

Figure B.14 Signal processing results of structure one subjected to dynamic load one (FFT diagram- Δt_1= 0.5%, u_0= (1/10)*D_{max})

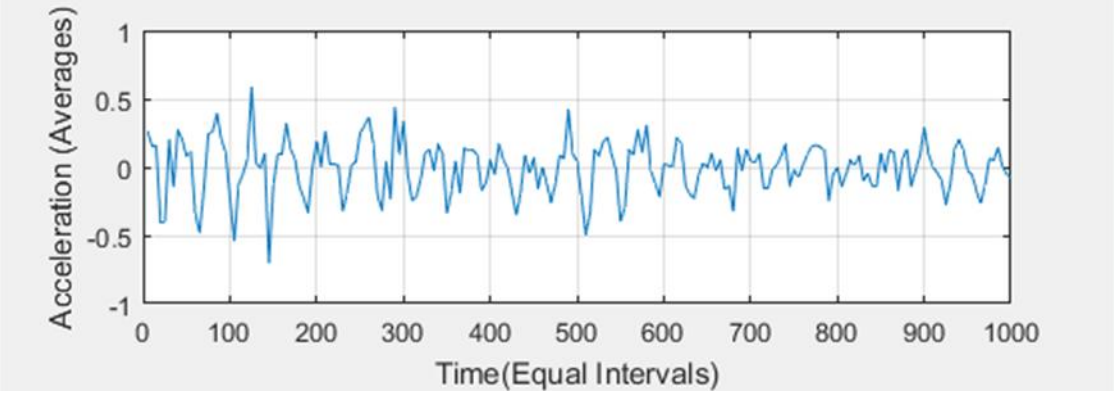

Figure B.15 Signal processing results of structure one subjected to dynamic load one (pseudo-free-vibration response diagram- Δt_1= 0.5%, u_0= (1/11)*D_{max})

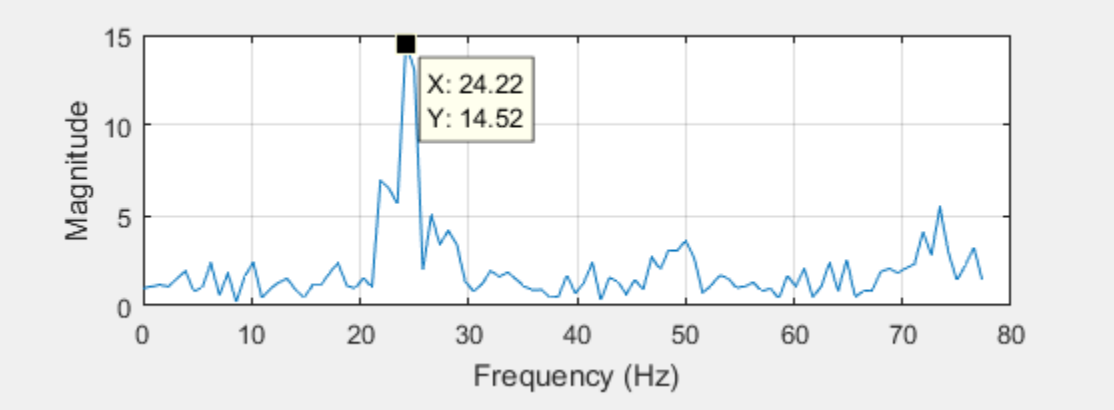

Figure B.16 Signal processing results of structure one subjected to dynamic load one (FFT diagram- Δt_1= 0.5%, u_0= (1/11)*D_{max})

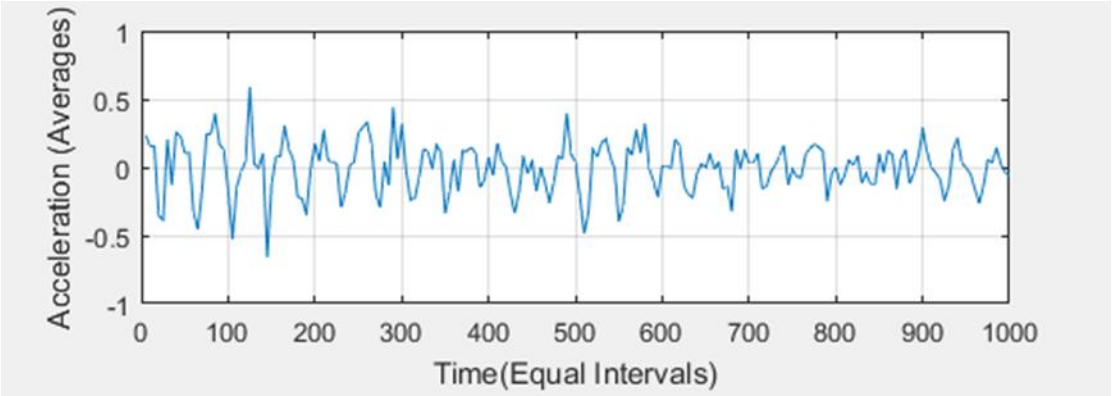

Figure B.17 Signal processing results of structure one subjected to dynamic load one (pseudo-free-vibration response diagram- Δt_1= 0.5%, u_0= (1/14)*D_{max})

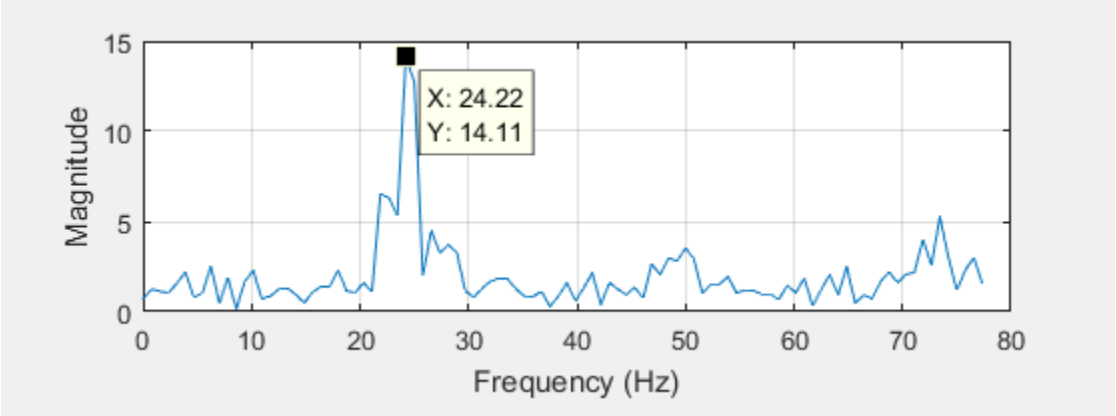

Figure B.18 Signal processing results of structure one subjected to dynamic load one (FFT diagram- Δt_1= 0.5%, u_0= (1/14)*D_{max})

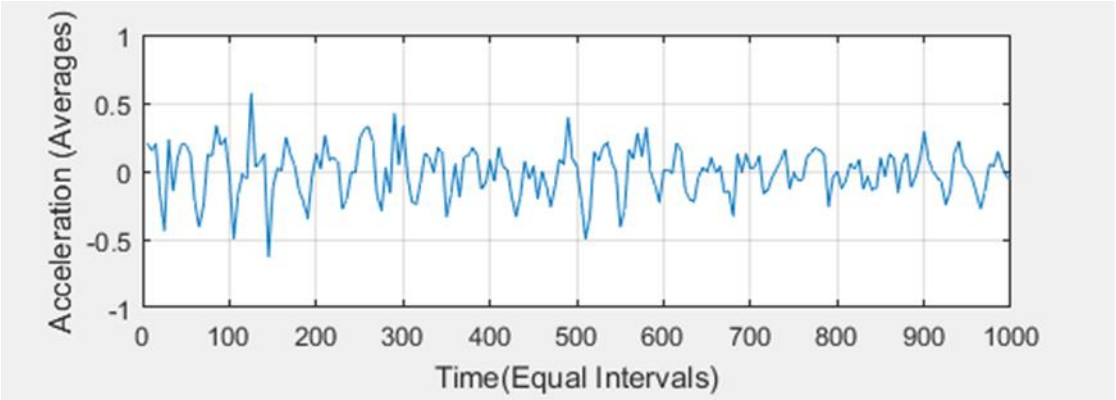

Figure B.19 Signal processing results of structure one subjected to dynamic load one (pseudo-free-vibration response diagram- Δt_1= 0.5%, u_0= (1/16)*D_{max})

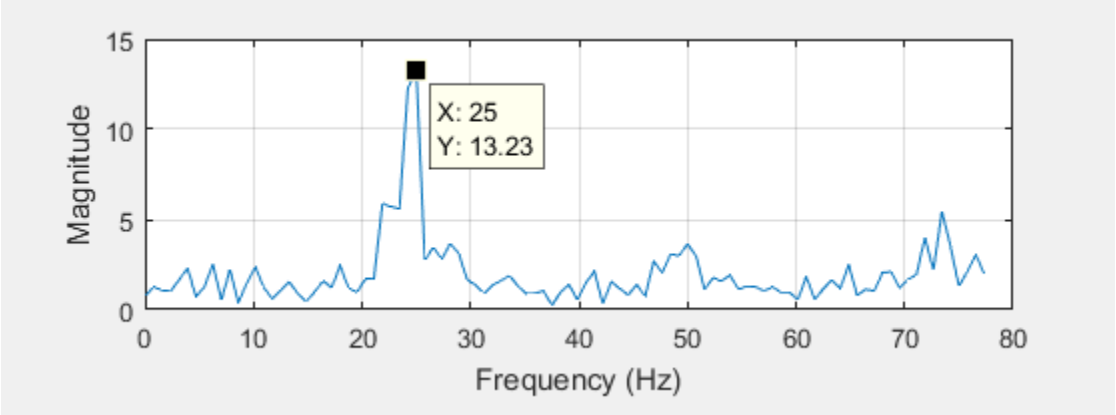

Figure B.20 Signal processing results of structure one subjected to dynamic load one (FFT diagram- Δt_1= 0.5%, u_0= (1/16)*D_{max})

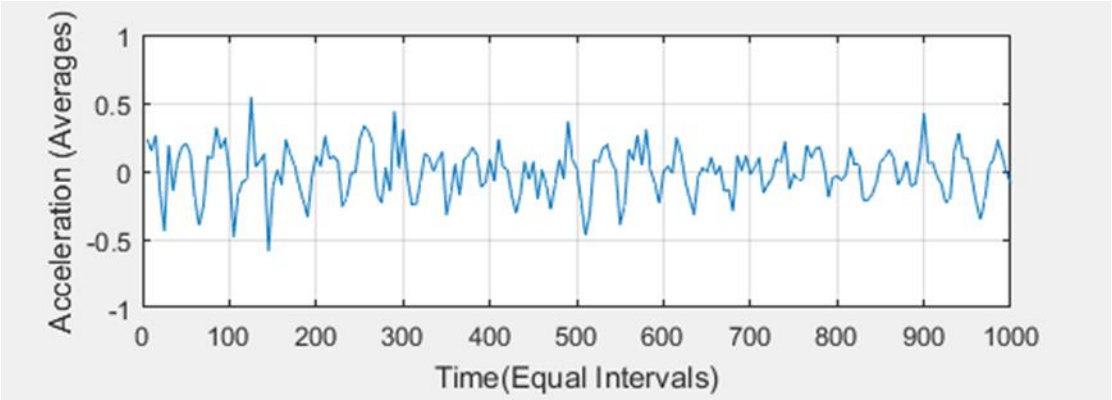

Figure B.21 Signal processing results of structure one subjected to dynamic load one (pseudo-free-vibration response diagram- Δt_1= 0.5%, u_0= (1/19)*D_{max})

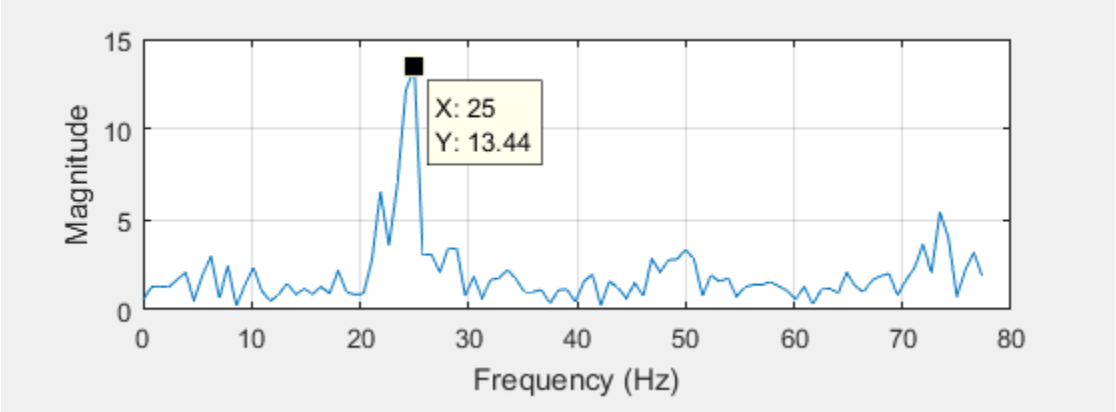

Figure B.22 Signal processing results of structure one subjected to dynamic load one (FFT diagram- Δt_1= 0.5%, u_0= (1/19)*D_{max})

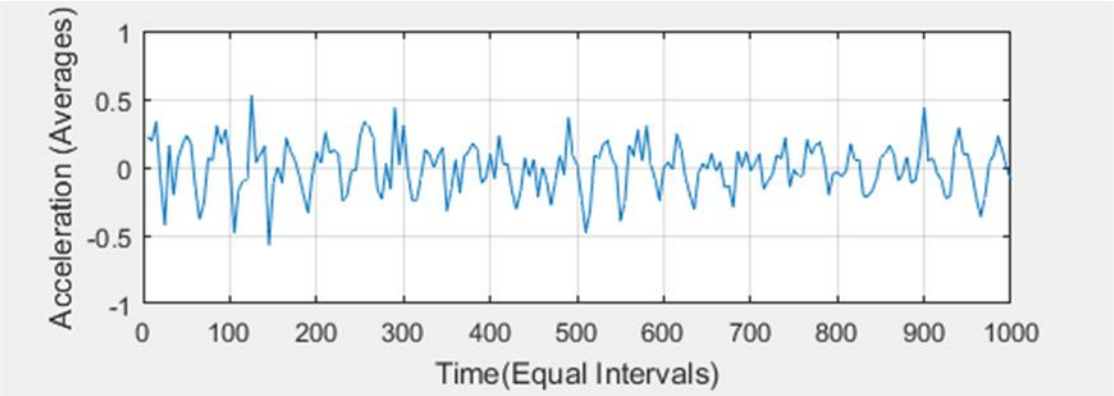

Figure B.23 Signal processing results of structure one subjected to dynamic load one (pseudo-free-vibration response diagram- Δt_1= 0.5%, u_0= (1/20)*D_{max})

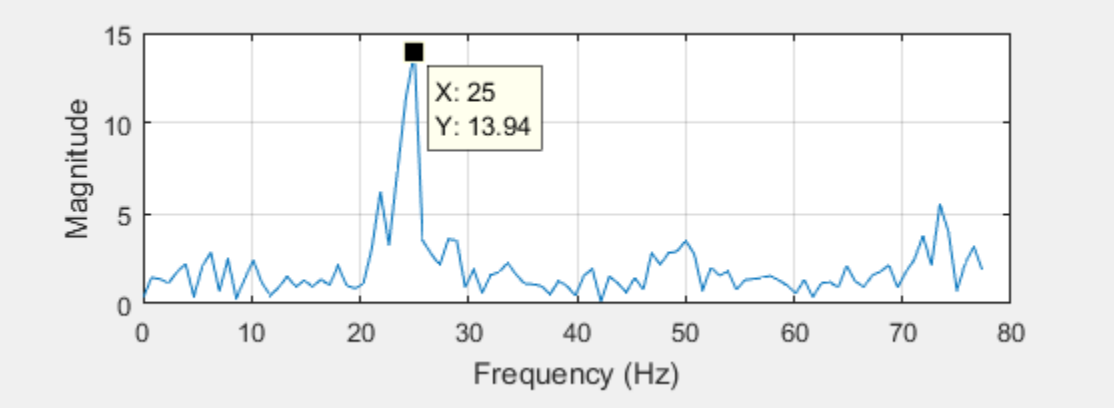

Figure B.24 Signal processing results of structure one subjected to dynamic load one (FFT diagram- Δt_1= 0.5%, u_0= (1/20)*D_{max})

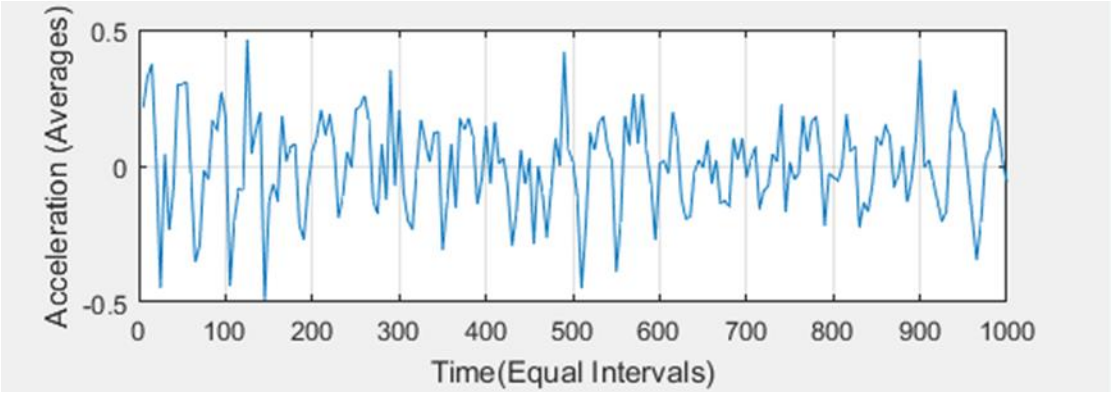

Figure B.25 Signal processing results of structure one subjected to dynamic load one (pseudo-free-vibration response diagram- Δt_1= 0.5%, u_0= (1/50)*D_{max})

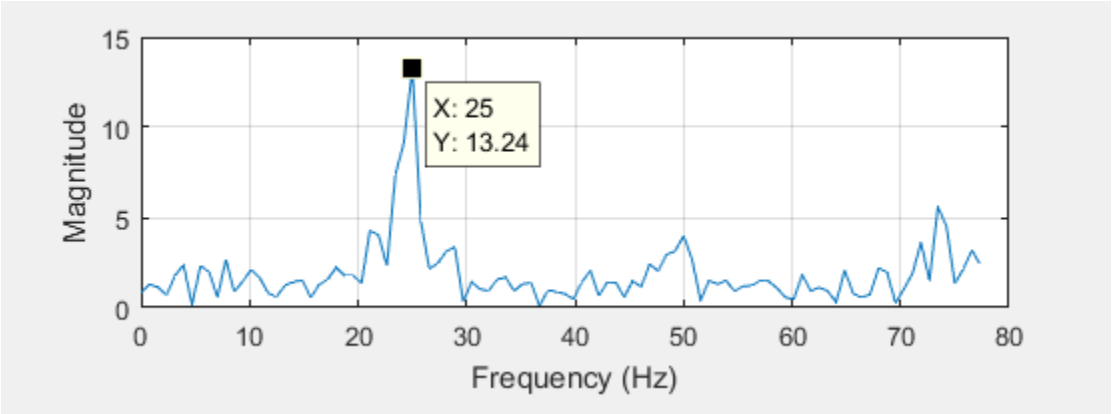

Figure B.26 Signal processing results of structure one subjected to dynamic load one (FFT diagram- Δt_1= 0.5%, u_0= (1/50)*D_{max})

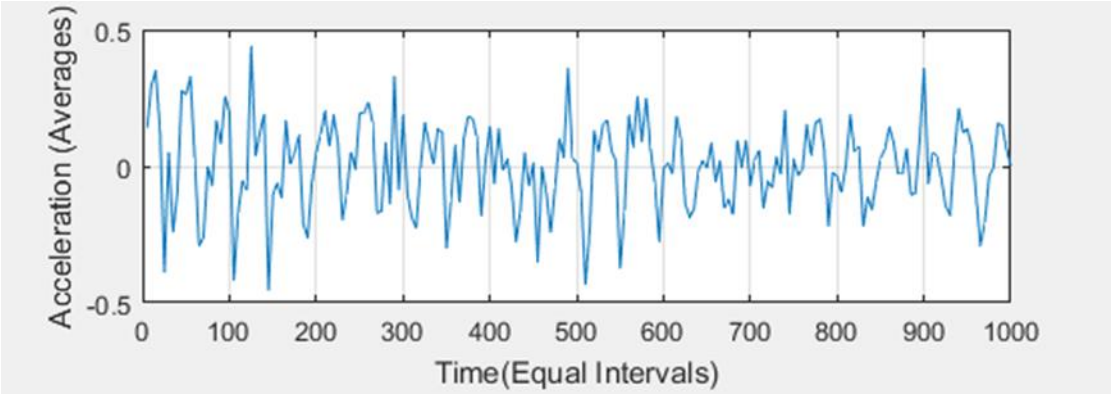

Figure B.27 Signal processing results of structure one subjected to dynamic load one (pseudo-free-vibration response diagram- Δt_1= 0.5%, u_0= (1/100)*D_{max})

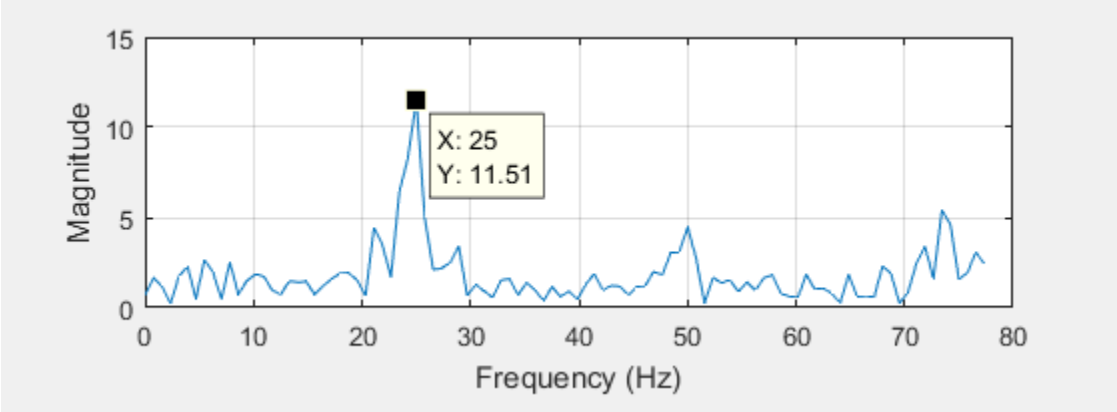

Figure B.28 Signal processing results of structure one subjected to dynamic load one (FFT diagram- Δt_1= 0.5%, u_0= (1/100)*D_{max})

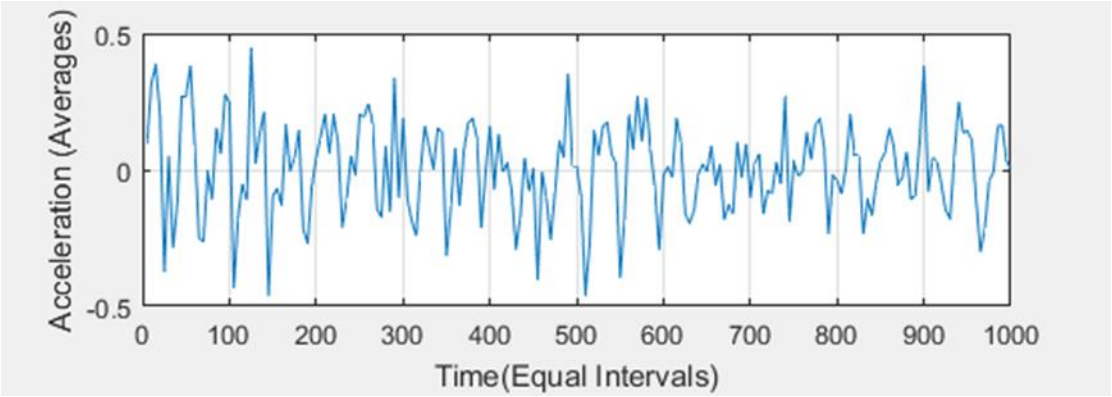

Figure B.29 Signal processing results of structure one subjected to dynamic load one (pseudo-free-vibration response diagram- Δt_1= 0.5%, u_0= (1/200)*D_{max})

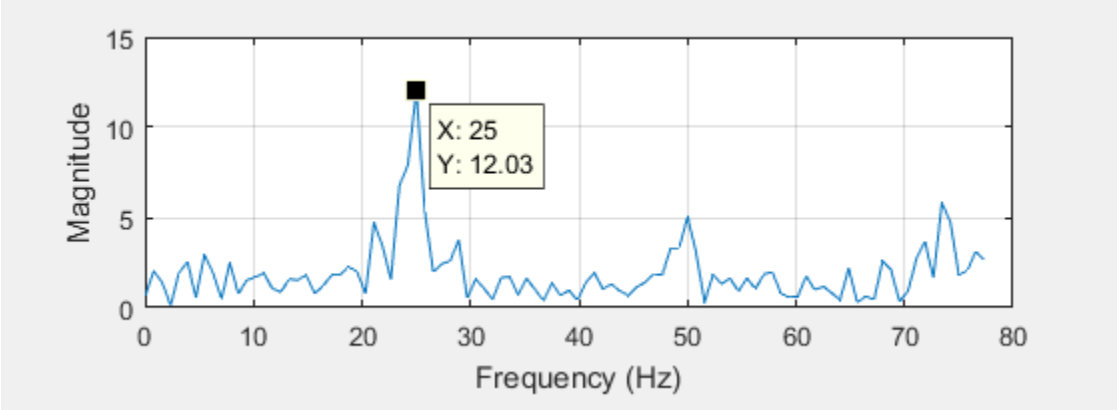

Figure B.30 Signal processing results of structure one subjected to dynamic load one (FFT diagram- Δt_1= 0.5%, u_0= (1/200)*D_{max})

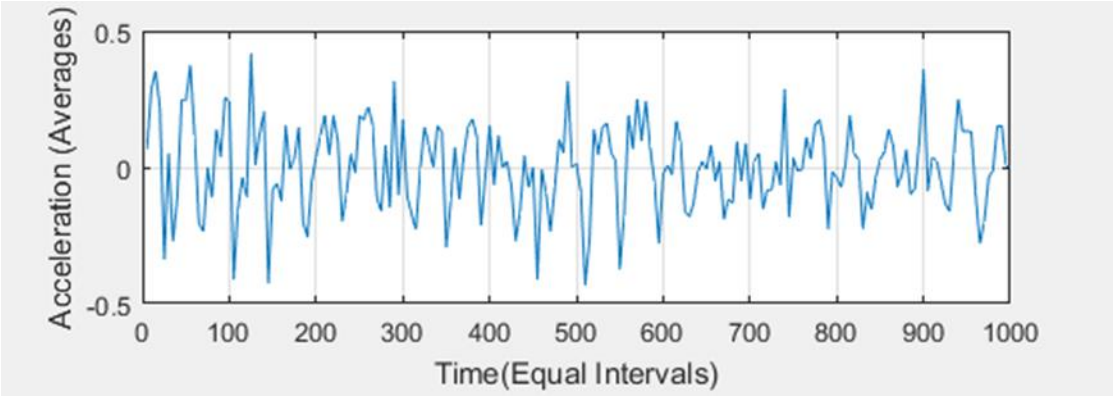

Figure B.31 Signal processing results of structure one subjected to dynamic load one (pseudo-free-vibration response diagram- Δt_1= 0.5%, u_0= (1/1000)*D_{max})

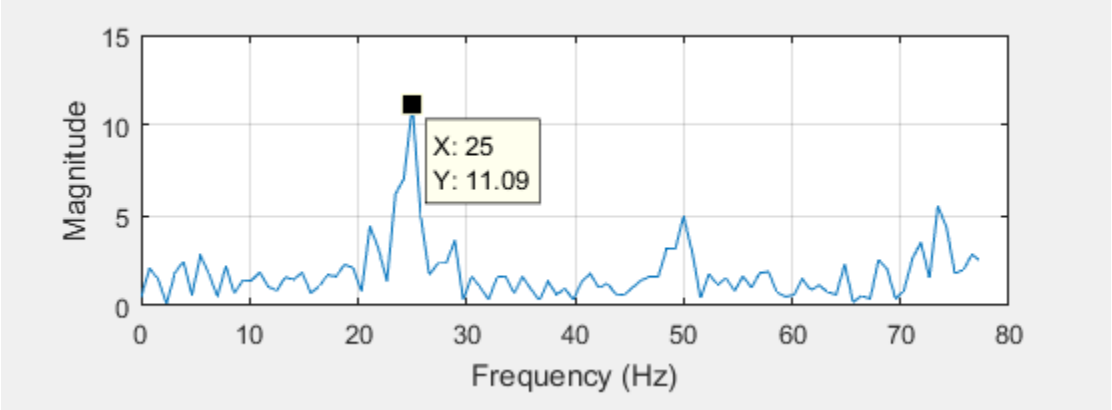

Figure B.32 Signal processing results of structure one subjected to dynamic load one (FFT diagram-ΔT_1= 0.5%, u_0= (1/1000)*D_{max})

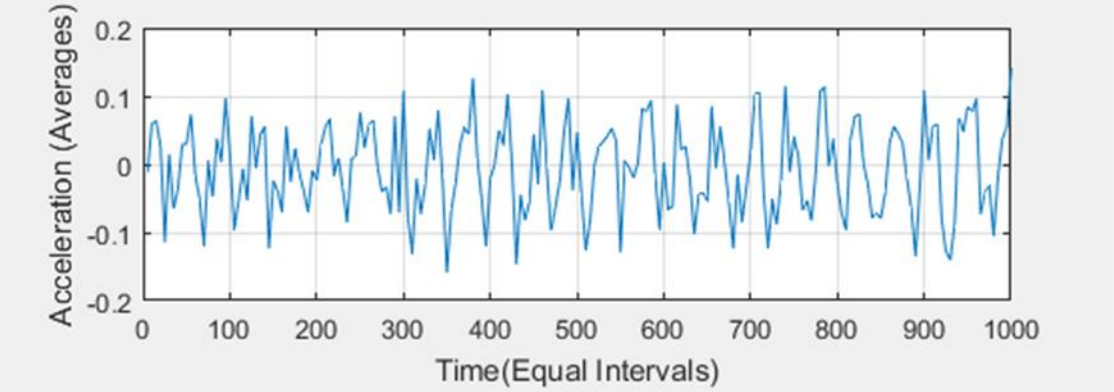

Figure B.33 Signal processing results of structure one subjected to dynamic load one (pseudo-free-vibration response diagram- Δt_1= 0.5%, u_0= (1/10000)*D_{max})

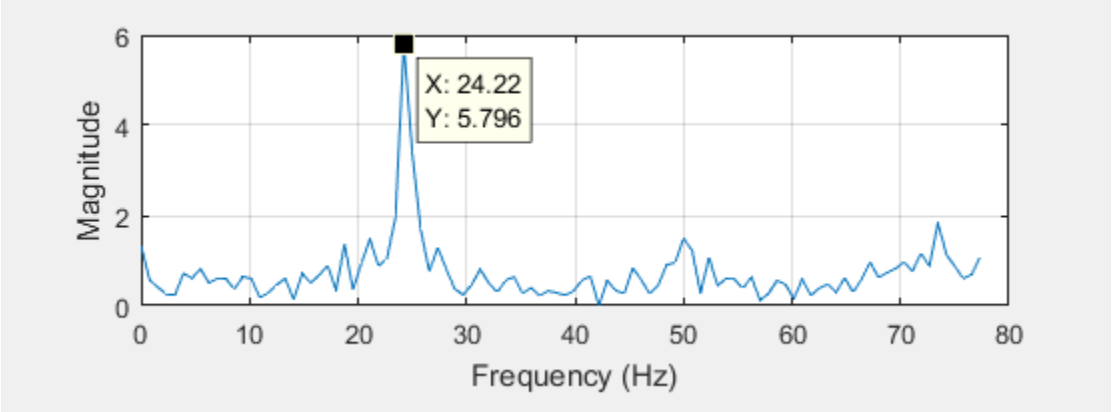

Figure B.34 Signal processing results of structure one subjected to dynamic load one (FFT diagram- Δt_1= 0.5%, u_0= (1/10000)*D_{max})

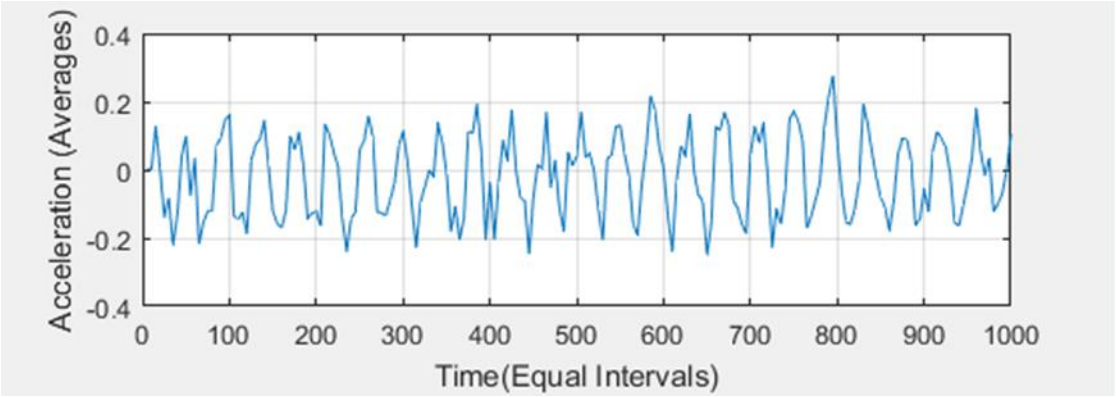

Figure B.35 Signal processing results of structure one subjected to dynamic load one (pseudo-free-vibration response diagram- Δt_1= 0.5%, u_0= (1/100000)*D_{max})

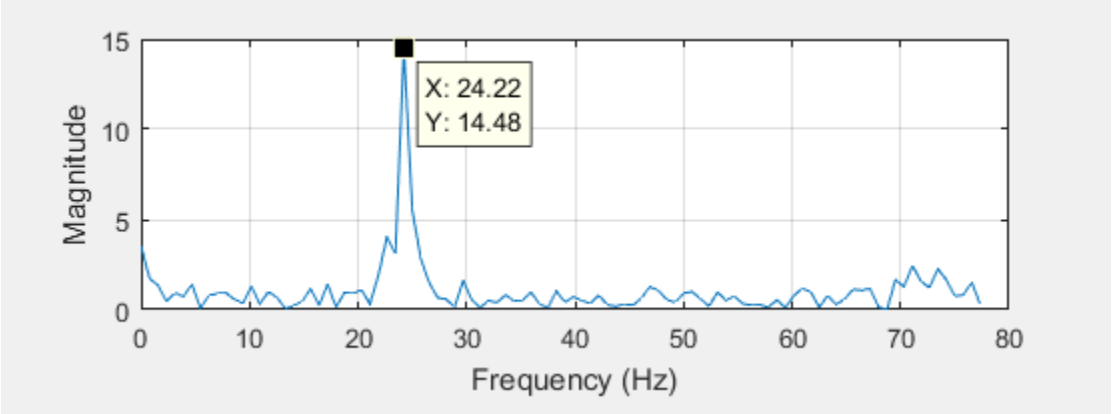

Figure B.36 Signal processing results of structure one subjected to dynamic load one (FFT diagram- Δt_1= 0.5%, u_0= (1/100000)*D_{max})

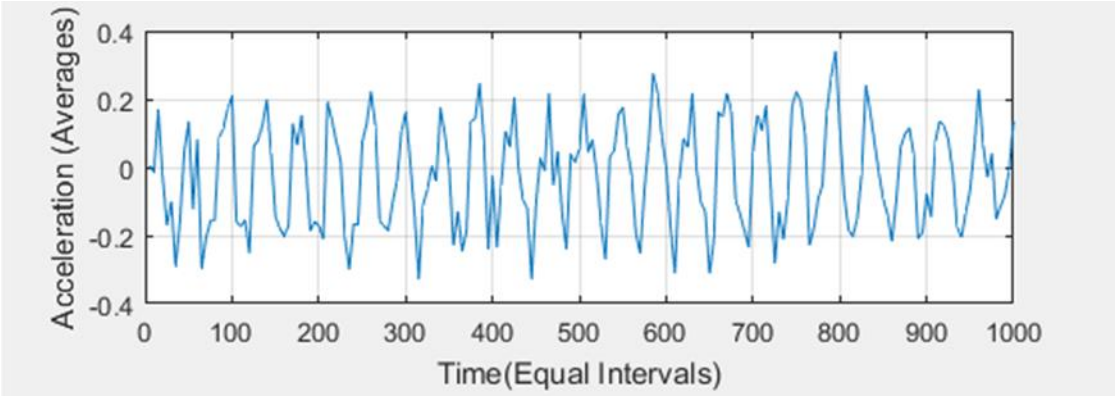

Figure B.37 Signal processing results of structure one subjected to dynamic load one (pseudo-free-vibration response diagram- Δt_1= 0.5%, u_0= (1/1000000)*D_{max})

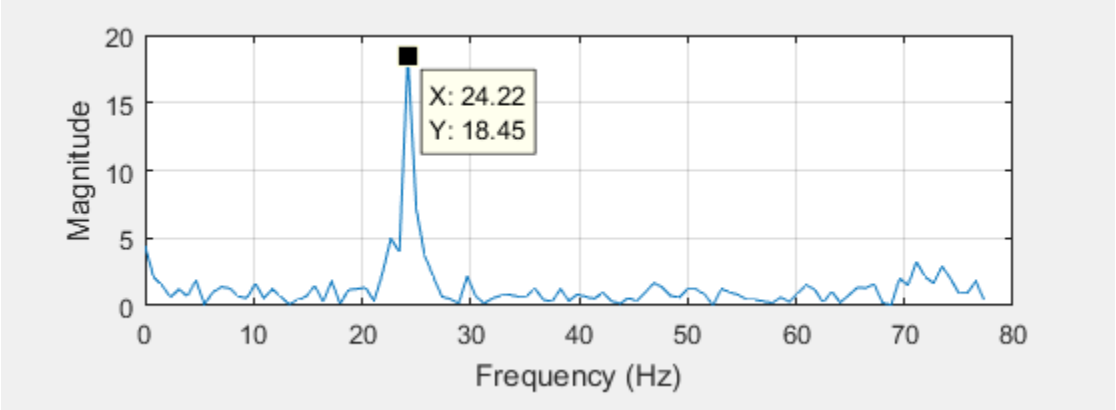

Figure B.38 Signal processing results of structure one subjected to dynamic load one (FFT diagram- Δt_1= 0.5%, u_0= (1/1000000)*D_{max})

Appendix C - MATLAB Codes

```
clc;
clear;
close all;
%INITIAL DATA PROVIDED BY USER

realTlimit=1000; %in sec., the maximum period of the expected free vibration frequency
theTimeStep=5; %in sec.(in percent), real time step we choose to be added to previous time
timeIncrement=1; %in sec., the time increment in the data file (time starts from 0 and increases
by this increment to the end
a=(1/10)*max(D(:,2));%the initial condition set as 1/10 of max

%END OF INITIAL DATA

mystep=theTimeStep/timeIncrement; %number of increments within the time step we chose
Tlimit=realTlimit/timeIncrement;%number of increments within the time limit
TM=mystep;%this is each step (in number of increments)

myData(1:Tlimit/mystep,1)=0.0;

while TM<=Tlimit
%disp('first while')
m=1;%this is number of row in the data, used to read the corresponding second column that is
value
n=0;%this is number of values found at the given TM for the given initial condition a
data=0;%summation of values with TM and initial a
Flag=false;%checking if we have already set the AD flag
AD=false;%flag to know if ascending or descending at the inital point of
while m+TM<length(D(:,1))
   if Flag==false
      if D(m,2)==a
         data=data+D(m+TM,2);
         n=n+1;
         if D(m+1,2)>D(m,2)
            AD=true;
         else
               AD=false;
         end
         Flag=true;
      elseif D(m+1,2)==a
         data=D(m+1+TM,2);
         n=n+1;
         if D(m+1,2)>D(m,2)
            AD=true;
         else
```

```
            AD=false;
        end
            Flag=true;
    elseif D(m,2)<a && a<D(m+1,2)
        ratio=(a-D(m,2))/(D(m+1,2)-D(m,2));
        data=data+D(m+TM,2)+ratio*(D(m+1+TM,2)-D(m+TM,2));
        n=n+1;
        AD=true;
        Flag=true;
    elseif D(m,2)>a && a>D(m+1,2)
        ratio=(a-D(m+1,2))/(D(m+1,2)-D(m,2));
        data=data+D(m+TM,2)+ratio*(D(m+1+TM,2)-D(m+TM,2));
        n=n+1;
        AD=false;
        Flag=true;
    end
end
if Flag==true
    if AD==true
        if D(m+1)>D(m)
            if D(m,2)==a
                data=data+D(m+TM,2);
                n=n+1;
                elseif D(m+1,2)==a
                    data=data+D(m+1+TM,2);
                    n=n+1;
                elseif (D(m,2)<a) && (a<D(m+1,2))
                    ratio=(a-D(m,2))/(D(m+1,2)-D(m,2));
                    data=data+D(m+TM,2)+ratio*(D(m+1+TM,2)-D(m+TM,2));
                    n=n+1;
            end
        end
     elseif AD==false
         if D(m+1)<D(m)
             if D(m,2)==a
                 data=data+D(m+TM,2);
                 n=n+1;
             elseif D(m+1,2)==a
                 data=data+D(m+1+TM,2);
                n=n+1;
             elseif D(m+1,2)<a && a<D(m,2)
                 ratio=(a-D(m,2))/(D(m+1,2)-D(m,2));
                 data=data+D(m+TM,2)+ratio*(D(m+1+TM,2)-D(m+TM,2));
                 n=n+1;
             end
         end
```

```
      end
   end
   m=m+1;
end
datapoint=data/n;
myData(TM/mystep,1)=TM*timeIncrement;
myData(TM/mystep,2)=datapoint;
TM=TM+mystep;
end
disp(myData(:,2))
% size(myData(:,2))
myData = myData; % The file name in Workspace
t=myData(:,1);
s=myData(:,2);
disp(s)
        Ts=mean(diff(t));
fs=1/Ts;
L=length(s);
disp(L)
NFFT=2^nextpow2(L); % Next power of 2 from length of y
M=L+1;
y=fft(s,NFFT);
mag=abs(y);
f=fs/2*linspace(0,1,NFFT/2+1);
r=real(y);
F=f*1000
a=r.^2;
i=imag(y);
b=i.^2;
c=a+b;
Energy=sum(c(:)) % Energy of signal
figure;
subplot(2,1,1);
plot(myData(:,1),myData(:,2));
xlabel('Time(Equal Intervals)')
ylabel('Acceleration (Averages)')
grid
F=f*1000
subplot(2,1,2)
plot(F(1:M/2),mag(1:M/2));
xlabel('Frequency (Hz)')
ylabel('Magnitude')
grid
disp(mag(1:M/2))
disp(F(1:M/2))'
```